# IMPACT OF MIXED CONVECTION ON WILLIAMSON NANOFLUID FLOW OVER A STRETCHING SURFACE

**By**

**Aqsa Mansha**


**NATIONAL UNIVERSITY OF MODERN LANGUAGES**
**ISLAMABAD**

**June, 2023**

# Impact of Mixed Convection on Williamson Nanofluid Flow over a Stretching Surface

**By**

**AQSA MANSHA**

A THESIS SUBMITED IN PARTIAL FULLFILMENT OF THE REQUIREMENT FOR THE DEGREE OF

**MASTER OF SCIENCE**

In Mathematics

**TO**

FACULITY OF ENGINEERING & COMPUTER SCIENCE


NATIONAL UNIVERSITY OF MODERN LANGUAGES ISLAMABAD


# THESIS AND DEFENSE APPROVAL FORM

**The undersigned certify that they have read the following thesis, examined the defense, are satisfied with overall exam performance, and recommend the thesis to the Faculty of Engineering and Computer Sciences for acceptance.**

**Thesis Title:** Impact of Mixed Convection on Williamson Nanofluid Flow over a Stretching Surface

**Submitted By:** Aqsa Mansha

**Registration #:** 1/MS/Math/S20

Master of Science in Mathematics (MS Math)
Title of the Degree

Mathematics
Name of Discipline

Dr. Anum Naseem
Name of Research Supervisor

Signature of Research Supervisor

Dr. Sadia Riaz
Name of HOD (MATH)

Signature of HOD (MATH)

Dr. Muhammad Noman Malik
Name of Dean (FE&CS)

Signature of Dean (FE&CS)

Date: 13 June, 2023

# AUTHOR'S DECLARATION

I Aqsa Mansha

Daughter of Muhammad Mansha

Registration #1/MS/MATH/S20

Discipline Mathematics

Candidate of **Master of Science in Mathematics** at National University of Modern Languages do here by declare that the thesis **Impact of Mixed Convection on Williamson Nanofluid Flow over a Stretching Surface** submitted by me in fractional fulfillment of **MS Mathematics** degree, is my original work, and has not been submitted or published earlier. I also solemnly declare that it shall not, in future, be submitted by me for obtaining any other degree from this or any other university or institution. I also understand that if evidence of plagiarism is found in my thesis/dissertation at any stage, even after the award of a degree, the work may be cancelled and degree revoked.

Signature of Candidate ……..

Name of Candidate…Aqsa Mansha……

Date: 13 June, 2023

# ABSTRACT

**Title: Impact of Mixed Convection on Williamson Nanofluid Flow over a Stretching Surface**

This research work deals with the mixed convection flow of a shear thinning nanofluid over a stretching surface. The surface is assumed to be porous and stretching exponentially. Two different cases of heat transfer, i.e., prescribed exponential surface temperature (PEST) and prescribed exponential heat flux (PEHF) are used for the analysis. Moreover, an inclined magnetic field is applied to the flow and the effects of chemical reaction, heat generation/absorption and viscous dissipation are considered. The boundary layer theory is applied to the fluid model and the resultant system of differential equations are presented and simplified with the help of useful similarity transformations. Homotopy analysis method is used to solve the governing nonlinear system using Mathematica Software. The velocity, temperature and concentration profiles are graphically analyzed under the influence of various flow parameters. From the results, it is found that increased values of local grashof number increases the velocity profile while the opposite behavior is seen for the temperature profile. An enhanced temperature profile corresponds to enhanced Eckert number and the enhanced chemical reaction parameter reduces the concentration profile. The friction drag, Nusselt number and Sherwood number are studied for varying dimensionless parameters. A comparison with the existing literature is also performed.

# TABLE OF CONTENTS

# LIST OF TABLES

# LIST OF FIGURES

# NOMENCLATURE

## Acronyms

| | |
|---|---|
| PEST | Prescribed exponential order surface temperature |
| PEHF | Prescribed exponential order heat flux |

## Symbols

| | |
|---|---|
| $x, y$ | Cartesian coordinates |
| $u,\ v$ | Velocity components |
| $T$ | Temperature |
| C | Concentration |
| $\alpha$ | Thermal diffusivity |
| $\sigma$ | Electrical conductivity |
| $\nu$ | Kinematic viscosity |
| $\rho$ | Density |
| $k_1$ | Permeability of the porous medium |
| $(\rho C_p)_f$ | Fluid heat capacity |
| $Q_0$ | Heat generation coefficient |
| $T_\infty$ | Ambient fluid temperature |
| $C_\infty$ | Ambient nanoparticles volume fraction |

| | |
|---|---|
| $D_B$ | Coefficient of brownian diffusion |
| $D_T$ | Coefficient of thermophoresis diffusion |
| Γ | Shear stress for time constant |
| $\lambda$ | Williamson parameter |
| $N_t$ | Thermophoresis motion parameter |
| $N_b$ | Brownian motion parameter |
| $Le$ | Lewis number |
| $Pr$ | Prandtl number |
| $Q$ | Heat soure/sink |
| $K$ | Porosity parameter |
| $M$ | Hartmann number |
| $Re$ | Reynolds number |
| $Ec$ | Eckert number |
| $Nu$ | Nusselt number |
| $Sh$ | Sherwood number |
| $Gr_t$ | Grashof number for temperature |
| $Gr_c$ | Grashof number for concentration |
| $\gamma$ | Chemical reaction parameter |
| $\beta_T$ | Temperature expansion coefficient |
| $\beta_c$ | Concentration expansion coefficient |

# ACKNOWLEDGEMENT

In the name of Allah, the most gracious and the most merciful. First and foremost, I am thankful to Almighty ALLAH for giving me the strength, knowledge, ability and opportunity to accomplish and complete this study satisfactorily.

I would like to express my deep and sincere gratitude to my research supervisor, Dr. Anum Naseem for giving me the opportunity to do research and providing invaluable guidance throughout this research. Her dynamism, vision, sincerity and motivation have deeply inspired me. She has taught me the methodology to carry out the research and to present it as clearly as possible. It was a great privilege and honor to work and study under her guidance. I am extremely grateful for what she has offered me. Her valuable expertise, suggestions, comments and instructions have greatly improved the novelty of this document. I am placing my earnest thanks to Dr. Anum Naseem. I am so grateful to work under the supervision of such a great person.

Finally, I must express my very profound gratitude to my parents and to my friends for providing me with unfailing support and continuous encouragement throughout my years of study and through the process of research and writing this thesis. This accomplishment would not have been possible without them. Thank you.

# DEDICATION

I dedicate my thesis to my parents and teachers for their endless support and encouragement throughout my pursuit for education. I hope this achievement will fulfill the dream they envisioned for me.

# Chapter 1

# Introduction

## 1.1 Williamson Nanofluid

Nanofluids triggered researchers' interest since they played an important role in a variety of heat-related equipments, technical gadgets and industrial items. Modern eras focus on finding ways to save energy and acquire better outcomes. Regarding this, improvement in thermal-exchanges can be one of the important features. Nanoparticles are employed in nanofluids which are usually metals, oxides, carbides or carbon nanotubes. They are nanometer sized particles possessing less than 100 nm diameter and have enhanced viscosity, greater thermal conductivity and are more stable when compared to the other fluids. Nanofluids are a new and different type of heat transfer flowing fluids laying foundations for nanotechnology and are produced by scattering and suspending nanoparticles in typical traditional fluids. The practice of nanofluid is quite efficient in many fields of engineering and science. They have prominent advantages in heat transport, nuclear reactor, solar energy, paper production, boiler, laser diode arrays etc. Their utility also extends to applications in medicine, chemical engineering and many others. Nanofluids possess special qualities that potentially make them useful for a variety of applications in heat transfer. Some of them include microfluidics, engine cooling, automotive thermal dissipation, household kitchen appliances, fuel cells and heat exchangers. The performance of numerous application, including heat transfer, medication delivery, higher oil recovery, lubrication and many others, is improved by the better rheological, thermal and wettability characteristics of nanofluid. Recent study and experiments have shown that with the introduction of nanofluids the physical features of traditional fluids can be improved. The properties of nanofluids are significantly influenced by the structure of its additives. Nanofluid can be created using either a single phase (solid phase) or a two phase approach (liquid phase). Nanofluids own superior thermophysical

properties when compared to the properties of base fluids (water or oil), they have excessive potential usage in countless fields. Choi [1] studied the nanoparticles and their properties. He found that the suspensions differ significantly from their conventional fluids in a number of ways, the most remarkable of which is that they have far better thermal performance than the corresponding base fluids.

It is a known fact that non-Newtonian fluids are defined as liquids that violate the Newtonian law of viscosity. Such fluids' viscosity is dependent on the tensile stress that is applied to the fluid. There are lots of cases of these fluid in common liquid items, including custards, plasma, soap, toothpaste, jelly, corn starch, paint, melted butter and a number of others. Non-Newtonian fluids can be expressed by a wide variety of fluid models. These fluids exhibit shear-thinning and shear-thickening properties. Scientists and academics have always been interested in non-Newtonian fluids because of how frequently they are used in industrial and biological operations. Blood, polymer solutions, ketchup, paper pulp, crude oil and biological applications are a few examples of these fluids. Due to their numerous and complicated structures, non-Newtonian's fluid flowing properties cannot be explained by a single constitutive equation. In many business and technological programs, non-Newtonian fluids have currently obtained extra interest and relevance than Newtonian fluids. For non-Newtonian fluids, the perceived viscosity is dependent on the geometry of the flow, shear rate and other variables rather than being constant at the specified pressure and temperature. Williamson fluid is familiarized as a shear thinning fluid that is a non-Newtonian fluid and was initially revealed by Williamson. Williamson [2] proposed a theory to investigate pseudoplastic elements and constructed a constitutive equation to explain the properties of pseudoplastic fluids. Experiments he carried out were based on the equations and supported the findings regarding the flow properties. Williamson fluid has extensive range of applications, particularly in the performance pertaining to pseudo-plastic fluids that is extensively applied in commercial applications. It also has its applications in biological engineering like hemodialysis and measuring heat and mass transport rate within the walls of blood vessels. Khan *et al*. [3] showed their interest in the work initiated by Williamson and examined the flow of Williamson fluid with chemical reaction effect by using the homotopy analysis technique. Kothandapani and Prakash [4] evaluated the consequences of peristaltic flow of Williamson nanofluid in an elastic medium under the process of a thermal emission. In the same year, Krishnamurthy *et al*. [5] examined the impact of nanoparticle on the persistent motion of MHD Williamson fluid flow via

porous media towards a horizontally stretching sheet. The influences of mixed convection and chemically reactive species on the Williamson fluid produced by a non-isothermal plate and cone in a porous media was studied by Khan *et al*. [6]. Nanoparticles have the ability to improve convective heat transfer within the boundary layer region. Hamid and Khan [7] examined the thermo-physical characteristics of Williamson nanofluid flow with the existence of mixed convection and with magnetic field. Ali *et al*. [8] investigated how the electric field affects the MHD and Williamson nano-fluid flow and heat transmission capabilities across a heated surface with varying thickness.

## 1.2 Mixed Convection

Mixed convection occurs when a flow is simultaneously influenced by an exterior forcing mechanism and internal forces related to volume. Mixed convections that is in actual both forced and free convection, often used as a mechanism of a heat transfer. When a flowing fluid, such as air or water, is moving, the heat transfer process takes place. Differences in temperature within the flowing fluid start causing convection. A porous media and the dissipative convective flow have numerous applications, including fiber insulation, geysers, soil pollution, electric kettles, and lights. Internal fluids' ability to transfer thermal energy is termed as a transmission of convectional heat. Convection happens when molecules in a liquid, gas or liquid-gas mixture move collectively. Although there is some initial conduction of heat between molecules, the majority of heat transmission occurs as molecules move around inside a fluid. In a lid-driven cavity with an arched wall and filled with a CuO-water nanofluid, Nada *et al*. [9] concentrated on the mathematical analysis of steady two-dimensional mixed convection flow. Rashidi *et al*. [10] looked into the outcomes of a magnetic field for the combined convective heat transfer for nanofluid flow within a vertical channel with periodic walls. The features of hydrodynamic fluid and heat analysis were also studied. Selimefendigil and ztop [11] used the finite element approach to analyze the effects of mixed convection for nanofluid in a three-dimensional flow with two internally spinning circular cylinders. Vertical walls were kept at a constant temperature whereas rotating cylindrical surfaces were considered to be adiabatic. For a partially layered non-Darcy porous medium, Aly

*et al*. [12] examined the mixed convection flow for a nanofluid. They also proposed an enhanced version of the incompressible smoothed particle hydrodynamics (ISPH) method in light of the advantages of particle-based methods.

## 1.3 Magnetohydrodynamics

Magnetohydrodynamics (MHD) deals with magnetic behavior observed in electrically conducting fluids like salt water, plasma and liquid metals. If a conducting fluid is exposed to a continuous magnetic flux, then an electromagnetic force is produced which in turn generates electric current. Magneto-hydrodynamics (MHD) research was first documented in astronomical and geophysical issues. Due to its numerous uses in the fields of medicine, engineering and petroleum refining, this research has drawn a great deal of focus over the past few years. Additionally, magnetohydrodynamics for nanofluid have demonstrated their value in a variety of sectors. Biomedicine, optical activators, metallurgical techniques, magnetic cell insulator, blood flow monitoring and optical control keys are a few of them. The fundamental concept of MHD holds that the magnetic fields can generate current in a conducting fluid, polarizing the fluid and therefore altering the magnetic field. Pal and Mandal [13] analyzed the flow of a nanofluid in magnetohydrodynamic flow that conducts electricity across a nonlinear elastic surface with pores. They discovered for larger amount of the heat generation/absorption parameter, dual solutions existed. Hayat *et al*. [14] explored three-dimensional and magnetohydrodynamic (MHD) flow of the Oldroyd-B nanofluid with the appearance of generating and absorbing heat and surface imitating conditions for convection. Using a nanofluid moving due to a semi-infinite flat plate as a boundary, Prasad *et al*. [15] investigated the impacts of radiation and chemical reaction on MHD free convective heat and also mass transfer flow. Mohyud-Din *et al*. [16] examined flow with the analysis of mass and heat transfer of a flowing fluid past a swiftly moving flat plate by applying Buongiorno's model.

## 1.4 Viscous Dissipation

Viscous dissipation demonstrates how kinetic energy is transformed into enthalpy. Viscous dissipation is a factor in the energy equation, while it serves as an energy source and modifies temperature distributions, thus affecting heat transfer rates. It is the energy loss brought on by the forces of friction between the fluid particles. Umavathi *et al*. [17] inspected a viscous fluid flowing via an ascending channel with temperature and thermal resistance to evaluate the transfer of heat and mass properties. Viscous dissipation affects the sheet in a different way depending on whether it is being heated or cooled. The analysis of heat transmission due to the presence of viscous dissipation is of tremendous interest in light of the extensive practical applications. Badruddin and Quadir [18] observed the impact of viscous dissipation and radiation in a square porous annulus subjected to inside and outside cold temperatures. Hsiao [19] inspected viscous dissipation impact on micropolar nanofluid for a stretched sheet and examined the heat and mass transfer in hydromagnetic flow. The flow of second-grade nanoliquid via a revolving disk is examined by Hayat *et al*. [20] and Joule heating while dissipation were the factors considered for studying heat transport. Saleem *et al*. [21] inspected the movement of a nanofluid caused due to a stretched surface with heat source and viscous dissipation. Thermophoresis and Brownian motion were also included.

## 1.5 Heat generation/absorption

Heat generation is the process by which one type of energy, such as electrical or chemical, is modified into thermal energy (heat energy) inside a body. Temperature changes across the boundaries require the heat transfer process. There are several industrial and engineering uses for heat propagating mechanisms such as in food processing, nuclear reactors, thermal transmission, etc. It is crucial to many energy-related applications, including automotive radiators, lubricants and coolants used in mechanical processes. Abbas *et al*. [22] used nanofluid flowing by a curved stretchable surface to investigate the effects of heat generation/absorption and magnetohydrodynamics. A numerical technique, shooting method was employed to investigate the

solutions numerically. The use of heat absorptive/generative transport done within a three-dimensional flow of Williamson fluid instigated by bidirectional surface stretching non-linearly was explored by Bilal *et al*. [23]. Upreti *et al.* [24] studied the effects of suction/injection, heat absorption/generation on MHD flow of Ag-water nanofluid past a stretching flat plate in a porous media with Ohmic-viscous dissipation. Saba *et al*. [25] looked at a boundary layer radiative flow in two dimensions with heat generation/absorption. The fluid flow was across a curved surface and involved CNTs (carbon nanotubes). Eid and Mahny [26] investigated the impact of steady flow and heat transfer in the presence of heat absorption and generation over a nonlinearly stretching surface in a porous medium saturated with a Sisko flowing fluid. The significant effects of radiation and heat generation/absorption for Maxwell nanofluid fluid model was taken by Hayat *et al.* [27] to further explore the MHD flow for in case of a stretched surface.

## 1.6 Chemical Reactions

Chemical reaction is the process by which one or more chemicals are changed into one or more other compounds. The atoms that constitute the reactants are rearranged during a chemical reaction to form different products. The evolution of the idea of a chemical reaction was crucial in shaping chemistry as we know it today. For thousands of years, people have studied and used chemical processes for a variety of purposes, such as the smelting of iron, burning of fuels, the brewing of beer and wine, the production of glass and pottery and the production of cheese. In addition to the Earth's geology, atmosphere and oceans, all biological systems exhibit complex chemical interactions on regular basis. Numerous instances of sophisticated chemical processes can be observed in all living systems, also in the geology, environment and ecosystems of the entire globe. Chemical processes must be distinguished from physical changes. State shifts can also occur during physical alterations, such as when ice melts into water or water evaporates into vapour. The physical characteristics of a material alter when it goes through a physical metamorphosis, but its chemical structure stays the same. When a substance undergoes a physical transformation, its physical characteristics will alter but its chemical composition won't with the existence of a heat sink, heat source and a chemical reaction, Nayak *et al*. [28] investigated the effects of mass and heat transfer in a boundary layer flow through a porous material of a

viscoelastic fluid subject to a longitudinal magnetic field. Using the combined effects of radiative heat and mass transfer in the presence of first-order chemical reaction, Saqib *et al.* [29] examined the effects of slip at a vertical plate for the originating flow of Casson flowing fluid. Mjankwi *et al.* [30] investigated the magnetohydrodynamic (MHD) flow of nanofluid across a shrinking surface that is inclined in the existence of thermally radiation and chemical process. Sabir *et al*. [31] worked to investigate the effects of chemical processes and gyrostatic microorganisms on the two-phase Casson nanofluid moving through a stretched sheet which was permeable and the effective numerical method known as the shooting approach was used to handle the resulting equations.

## 1.7 Thesis Organization

The thesis comprises of six chapters.

Chapter. 1 is about a detailed introduction related to the existing work.

Chapter. 2 is related to a detailed literature review. It includes the literature that is the foundation of the current work.

Chapter. 3 contains important definitions and concepts that are used in our study. The fundamental laws for analysis of subsequent chapters are also included in this chapter.

In Chapter. 4, the analysis of Williamson nanofluid flow in two dimensions caused by a stretched surface with exponential velocity is carried out. The fluid characteristics are affected by the consideration of MHD and production and absorption of heat. Through the utilization of the homotopy analysis approach, a system of PDEs which are the model equations is solved.

Chapter. 5 is devoted to the mixed convective nanofluidic flow analysis of a shear thinning fluid studied due to an exponentially stretching surface. The phenomenon of magnetohydrodynamics and in addition chemical reaction are also responsible for obtaining important results. The considered equations are converted into the nonlinear ODEs and the ensuing

system is solved using homotopy analysis techniques. A complete analysis on the obtained results has been carried out.

Chapter. 6 is about the conclusions of a review and extended work. It also contains some future potential studies.

# Chapter 2

# Literature Review

Analysis on non-Newtonian nanofluid has received attention of scientists and researchers since the last decades. The significance and practicality of nanofluid have piqued researchers' interests in both numerical and experimental research. Williamson fluid is introduced to be a shear thinning non-Newtonian fluid, initially introduced by Williamson. Waqas *et al.* [32] examined the heat generation and absorption for a Williamson fluid flowing due to a stretching surface with modified Fick's and Fourier idea and the occurrence of mixed/forced nonlinear convection alters the flow. Ali *et al*. [33] studied the application of PEST and PEHF (two conditions of heat) in magnetohydrodynamic Williamson nanofluid flow in accordance with suction/injection. Yusuf *et al*. [34] investigated the impact of magnetic field on a Williamson fluid flow over a porous material in the presence of heat source that was not uniform, thermal radiation and chemical process. Nazir *et al*. [35] considered the work on mass and energy transfer for Williamson fluid by considering non-Fourier model. It is assumed that the Williamson fluid exhibits thermal relaxation behavior, which causes the fluid to avoid thermal changes in order to preserve its thermal equilibrium. Srinivasulu *et al*. [36] examined outcomes of magnetohydrodynamics applied at an angle on Williamson nanofluid flow while heat transfer and mass transfer for an extending sheet was studied. In a nonlinear stretching plate, Williamson fluid was examined by Dawar *et al*. [37]. In addition, they also considered the characteristics of activation energy. Habib *et al*. [38] focused on comparing the results obtained by the flow of micropolar, Maxwell, Williamson and Newtonian fluids over stretching surfaces. The comparison was done in the presence of magnetic field and double diffusion. Loganathan *et al.* [39] analyzed how nanoparticles suspended in Williamson

fluid can increase the speed of mass transfer and thermal conductivity for a vertical surface. Patil *et al*. [40] evaluated the mixed as well as bio-convection in a Williamson flow that has liquid oxygen diffusion. Sharma *et al*. [41] reviewed the results of chemical process and heat radiation for the flow of Williamson nanofluid over a linearly extending sheet. The irregular unsteady fluid flow and transmission of heat across a non-Newtonian fluid subjected to elongating surface was analyzed by Reddy and Machireddy [42]. Reddy *et al*. [43] employed the Cattaneo-Christov model including MHD and radiation for Williamson fluid flow for a surface that has pores and this examination was done in the presence of chemical interaction and suction/injection. Sulochana and Belagumpi [44] examined the time-independent magnetohydrodynamic Williamson fluid's thermal transfer properties past a surface in the existence of a chemical equilibrium process. Song and Ying [45] explored the unsteady magneto-Williamson mixed convection flow brought by extended container with substantial irregular heat source/sink properties.

Mixed convection is the most prevalent type of convection, which happens when both forced and natural convection are taking place at the same time. Due of its numerous astonishing and contemporary uses, this work has drawn many scholars. Hussain and Malik [46] worked on gyrostatic swimming bacteria movement within a nanoliquid flowing above a stretching cylinder in the existence of magnetohydrodynamics and mixed convection. Using the Runge-Kutta-Fehlberg (R-K-F) method, the governing equations' numerical solution was obtained. Zhang *et al.* [47] looked into the implications of Joule heating, convection as well as mass repulsion in a two-dimensional magnetohydrodynamics flow of a tiny liquid its stagnation point, flowing over a curved elastic surface that can be stretched or contracted. Ali and Bagh [48] investigated the bio convection nanofluid flow for a rotating sphere near a stagnation area. Arafa *et al.* [49] studied nanofluidic peristaltic motion across a porous media. It was simulated using the non-homogeneous nanofluid model and studied how the mixture's characteristics and behavior with respect to the size and form of the nanoparticles changes. Sharada *et al.* [50] evaluated the outcome of magnetism, Dufour and Soret impacts on the flow of a fluid that is non-Newtonian viscoelastic liquid. Arshad *et al*. [51] analyzed the motion of fluid and mass and heat transfer occurring on a porous, flat surface during the presence of mixed convection and magnetic field. Haq *et al*. [52] explored the mixed convection flow of nanofluid over an inclined uneven area with the consideration of heat source and chemical process. Hameezah *et al*. [53] observed the various boundary conditions for

the CNT-water nanofluid combined convection and entropy formation. Using Buongiorno's model, Safdar *et al*. [54] examined radiating Maxwell nanofluid flow under mixed convection phenomenon. While buoyancy forces work in bio convection, the concept of the microbe was employed to stabilize the suspended nanoparticles. Sudarsana and Sreedevi [55] took into account chemical reaction process, radiation, induced electric field, solid-state stratification and the liquid was incorporated in a porous media when analyzing the nanofluid flow across a stretched surface. Almaneea and Abdulmajeed [56] analyzed nanofluid flow and homogeneous/heterogeneous chemical reactions affecting the flow. The fluid flowing was also impacted by the phenomenon of mixed convection.

Magnetohydrodynamics (MHD) may regulate fluid flow and enhance heat analysis in the presence of electrically conductive fluids. Thus, MHD flow research is crucial for engineering and industry applications. Salawu *et al.* [57] scrutinized the results of mass and heat transport for the flow of a Maxwell nanofluid having variable properties. The Arrhenius pre-exponential kinetics were used to create the species molecular mixture and the Non-Newtonian fluid was described using the Maxwell theory. Zhou *et al.* [58] evaluated the unstable Casson fluid flow above a dimensionally stable surface close to a stagnation point. The flow model also incorporated effects of an irregular heat source, thermal radiation, MHD and slipping. Adigun *et al*. [59] discussed influence of magnetohydrodynamics on the flow of viscoelastic nanofluid. The nanofluid was flowing towards an inclined cylinder which was stretching linearly and effects of stagnation point were also examined. Warke *et al.* [60] studied on steady, magnetohydrodynamic flow of a micro polar liquid in two dimensions under the appearance of chemical reaction process and heat sink/source. Yahya *et al.* [61] investigated thermal transport of a hybrid fluid considering the existence of magnetic field, heat source and thermal dissipation above a penetrable surface. The results of employing catalyst and viscosity dielectric breakdown on electrically conducting nanofluid flowing over sustained porous sheet were evaluated by Gopal *et al.* [62]. Brownian motion and diffusion due to thermophoresis were also considered with the Buon-giorno fluid model. For the magnetohydrodynamics (MHD) and stagnation point theory, Hayat *et al.* [63] inspected the movement of Jeffrey's liquid towards a surface that stretches nonlinearly and has suitable surface roughness. The properties of heat transfer were investigated using melting effect, viscous dissipation and internal heat generation. A magnetic flux that is not uniform was taken

into account. Megahed *et al*. [64] inspected variable fluid properties during modeling of unstable flowing fluid over a surface. Additionally, they reviewed the effects of injection/suction in the considered stream. Vinodkumar *et al.* [65] used this concept and explored results for a convection flow in MHD Maxwell nanofluid flow using a flexible stretched sheet and the Cattaneo-Christov flux model. Heat and mass transmission were brought into consideration during the study. Abdelmalek *et al.* [66] discussed Buon-giorno nano-model due to the existence of mass and heat transfer for MHD and Prandtl-Eyring flowing nanofluid. Biswas and Rajib [67] analyzed the conduct of a 2-dimensional Maxwell nanofluid flowing because of a stretched surface in studied Brownian motion involving magnetohydrodynamics (MHD). Bejawada *et al.* [68] assessed the results of a heat source, chemical reaction and radiation for the flow of MHD Casson flowing fluid through an inclined nonlinear stretched surface.

Viscous dissipation is the terminology used to describe the unchangeable process through which work is performed by the fluid between its adjacent layers after the application of shear force and results in heat generation. Hamid and Amair [69] examined the remarkable benefits of nonlinear thermal radiation, heat source and sink for Casson nanofluid flow past a vertical thin needle with the consideration of ohmic-viscous dissipation. A non-linear shrinking sheet was involved for the stability analysis of a Cu-Al2O3/water hybrid nanofluid and this was investigated by Lund et al. [70]. To create a Cu-Al2O3/water hybrid nanofluid, the nanomaterials were added to the resulting water-soluble (basic fluid) while Cu and Al2O3 make up the hybrid nanomaterial. Chu *et al*. [71] studied the important role of viscous dissipation and magneto-hydrodynamics for a cross or secondary flow. For particular values of dimensionless parameter, dual solutions were produced. Aziz with Asim [72] analyzed the significance of viscous dissipation with linear radiant energy for the entropy assessment of Powell-Eyring hybrid nanofluid. The fluid is flowing and heat transfer is performed via convection with the volumetric entropy production. Abbas and Munawwar [73] analyzed the micro polar fluid with entropy generation study and the flow was considered above a surface that was being stretched and was affected by thermal radiation, viscous dissipation as well as the magnetic field. The inconsistent mixed convection of a chemically reactive and radiating nanofluid was examined by Rikitu *et al.* [74]. The fluid's varying characteristics in a porous medium were also a part of the study. Saeed and Anwa [75] studied the influences of chemical reaction, Joule heating, viscous dissipation and thermal radiation in

correspondence with the Casson fluid flowing owing to a stretchable surface. Nandi and Kumbhakar [76] looked into the magnetohydrodynamic flow for tangent hyperbolic nanofluid due to a stretching wedge and focused on convective heating and Navier's velocity boundary slip. The results of radiation and viscous dissipation on MHD free convective mass and heat transfer of an incompressible, viscous fluid flow via a stretched surface was found by Navivela *et al*. [77]. The numerical computation of cross-flow of a non-Newtonian fluid flow is the focus of Hussian *et al.* [78] research. They considered a homogeneous channel with porous walls on and studied flow dynamics. Tangent-Hyperbolic fluid flow in two dimensions has been considered in presence of regard to magnetic fields that act transversely. According to research, the chemical and mechanical industries usually deal with various types of highly viscous flows that can efficiently use porous walls and channels that are slippery. Khan *et al*. [79] examined the important aspect of friction drag for heat generation and viscous dissipation the study was done for fluid flow and heat transmission.

Heat generation or absorption phenomenon is common in numerous engineering and industrial uses. Chen [80] has looked into the problem related to heat transfer with mixed convective fluid flowing with the consideration of heat generation and also absorption and considered stretched surface with thermal radiation. The flow analysis and heat transfer mechanism of a fluid flow with carbon nanotubes in an asymmetric framework with flexible walls was explored statistically by Ahmed *et al*. [81] with the existence of heat generation/absorption. Additionally, a number of researchers have looked into a variety of phenomenon, including diverse geometries, with expanding and contracting surfaces for nanofluids. Temperature changes across boundaries requires the heat transfer process. In relation to this. Nuwairan *et al*. [82] studied the behavior of nanofluid under the consideration of a magnetic field while taking heat generation /absorption into account. The task employed the Lattice Boltzmann technique to investigate the heat transport through natural convection in a two-dimensional container filled with a nanofluid and three different wall shapes were analyzed. Walters' B fluid flow due to porous material under the effects of thermal radiation, heat prodution and also absorption was investigated by B. Johnson and Olajuwon [83] they concluded the consequences arising from the factors of thermal diffusion, radiation and chemical reaction. Yaseen *et al*. [84] conducted research on the significance of nanofluid flow between two alike permeable plates with the existence of heat absorption and

generation process. Eid *et al*. [85] examined the flow and heat transmission caused by a sheet stretching in an exponential manner and two nanoparticles were added to the considered fluid and heat generation was also an important part of the study. Yesodha *et al*. [86] analyzed the flow of a nanofluid in three dimensions past a stretched sheet. The nanofluid velocity decreases as the stretching sheet becomes porous, while both of the temperature as well as the concentration increase simultaneously. Shah *et al*. [87] studied the CuO-water nanofluid flow with mixed convection and heat generation/absorption. The adiabatic obstructions cold and heated surfaces were considered. Because of its prominence in physical features of the flow, the heat generation or absorption was examined for Casson nanofluid and the results were studied by Gajbhiye *et al.* [88]. Considerations were done for the constant, laminar, electromagnetic flow of Casson nanofluid over parallel plates under the impact of Hall current, chemical reactions and also Joule heating.

Chemical reactions are a fundamental component of technology, society and life itself. In view of this, Khan *et al*. [89] viewed the thermo physical aspects of higher-order chemical reaction and viscous dissipation for nanofluid flow while also taking a continually extending porous sheet into consideration. The flow model involved a porous medium and assumed laminar, time-invariant, MHD, incompressible Newtonian nanofluid with two spatial coordinates. The flow of Walter-B nanofluid with chemical reactions, non-linear thermal radiation and stationary point region was investigated by Khan *et al.* [90]. Brownian and thermophoresis motion consequences were used to investigate the properties of nanofluid. Fluid conducts electricity when a uniform magnetic field was present. Furthermore, the impacts of Joule heating and activation energy were used to study the phenomenon of mass and also heat transfer. Uddin *et al.* [91] analyzed the MHD and chemically reacting flow of Prandtl-Eyring nanofluid with the involvement of enthalpy change and heat transfer was also a part of the research. The improvement in heat transmission was studied by Punith *et al*. [92] by selecting a suitable ferromagnetic fluid or base fluid as an active liquid. In this regard, the flow was examined across a stretched flat sheet with pores and chemical reaction was taken into consideration. A third grade magnetohydrodynamic fluid flow model with the existence of chemical reactions and heat source or sink was explored by Raja *et al*. [93] using an Artificial Neural Network. Varun *et al.* [94] explored the role of chemical reactions and the magnetic field effect on the Casson nanoliquid flow across a curved stretching sheet. Furthermore,

Brownian motion, thermophoresis effects and exponential heat sources were used to examine the mass and heat transfer characteristics.

The above investigations lead to the conclusion that the phenomenon of mixed convection for Williamson nanofluid flowing across an exponentially porous stretched surface with mass suction, inclined magnetic field and heat absorption/generation has not been explored yet. Thus the main purpose here is to investigate the consequence of mixed convection on Williamson nanofluid flow over an exponentially stretchable sheet. The flow problem has been mathematically modelled keeping in view the basic laws of fluid mechanics and heat transmission. Application of suitable similarity transformations change the fluid model equations into a set of ODEs. The resulting system is then solved through homotopy analysis method. The results of the fluid flow and mass and heat transfer are graphically analyzed under the effects of different flow parameters. The findings are obtained for different physical flow parameters in terms of skin friction coefficient, velocity, local Nusselt number, temperature, concentration and the Sherwood number. The results of the current work are anticipated to be helpful for the future studies to advance the development in the scientific and technical sectors.

# Chapter 3

# Preliminaries

The current chapter includes certain relevant definitions and important fundamental laws for analysis of next chapters.

## 3.1 Fluid [97]

Fluid is a material that deforms continuously when an external force is applied. Examples of fluids are liquid, gasses and plasmas.

## 3.2 Fluid Mechanics [97]

Fluid mechanics studies the nature and characteristics of fluids both in motion and at rest. It consist of two dominant branches.

### 3.2.1 Fluid statics [97]

It comprises of the study related to behavior of fluid's particles at rest.

### 3.2.2 Fluid dynamics [97]

It includes the study on behavior of fluid's particles in motion.

## 3.3 Stress [98]

It is illustrated as the average force per unit of a body's surface area on which various forces act.

$$\text{Stress} = \frac{\text{Force}}{\text{Area}}. \tag{3.1}$$

It is measured in $Nm^{-2}$ or $kg/m.s^2$ in SI system and has dimensions $\left[\frac{M}{LT^2}\right]$. Stress consist of two parts.

### 3.3.1 Shear Stress [98]

It is referred to as a force that tends to cause a material to slip across a plane and is applied parallel to the considered material's cross-section.

### 3.3.2 Normal Stress [98]

It is noted to be a form of stress when a force is assumed to work normally on the cross section of the considered material.

## 3.4 Strain [98]

If a force is acted upon a considered material, then strain is expressed as a measurement of the relative deformation that occurs. It is a non-dimensional property of the fluid.

## 3.5 Viscosity [98]

Viscosity is a physical trait of fluids associated with the shear deformation of fluid's particles exposed to applied forces. Viscosity can be described in two ways which are as follows:

### 3.5.1 Dynamic Viscosity [98]

A measure of the proportion of shear stress to velocity slope is termed as dynamic viscosity or absolute viscosity $(\mu)$ and

$$\mu = \frac{\text{Shear stress}}{\text{Velocity gradient}}. \tag{3.2}$$

The dynamic viscosity is measured in $Ns/m^2$ or $kg/m.s$ (SI-System) and the related dimensions are noted to be $\left[\frac{M}{LT}\right]$.

### 3.5.2 Kinematic Viscosity [97]

The relation between absolute viscosity and density can be expressed by kinematic viscosity $(\nu)$. Mathematically, it is written as:

$$\nu = \frac{\mu}{\rho}. \tag{3.3}$$

It has units of $m^2/s$ and the dimensions are $\left[\frac{L^2}{T}\right]$.

## 3.6 Newton's Law of Viscosity [98]

It is demonstrated as the application of shear stress on a fluid, leads to directly proportional relation of stress and velocity gradient. Newton's law of viscosity is mathematically written as

$$\tau_{yx} \propto \frac{du}{dy}, \tag{3.4}$$

$$\tau_{yx} = \mu \frac{du}{dy}, \tag{3.5}$$

where $\tau_{yx}$ represents shear stress applied on the fluid element and $\mu$ is proportionality constant.

## 3.7 Newtonian Fluids [98]

Newtonian fluids are those that adhere to Newton's viscosity law i.e., there is a linear relation between velocity gradients and shear stress $\tau_{yx}$ . Examples of Newtonian fluids include water, air and alcohol etc.

## 3.8 Non-Newtonian Fluids [98]

The kind of fluids which signifies a nonlinear connection between shear stress and strain rate or those fluids that are not in accordance with Newton's law of viscosity are noted to be Non-Newtonian fluids

$$\tau_{yx} \propto \left(\frac{du}{dy}\right)^n, \quad n \neq 1, \tag{3.6}$$

$$\tau_{yx} = k(\frac{du}{dy})^n. \tag{3.7}$$

Above equation is reduced to Newton's law of viscosity with respect to $n = 1$ and $k = \eta$

$$\tau_{yx} = \eta(\frac{du}{dy}), \tag{3.8}$$

$$\eta = k(\frac{du}{dy})^{n-1}, \tag{3.9}$$

where $\eta$ is denoted for apparent viscosity, $k$ is symbolized for consistency index and $n$ is indicated for flow behavior index. Toothpaste, blood and ketchup are some examples of non-Newtonian fluids.

## 3.9 Nanofluids [98]

Nanofluids are a special kind of fluid which consist of nanometer-sized particles involving base fluid. Nanoparticles include metals, non-metals and metal carbides etc. Base fluid include

water, oil and other lubricants. Nanofluids are used in cosmetics, heat exchangers, electronic cooling system etc.

## 3.10 Williamson Nanofluid [98]

Williamson fluid is introduced as a shear thinning fluid that is non-Newtonian. It has wide range of implementations, particularly in the performance of pseudoplastic fluid, which is extensively used for industrial purposes.

The tensor $\vec{S}$ for our considered fluid is indicated as Nadeem *et al*. [95].

$$\vec{S} = -p\vec{I} + \vec{\tau}, \tag{3.10}$$

and

$$\vec{\tau} = [\mu_{\infty} + \frac{(\mu_0 - \mu_{\infty})}{1 - \Gamma\dot{\gamma}}]A_1, \tag{3.11}$$

in which $\tau$ stand for extra stress tensor, $\mu_0$ and $\mu_{\infty}$ for limiting viscosity at zero shear rate and infinite shear rate, $\Gamma > 0$ for time constant, $A_1$ represent first Rivlin-Erickson tensor and $\dot{\gamma}$ is define as

$$\dot{\gamma} = \sqrt{\frac{1}{2}\pi}, \tag{3.12}$$

$$\pi = trace(A_1^2), \tag{3.13}$$

The tensor reduces to

$$\tau = \mu_0[1 + \Gamma\dot{\gamma}]^{-1}A_1, \tag{3.14}$$

## 3.11 Flow [98]

There are different types of flow discussed as:

### 3.11.1 Compressible Flow [98]

A flow in which the fluid's density keeps on changing with the flow is indicated as compressible flow.

### 3.11.2 Incompressible Flow [98]

A flow in which the subsequent fluid's density does not vary throughout the flow corresponds to incompressible flow.

### 3.11.3 Turbulent Flow [98]

If each liquid particle does not follow a clear path and the path of one particle crosses the other particle's path, then it is termed as turbulent flow.

### 3.11.4 Laminar Flow [98]

This flow is observed if liquid particles travels in regular paths under no interference among them.

### 3.11.5 Unsteady Flow [98]

An unsteady flow is expressed as a flow through which amount of liquid flowing per second changes. i.e., for any studied fluid property $\Omega$, we can see the following relation

$$\frac{\partial \Omega}{\partial t} \neq 0. \tag{3.15}$$

### 3.11.6 Steady Flow [98]

A steady flow is the one for which the flow rate of the liquid through any section is observed to be constant, i.e., if any fluid property is denoted by $\Omega$, then

$$\frac{\partial \Omega}{\partial t} = 0. \tag{3.16}$$

## 3.12 Methods of Heat Transfer [99]

There are three significant forms of heat transfer from one position to another.

### 3.12.1 Conduction [99]

It describes a mechanism of heat transfer which studies heat flows from hot to cold body due to collision of molecules or atoms in solids and liquids which are in contact. Mathematically it can be expressed as

$$\tilde{q} = -k \times \nabla T. \tag{3.17}$$

In above representation, negative sign represents that heat is transferred from higher to lower temperature, $\tilde{q}$ denotes local heat flux density, $A$ is surface area, $k$ represents thermal conductivity and $\nabla T$ indicates temperature gradient.

### 3.12.2 Convection [99]

Convection is a heat transfer mechanism in which heat is transferred from a hot to a cold region, owing to the fluid's particles movement this method of heat transfer is known as convection. In mathematics,

$$Q = h \times A \times \nabla T, \tag{3.18}$$

where $h$ is coefficient of convective heat transfer, $A$ is a surface area and $\nabla T$ is temperature gradient.

#### 3.12.2.1 Forced Convection [99]

Forced convection is a different type of heat transfer during which the heat is conducted owing to an external force. Examples are air conditioners, fans and pumps etc.

#### 3.12.2.2 Natural Convection [99]

As the internal temperature of the fluid changes, so does the density in the gravitational field. Buoyancy forces cause natural convection or free convection due to density fluctuations. Examples of natural convection is the rise of warm air, sea breeze and land breeze etc.

#### 3.12.2.3 Mixed Convection [99]

Mixed convection is the most common type of convection, which occurs when both forced and natural convection occur simultaneously. This results from the interaction between buoyancy and external forces. The technique of mixed convection is used in various technical devices.

### 3.12.3 Radiation [99]

Radiation is the movement of heat energy as waves or particles through a material medium. Sunlight or heat from the sun, microwaves from an oven and X-rays from an X-ray tube are few related examples.

## 3.13 Thermal Conductivity [99]

The ability of a thing to transmit heat is referred as thermal conductivity. Mathematically,

$$\text{Thermal conductivity} = \frac{\text{distance} \times \text{heat}}{\text{temperature gradient} \times \text{area}}, \tag{3.19}$$

so

$$k = \frac{Q \times L}{A \times \Delta T}, \tag{3.20}$$

where $A$ is denoted for the cross-sectional area, $k$ for designated as thermal conductivity, $Q$ for typified for the heat flow per unit time and $\Delta T$ for temperature difference.

The SI unit for thermal conductivity is written as $W/m.K$ or $kg.m/s^3.K$ and have dimensions $\left[\frac{ML}{T^3\theta}\right]$.

## 3.14 Thermal Diffusivity [99]

Thermal diffusivity is the relationship between heat conduction and the product of density and specific heat. Mathematically, we have

$$\alpha = \frac{k}{\rho c_p}, \tag{3.21}$$

where $k$ is characterized as thermal conductivity, $\rho$ represents density and $c_p$ symbolizes specific heat capacity. SI system provides $m^2 / s$ as its units and $\left[\frac{L^2}{T}\right]$ are its dimensions.

## 3.15 Viscous Dissipation [101]

The energy produced by the fluid's motion during a viscous fluid flow is captured by its viscosity and transformed into its internal energy and this phenomenon is known as viscous dissipation. It is a permanent process and helps in lifting the fluid's temperature.

## 3.16 Magnetohydrodynamics (MHD) [101]

Magnetohydrodynamics analyzes the motion corresponding to electrically conducting fluid with in a magnetic field. In MHD, magnetic fields and fluids that conduct electricity are involved. The phrase "magneto hydro-dynamics" (MHD) relates to the phrase "magneto" refering to a magnetic field, "hydro" meaning liquid and "dynamics" referring to motion. Examples of electrically conducting fluids are rain water, salt solution, liquid soap etc.

## 3.17 Permeability [101]

Permeability can be expressed as an intensity of spongy substance that allows liquids to travel through it. Large pores in surfaces make them highly permeable.

## 3.18 Dimensionless numbers [101]

### 3.18.1 Reynolds Number [101]

The relationship between inertial and viscous forces can be described through Reynolds number.

We have

$$\mathrm{Re} = \frac{\text{Inertial force}}{\text{Viscous force}}, \tag{3.22}$$

i.e.

$$\mathrm{Re} = \frac{\rho v^2 L^2}{\mu v L} = \frac{vL}{\upsilon}. \tag{3.23}$$

Here $\rho$ is noted for density, $v$ for mean velocity, $L$ for characteristic length, $\mu$ for dynamic viscosity and $\upsilon$ for kinematic viscosity.

### 3.18.2 Prandtl Number [101]

The Prandtl number, which has no dimensions, measures the relationship between momentum diffusivity $(\nu)$ and heat diffusivity $(\alpha_1)$.

The formula for the Prandtl number in mathematics is

$$\mathrm{Pr} = \frac{\text{Viscous diffusion rate}}{\text{Thermal diffusion rate}}, \tag{3.24}$$

i.e.

$$\mathrm{Pr} = \frac{\upsilon}{\alpha_1} = \frac{c_p \mu}{k}, \tag{3.25}$$

where $\upsilon$ represents the kinematic viscosity, $\alpha_1$ is thermal diffusivity, $k$ represents thermal conductivity and $c_p$ shows the specific heat at constant pressure. Momentum diffusivity prevail

for $\Pr >> 1$ while influence of thermal diffusivity is seen for $\Pr << 1$ .

Prandtl number strongly affects the relationship between the respective closeness of momentum boundary layers and also thermal boundary layers. Higher Pr values indicate that the boundary layer for momentum is stronger than that of thermal boundary layer.

Prandtl number is crucial for free and as well as forced convection. For various fluids, the Prandtl number can have a broad range of values. It can range from 0.7 to 1 for gases, water has a Pr value between 1 and 10, and it ranges from 0.001 to 0.03 for liquid metals and from 50 to 2000 for oils.

### 3.18.3 Grashof Number [101]

It reflects the behavior of the buoyancy forces against the viscous forces in a flowing fluid. It is employed to establish the fluid boundary layer flow regime in laminar systems.

Mathematically, it can be written as

$$Gr = \frac{L^3}{\nu^2}\, g\beta(T - T_\infty), \tag{3.26}$$

where $\beta$ denotes volumetric thermal expansion coefficient, $g$ denotes acceleration due to gravity, $\nu$ denotes kinematic viscosity, $L$ denotes characteristic length, $T$ and $T_\infty$ are fluid and surrounding temperatures respectively.

### 3.18.4 Eckert Number [101]

The relationship of kinetic energy to enthalpy of the heat flow is referred to as the Eckert number.

Mathematically, it can be expressed as

$$Ec = \frac{\text{Kinetic energy}}{\text{Enthalpy}} = \frac{\text{v}^2}{c_p \Delta T}, \tag{3.27}$$

where $\upsilon$ is represented the fluid's velocity, $c_p$ for specific heat and $\Delta T$ for temperature difference.

If the Eckert number $(Ec << 1)$ is noticeably low, the part in the energy equation representing the

effect of Joule heating is usually omitted. To determine the viscous energy dissipation when the flow speed is low, the multiplication of the Eckert number and Prandtl number is utilized, i.e.

$$Ec.\Pr = \frac{\mu v^2}{k(\Delta T)}. \tag{3.28}$$

### 3.18.5 Nusselt Number [101]

Nusselt number is distinguished as dimensionless number and described to be the ratio of convective and conduction heat transfer at a fluid's boundary.
Mathematically, it can be expressed as

$$Nu_L = \frac{\text{Convective heat transfer}}{\text{Conductive heat transfer}}, \tag{3.29}$$

$$Nu_L = \frac{h^* \Delta T}{k\Delta T / l} = \frac{h^* l}{k}, \tag{3.30}$$

where $h^*$ represents coefficient of heat transfer, $l$ denotes characteristic length and $k$ shows the thermal conductivity.

### 3.18.6 Sherwood Number [101]

The Sherwood number which is also noted as mass transfer Nusselt number is an important dimensionless number and is readily seen in mass-transfer phenomenon. It is found to be the ratio of the convective mass transport to rate of diffusive mass transport. Mathematically, it is expressed as

$$Sh = \frac{h \times L}{D_B} = \frac{\text{Convective mass transfer rate}}{\text{Diffusion rate}}, \tag{3.31}$$

where $L$ is symbolized for characteristic length, $D_B$ for mass diffusivity while $h$ for convective mass transfer layer coefficient.

### 3.18.7 Skin Friction [101]

Skin friction is a type of friction that results from the relative motion of a solid's surface with in a fluid. Mathematically, it can be written as

$$C_f = \frac{2\tau_w}{\rho U^2}, \tag{3.32}$$

where $U$ signifies velocity, $\tau_w$ represents shear stress at the wall and $\rho$ is indicated for density. Skin friction is created by the drag that results from the viscous strains at the boundary layer. Compared to turbulent flow, the boundary layer is thinner in laminar flow, thus skin friction has a less impact. If an object is shaped in a way that promotes laminar flow, skin friction can be minimized.

## 3.19 Basic Equations [101]

### 3.19.1 Equation of Continuity [101]

The physical illustration of continuity equation, also named as law of mass conservation, indicates that net mass of the system is always conserved. Mathematically, it is noted to be:

$$\nabla.(\rho\vec{V}) + \frac{\partial\rho}{\partial t} = 0, \tag{3.33}$$

The density does not vary for incompressible fluids, so equation changes as

$$\nabla.\vec{V} = 0, \tag{3.34}$$

If two dimensional flow is talked about, then

$$\frac{\partial\tilde{u}}{\partial x} + \frac{\partial\tilde{v}}{\partial y} = 0, \tag{3.35}$$

and for three dimensional flow,

$$\frac{\partial \tilde{u}}{\partial x}+\frac{\partial \tilde{v}}{\partial y}+\frac{\partial \tilde{z}}{\partial z}=0. \tag{3.36}$$

The net flux of the system can be demonstrated through this law.

### 3.19.2 Momentum Equation [101]

This equation is physically related to law of conservation of momentum and therefore demonstrates that the total momentum of system will always be conserved. If incompressible fluid is taken into account, then the equation is written as:

$$\rho \frac{d\vec{V}}{dt} = div\,\boldsymbol{\tau} + \rho \vec{b}, \tag{3.37}$$

where $\rho$ represents density, $\vec{V}$ signifies velocity, $\boldsymbol{\tau}$ characterizes Cauchy stress tensor, $\mathrm{div}\,\boldsymbol{\tau}$ exhibits surface forces, $\rho\vec{b}$ means body force per unit volume and $\rho\frac{d\mathbf{V}}{dt}$ points towards inertial forces. The component form of momentum equation is as follows:

$x$ -component;

$$\rho[\frac{\partial \tilde{u}}{\partial t}+\tilde{u}\frac{\partial \tilde{u}}{\partial x}+\tilde{v}\frac{\partial \tilde{u}}{\partial y}+\tilde{w}\frac{\partial \tilde{u}}{\partial z}=-\frac{\partial p}{\partial x}+\frac{\partial}{\partial x}\left(\frac{2}{3}\mu\nabla.V-2\mu\frac{\partial \tilde{u}}{\partial x}\right)+\frac{\partial}{\partial y}[\mu\left(\frac{\partial \tilde{v}}{\partial x}+\frac{\partial \tilde{u}}{\partial y}\right)+\frac{\partial}{\partial y}[\mu\frac{\partial \tilde{u}}{\partial z}+\frac{\partial \tilde{w}}{\partial x}]\rho b_x \tag{3.38}$$

$y$ -component;

$$\rho[\frac{\partial \tilde{v}}{\partial t}+\tilde{u}\frac{\partial \tilde{v}}{\partial x}+\tilde{v}\frac{\partial \tilde{v}}{\partial y}+\tilde{w}\frac{\partial \tilde{v}}{\partial z}=-\frac{\partial p}{\partial x}+\frac{\partial}{\partial y}\left(\frac{2}{3}\mu\nabla.V-2\mu\frac{\partial \tilde{v}}{\partial y}\right)+\frac{\partial}{\partial x}[\mu\left(\frac{\partial \tilde{u}}{\partial y}+\frac{\partial \tilde{v}}{\partial x}\right)+\frac{\partial}{\partial z}[\mu\frac{\partial \tilde{v}}{\partial z}+\frac{\partial \tilde{w}}{\partial y}]\rho b_y \tag{3.39}$$

$z$ -component;

$$\rho[\frac{\partial \tilde{w}}{\partial t}+\tilde{u}\frac{\partial \tilde{w}}{\partial x}+\tilde{v}\frac{\partial \tilde{w}}{\partial y}+\tilde{w}\frac{\partial \tilde{w}}{\partial z}=-\frac{\partial p}{\partial x}+\frac{\partial}{\partial z}\left(\frac{2}{3}\mu\nabla.V-2\mu\frac{\partial w}{\partial z}\right)+\frac{\partial}{\partial y}[\mu\left(\frac{\partial \tilde{v}}{\partial z}+\frac{\partial \tilde{w}}{\partial y}\right)+\frac{\partial}{\partial x}[\mu\frac{\partial \tilde{u}}{\partial z}+\frac{\partial \tilde{w}}{\partial x}]\rho b_z \tag{3.40}$$

### 3.19.3 Energy Equation [101]

The energy equation is based on the conservation of the respective total energy. Mathematically,

$$(\rho c_p)\,\rho\frac{dT}{dt} = \text{div}\,\tilde{q}\,, \tag{3.41}$$

$$\tilde{q} = -\,k\,\nabla T\,, \tag{3.42}$$

where $\rho$ depicts density, $c_p$ symbolizes specific heat, $\tilde{q}$ identifies heat flux, $T$ indicates temperature and $k$ typifies thermal conductivity, $(\rho C_p)\frac{dT}{dt}$ is indicated for total internal energy and div $\tilde{q}$ for total heat flux.

### 3.19.2 Concentration Equation [101]

This equation physically means that concentration of the system is conserved and is derived from Fick's law. The equation in mathematical form is

$$\frac{dC}{dt} = D\,\nabla^2 C. \tag{3.43}$$

For two dimensional flow field;

$$\tilde{u}\frac{\partial C}{\partial x} + \tilde{v}\frac{\partial C}{\partial y} = D\left(\frac{\partial^2 C}{\partial x^2} + \frac{\partial^2 C}{\partial y^2}\right), \tag{3.44}$$

where $C$ is denoted to be the concentration and $D$ is noted for diffusion coefficient.

## 3.20 Homotopy analysis method [102]

The homotopy analysis technique (HAM) is a powerful tool for solving highly nonlinear differential equations analytically. Liao (1992) was the one who introduced this method and it was adopted by many researchers as it guarantees convergence of the desired solution and it provides a great freedom to choose initial guesses for the desired solution.

To illustrate method of homotopy analysis, consider the differential equation

$$N[w(x)] = 0, \tag{3.45}$$

where $N$ is denoted for a nonlinear operator, $w(x)$ represents unknown function and $x$ is denoted for the independent variable. The following is the Zeroth-order deformation equation

$$(1-r)\mathcal{L}\left[\widehat{w}(x;r) - w_0(x)\right] = r\hbar N\left[\widehat{w}(x;r)\right]. \tag{3.46}$$

Here $r$ is symbolized as embedding parameter with varying values from $0$ to $1$, $L$ is represented as auxiliary linear operator, $h$ is noted as nonzero auxiliary parameter, $w(x;r)$ is considered as unknown function and $w_\circ(x)$ stands for the initial approximation.

Equations corresponding to $r = 0$ and $r = 1$ are as follows

$$\widehat{w}(x;0) = w_0(x), \qquad \text{and} \qquad \widehat{w}(x;1) = w(x). \tag{3.47}$$

The solution $\widehat{w}(x;r)$ modifies from initial approximation $w_0(x)$ to the final solution $r(x)$ with the conversion of $r$ from $0$ to $1$. Taylor's series expansion leads to the following expressions

$$\widehat{w}(x;r) = w_0(x) + \sum_{n=1}^{\infty} w_n(x) r^n, \quad w_n(x) = \frac{1}{n!}\frac{\partial^n \widehat{w}(x;r)}{\partial r^n}\bigg|_{r=0}. \tag{3.48}$$

If $r = 1$, then

$$w(x) = w_0(x) + \sum_{n=1}^{\infty} w_n(x). \tag{3.49}$$

We obtain the following $n$th order deformation equation by differentiating $n$ times the Zeroth-

order deformation equation, with respect to $r$ , dividing the resulting equation by $n!$ and setting $r = 0,$ we get

$$\mathcal{L}[w_n(x) - \chi_n w_{n-1}(x)] = \hbar \mathcal{R}_n(x), \tag{3.50}$$

$$\mathcal{R}_n(x) = \frac{1}{(n-1)!} \frac{\partial^n N\left[\widehat{w}(x;r)\right]}{\partial r^n}\bigg|_{r=0}, \tag{3.51}$$

where

$$\chi_n = \begin{cases} 0, & n \leq 1 \\ 1, & n > 1 \end{cases}. \tag{3.52}$$

### 3.20.1 Example

Solve the differential equation

$$y' + y^2 = 1, \tag{3.53}$$

subject to the condition

$$y(0) = 0. \tag{3.54}$$

Assume that $y(x)$ can be expressed by

$$y(x) = \sum_{n=0}^{\infty} C_n e^{-nx}, \tag{3.55}$$

where $C_n$ is a coefficient.

Let

$$y_0(t) = 1 - e^{-x}. \tag{3.56}$$

Choosing the auxiliary linear operator

$$L_\phi = \frac{d\phi}{dx} + \phi \quad , \quad L = \frac{d}{dx} + 1, \tag{3.57}$$

as

$$L[y_m - \chi_m y_{m-1}] = hH[y_{m-1} + \textstyle\sum_{J=0}^{m-1} y_J \dot{y}_{m-1-J} - (1 - \chi_m)], \tag{3.58}$$

where

$$\chi_m = \begin{cases} 0 & , \quad m \leq 1 \\ 1 & , \text{otherwise} \end{cases} \tag{3.59}$$

put $m = 1$ in eq. (3.57 ) we get

$$y_1(x) = -\frac{h}{2}e^{-x} + he^{-2x} - \frac{h}{2}e^{-3x}. \tag{3.60}$$

For $m = 2$

$$y_2(x) = -\frac{h}{2}\left(1 + \frac{h}{2}\right)e^{-x} + h\left(1 + \frac{h}{2}\right)e^{-2x} - \frac{h}{2}(1 + h)e^{-3x} + \frac{h^2}{2}e^{-4x} - \frac{h^2}{4}e^{-5x}. \tag{3.61}$$

It is found that the corresponding *mth*-order approximation of $y(x)$ can be expressed by

$$y(x) \approx \sum_{n=0}^{2m+1} r_{m,n}(h)e^{-nx}, \tag{3.62}$$

where $r_{m,n}(h)$ is a coefficient dependent of *h*.

# Chapter 4

# The Magnetohydrodynamic Flow of Williamson Nanofluid over a Permeable Stretchable Sheet

## 4.1 Introduction

The incompressible, steady, two-dimensional and Williamson nanofluid flow owing to a stretching surface is analyzed. The surface is taken as porous and stretching exponentially. The influential elements of MHD and heat generation/absorption are also considered. The system of differential equations are rearranged as a system of less complicated differential equations by implementing pertinent similarity transformations. The solution of the obtained equations are derived by employing homotopy analysis method. The impact of consequential parameters for velocity, temperature and in addition concentration profiles are inspected graphically. Moreover, the conduct of skin friction coefficient, Nusselt number and Sherwood number is plotted for prominent parameters. The validity of the results is confirmed through a comparative study with the existing literature.

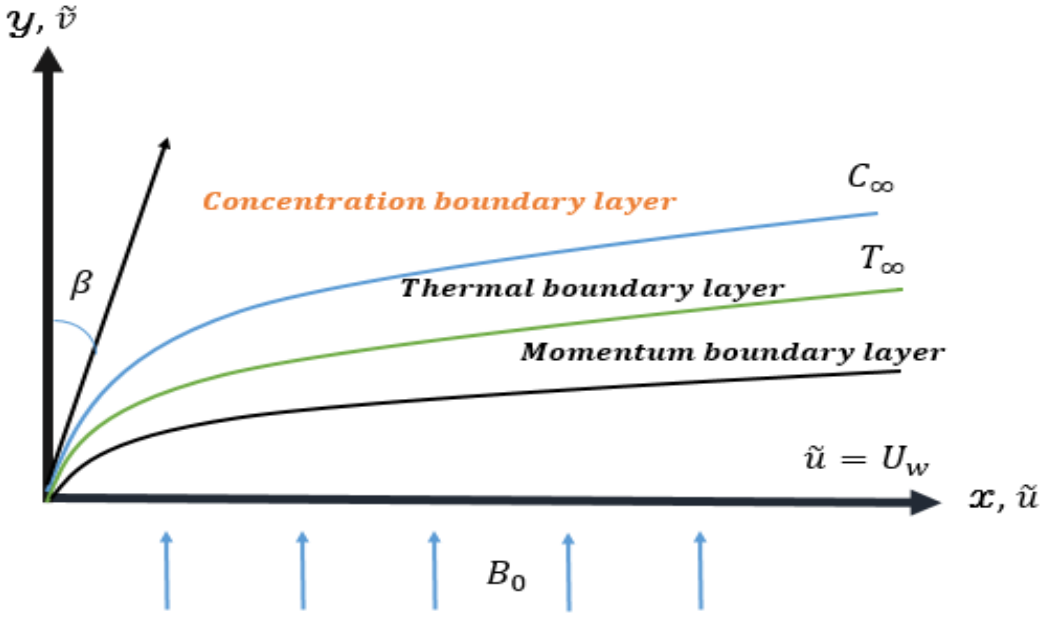


Fig. 4.1. Physical Model.

## 4.2 Mathematical construction of models

Let us inspect steady and two-dimensional flow based on Williamson nanofluid induced by a porous sheet. The sheet is believed to be stretching exponentially with a velocity $U_w$ directed along $x$-axis. An external magnetic field experiencing strength $B_0$ is applied at an angle $\beta$ to the surface. The assumed flow is further influenced due to the consideration of heat generation/absorption. The Cartesian coordinate system $(x, y)$ is the foundation for this system in which velocity field is expressed to be

$$\vec{v} = [\tilde{u}(x, y), \tilde{v}(x, y), 0]. \tag{4.1}$$

The continuity along with momentum and also energy equations Lie *et al*. [96] are observed as

$$\nabla . \vec{v} = 0, \tag{4.2}$$

$$\rho \frac{\partial \vec{v}}{dt} = \vec{\nabla}.\vec{S} + \vec{J} \times \vec{B} - \rho \vec{g}, \tag{4.3}$$

$$(\rho c_p)_f \frac{dT}{dt} = \vec{\nabla}.\left( k \ \vec{\nabla} T \right) + (\rho c_p)_p \left[ D_B \ \vec{\nabla} C.\vec{\nabla} T + \frac{D_T}{T_\infty} \left( \nabla T.\vec{\nabla} T \right) \right] + Q_0 (T - T_\infty), \tag{4.4}$$

$$\frac{dC}{dt} = \vec{\nabla}.\left( D_B \ \vec{\nabla} C + D_T \frac{\vec{\nabla} T}{T_\infty} \right), \tag{4.5}$$

where $\rho$ is noted for nanofluid density, $\vec{B}$ the total magnetic flux, $\vec{S}$ for stress tensor, $\vec{J}$ for electric current density, $\vec{g}$ for gravitational field, $(\rho c_p)_f$ and $(\rho c_p)_p$ for heat capacities of considered fluid and assumed nanoparticles respectively, $T$ for temperature, $D_B$ for Brownian diffusion coefficient, $C$ for nanoparticle volumetric fraction, $D_T$ for thermophoresis diffusion coefficient , $Q_0$ for heat generation coefficient and $T_\infty$ for ambient fluid temperature.

The tensor $\vec{S}$ for our considered fluid is indicated as Nadeem *et al*. [95].

$$\vec{S} = -p\vec{I} + \vec{\tau}, \tag{4.6}$$

and

$$\vec{\tau} = \left[ \mu_\infty + \frac{(\mu_0 - \mu_\infty)}{1 - \Gamma \dot{\gamma}} \right] A_1, \tag{4.7}$$

where $\tau$ is denoted for extra stress tensor, $\mu_0$ for limiting viscosity at zero shear rate and $\mu_\infty$ for limiting viscosity at infinite shear rate, $\Gamma > 0$ for time constant, $A_1$ for first Rivlin-Erickson tensor and $\dot{\gamma}$ is defined

$$\dot{\gamma} = \sqrt{\frac{1}{2}\pi}, \tag{4.8}$$

$$\pi = trace(A_1^2). \tag{4.9}$$

The tensor reduces to

$$\tau = \mu_0 [1 + \Gamma \dot{\gamma}]^{-1} A_1. \tag{4.10}$$

The component of extra stress tensor are

$$\begin{aligned} \tau_{xx} &= 2\mu_0[1+\Gamma\ \dot{\gamma}]\tfrac{\partial \tilde{u}}{\partial x}, \\ \tau_{xy} &= \tau_{yx} = 2\mu_0[1+\Gamma\ \dot{\gamma}](\tfrac{\partial \tilde{u}}{\partial y} + \tfrac{\partial \tilde{u}}{\partial x}), \\ \tau_{yy} &= 2\mu_0[1+\Gamma\ \dot{\gamma}]\tfrac{\partial \tilde{u}}{\partial y}, \end{aligned} \tag{4.11}$$

and $\tau_{xz} = \tau_{yz} = \tau_{zx} = \tau_{zy} = \tau_{zz} = 0$

Electromagnetic force is demonstrated when $\vec{\mathrm{E}} = 0$

$$\vec{\mathrm{J}} \times \vec{\mathrm{B}} = -\sigma B_{\circ}^{2} sin^2 \beta \tilde{u}, \tag{4.12}$$

where $B_0$ represents magnetic field in perpendicular direction to the surface and $\sigma$ epitomizes electrical conductivity.

Making use of above equation in $(4.2-4.5)$ and applying boundary layer assumptions, we get the equations given as below Lie *et al*. (2021):

$$\frac{\partial \tilde{u}}{\partial x} + \frac{\partial \tilde{v}}{\partial y} = 0, \tag{4.13}$$

$$\tilde{u}\,\frac{\partial \tilde{u}}{\partial x} + \tilde{v}\,\frac{\partial \tilde{u}}{\partial y} = \tilde{v}\,\frac{\partial^2 \tilde{u}}{\partial y^2} + \sqrt{2}\nu\,\Gamma\,\frac{\partial \tilde{u}}{\partial y}\frac{\partial^2 \tilde{u}}{\partial y^2} - \nu\,\frac{\tilde{u}}{k_1} - \frac{\sigma B_0^2}{\rho}\sin^2\beta\tilde{u}\,, \tag{4.14}$$

$$\tilde{u}\,\frac{\partial T}{\partial x} + \tilde{v}\,\frac{\partial T}{\partial y} = \alpha\,\frac{\partial^2 T}{\partial y^2} + \frac{Q_{\circ}}{(\rho C_p)_f}(T - T_{\infty}) + \frac{(\rho C_p)_p}{(\rho C_p)_f}\left[ D_B\,\frac{\partial T}{\partial y}.\frac{\partial C}{\partial y} + \frac{D_T}{T\infty}\left(\frac{\partial T}{\partial y}\right)^2 \right], \tag{4.15}$$

$$\tilde{u}\,\frac{\partial C}{\partial x} + \tilde{v}\,\frac{\partial C}{\partial y} = D_B\left(\frac{\partial^2 C}{\partial y^2}\right) + \frac{D_T}{T_{\infty}}\left(\frac{\partial^2 T}{\partial y^2}\right). \tag{4.16}$$

The boundary conditions for mentioned system are

$$\begin{aligned} &\tilde{u} = U_w = U_0 e^{\frac{x}{l}},\ \ v_w = -\delta(x); \\ &T = T_w,\ \ C = C_w \text{ at } y = 0, \end{aligned} \tag{4.17}$$

and for PEST and PEHF cases , the conditions given respectively as

$$T = T_w = T_{\infty} + (T_w - T_{\infty})\, e^{\frac{x}{2l}}\ at\ y = 0, \tag{4.18}$$

$$-k\left(\frac{\partial T}{\partial y}\right)_w = (T_w - T_{\infty})e^{\frac{x}{l}} \text{ at } y = 0, \tag{4.19}$$

and

$$\tilde{u} = u_e \to 0,\ T \to T_\infty, C \to C_\infty \text{ when } y \to \infty. \tag{4.20}$$

For the expressed equations, $u$ and $v$ are symbolized as the velocity components in the respective directions, $U_0$ as reference velocity, $\sigma$ as the electrical conductivity, $T_\infty$ as the ambient temperature, $\alpha$ as the thermal diffusivity, $k_1$ as the permeability of the porous medium, $\nu$ as kinematic viscosity, $C$ as concentration, $C_\infty$ as the ambient nanoparticle volume fraction, $Q_\circ$ as the heat generation coefficient.

Employing following similarity transformations

$$\begin{aligned} \tilde{u} &= U_0 e^{\frac{x}{l}} f'(\eta), \\ v_w &= -\sqrt{\frac{\nu U_\circ}{2l}} e^{\frac{x}{2l}} [(f(\eta) + \eta f'(\eta)], \\ \eta &= \sqrt{\frac{U_\circ}{2\nu l}} y e^{\frac{x}{2l}}. \end{aligned} \tag{4.21}$$

**Case for PEST:**

$$\begin{aligned} T &= T_\infty + (T_w - T_\infty) e^{\frac{x}{2l}} \theta(\eta), \\ h &= \frac{C - C_\infty}{C_w - C_\infty}. \end{aligned} \tag{4.22}$$

**Case for PEHF:**

$$\begin{aligned} T &= T_\infty + \frac{T_w - T_\infty}{k} e^{\frac{x}{2l}} \sqrt{\frac{2\nu l}{U_\circ}}\, \phi(\eta), \\ h &= \frac{C - C_\infty}{C_w - C_\infty}. \end{aligned} \tag{4.23}$$

Apply similarity transformations, Eq. $(4.13)$ is identically satisfied while equations $(4.14 - 4.16)$ becomes

$$f''' - 2(f')^2 + ff'' + \lambda f''' f'' - (K + M \sin^2 \beta) f' = 0. \tag{4.24}$$

**PEST case**

$$\theta'' + \Pr\left(f\theta' - f'\theta + N_b h'\theta' + N_t \theta'^2 + Q\theta\right) = 0, \tag{4.25}$$

$$h'' + Le\,\mathrm{Pr}(fh') + \frac{N_t}{N_b}\theta'' = 0 \tag{4.26}$$

**PEHF case**

$$\phi'' + \mathrm{Pr}\left(f\phi' - f'\phi + N_b h'\phi' + N_t \phi'^2 + Q\phi\right) = 0, \tag{4.27}$$

$$h'' + Le\,\mathrm{Pr}(fh') + \frac{N_t}{N_b}\phi'' = 0. \tag{4.28}$$

After the use of the same similarity transformations for the boundary conditions, we get

$$f(0) = v_w, \quad f'(0) = 1, \quad f'(\infty) = 0. \tag{4.29}$$

**PEST case**

$$\theta(0) = 1, \ \theta(\infty) = 0, \ h(0) = 1, \ h(\infty) = 0. \tag{4.30}$$

**PEHF case**

$$\phi'(0) = -1, \quad \phi(\infty) = 0, h(0) = 1, \ h(\infty) = 0 \ , \tag{4.31}$$

where $\lambda$ is denoted as Williamson parameter, $K$ as porosity parameter, $M$ as magnetic number, $\mathrm{Pr}$ as Prandtl number, $N_b$ and $N_t$ as the Brownian and thermophoresis motion parameter, $Q$ as the heat source/sink parameter and $Le$ as the Lewis number. These parameters are presented as

$$\begin{gathered} \lambda = \frac{\Gamma}{\sqrt{\nu l}} U_\circ^{3/2} e^{\frac{3x}{2l}}, \ M = \frac{2\sigma B_\circ^2 l}{\rho U_0} e^{-\frac{x}{l}}, \ K = \frac{2\nu l}{k_1 U_\circ} e^{-\frac{x}{l}}, \\ \mathrm{Pr} = \frac{\nu}{\alpha}, \ Q = \frac{Q_\circ}{(\rho C_p)_f} \frac{2l}{U_\circ} e^{-\frac{x}{l}}, \quad Le = \frac{\alpha}{D_B}, \\ N_t = \frac{D_T}{T_\infty} \frac{(\rho C_p)_p}{(\rho C_p)_f} \frac{(T_w - T_\infty)}{\nu} e^{\frac{x}{2l}}, \quad N_b = \frac{D_B}{\nu} \frac{(\rho C_p)_p}{(\rho C_p)_f} (C_w - C_\infty). \end{gathered} \tag{4.32}$$

Skin friction coefficient, local Nusselt number along with Sherwood number are given as

$$C_f = \frac{\tau_w}{\rho U_w^2}, \ \ Nu_x = \frac{x\,\tilde{q}_w}{k(T_w - T_\infty)}, \ \ Sh = \frac{x\tilde{q}_m}{D_B(C_w - C_\infty)}, \tag{4.33}$$

$$\tau_w = \mu\left[\frac{\partial \tilde{u}}{\partial y} + \frac{\Gamma}{\sqrt{2}}\left(\frac{\partial \tilde{u}}{\partial y}\right)^2\right]_{y=0}, \quad \tilde{q}_w = -k\left[\frac{\partial T}{\partial y}\right]_{y=0}, \quad \tilde{q}_m = -D_B\left[\frac{\partial C}{\partial y}\right]_{y=0},$$

Where $\tau_w$, $\tilde{q}_w$, $\tilde{q}_m$ are noted for local wall shear stress, local heat flux and mass flux respectively. Due to the similarity transformations, Eq. (4.33) attain the following forms

$$(2\,\mathrm{Re}_x)^{1/2} C_f = (f'' + \frac{\lambda}{2} f''^2)_{\eta=0}, \quad e^{-\frac{x}{2l}} (2\,\mathrm{Re}_x)^{-1/2} Nu = -\theta'(0), \tag{4.34}$$

$$e^{-\frac{x}{2l}} (2\,\mathrm{Re}_x)^{-1/2} Sh = -h'(0).$$

Where $\mathrm{Re} = \frac{U_0 x^2 e^{\frac{x}{l}}}{2\nu}$ is the key factor known to be Reynolds number.

## 4.3 Solutions through homotopy analysis method

The requisite initial guesses $(f_0, \theta_0, h_0)$ and associated linear operators ( $\mathcal{L}_f, \mathcal{L}_\theta, \mathcal{L}_h$) for the momentum, energy and also concentration equations can be adopted in the following way:

$$f_0(\eta) = 1 + v_w - \exp(-\eta), \quad \theta_0(\eta) = \exp(-\eta), \quad h_0(\eta) = \exp(-\eta), \tag{4.35}$$

$$\mathcal{L}_f(f) = \frac{d^3 f}{d\eta^3} - \frac{df}{d\eta}, \ \mathcal{L}_\theta(\theta) = \frac{d^2\theta}{d\eta^2} - \theta, \ \mathcal{L}_h(h) = \frac{d^2 h}{d\eta^2} - h, \tag{4.36}$$

and

$$\mathcal{L}_f \left[ a_1 + a_2 \exp(\eta) + a_3 \exp(-\eta) \right] = 0, \tag{4.37}$$

$$\mathcal{L}_\theta \left[ a_4 \exp(\eta) + a_5 \exp(-\eta) \right] = 0, \tag{4.48}$$

$$\mathcal{L}_h \left[ a_6 \exp(\eta) + a_7 \exp(-\eta) \right] = 0, \tag{4.39}$$

where $a_i$ $(i = 1-7)$ are indicated to be arbitrary constants. To further proceed, the deformation problems in line with the zeroth and nth ordered problems are expressed as:

### 4.3.1 Zeroth-order deformation problem (PEST case)

$$(1-r)\,\mathcal{L}_f\left[\hat{f}(\eta;r)-f_0(\eta)\right]=r\hbar_f\mathcal{N}_f\left[\hat{f}(\eta;r)\right], \tag{4.40}$$

$$(1-r)\,\mathcal{L}_\theta\left[\hat{\theta}(\eta;r)-\theta_0(\eta)\right]=r\hbar_\theta\mathcal{N}_\theta\left[\hat{f}(\eta;r),\hat{\theta}(\eta;r),\hat{h}(\eta;r)\right], \tag{4.41}$$

$$(1-r)\,\mathcal{L}_h\left[\hat{h}(\eta;r)-h_0(\eta)\right]=r\hbar_h\mathcal{N}_h\left[\hat{f}(\eta;r),\hat{\theta}(\eta;p),\hat{h}(\eta;r)\right], \tag{4.42}$$

$$\hat{f}(0;r)=v_w,\quad \frac{\partial\hat{f}}{\partial\eta}(0;r)=1,\qquad \frac{\partial\hat{f}}{\partial\eta}(\infty;r)=0, \tag{4.43}$$

$$\hat{\theta}(0;r)=1,\quad \hat{\theta}(\infty;r)=0, \tag{4.44}$$

$$\hat{h}(0;r)=1,\qquad \hat{h}(\infty;r)=0, \tag{4.45}$$

$$\mathcal{N}_f\left[\hat{f}(\eta,r)\right]=\left[\begin{array}{c}\frac{\partial^3\hat{f}(\eta;r)}{\partial\eta^3}-2\left(\frac{\partial\hat{f}(\eta;r)}{\partial\eta}\right)^2+\hat{f}(\eta;r)\frac{\partial^2\hat{f}(\eta;r)}{\partial\eta^2}+\lambda\frac{\partial^3\hat{f}(\eta;r)}{\partial\eta^3}\frac{\partial^2\hat{f}(\eta;r)}{\partial\eta^2}\\ -(K+M\sin^2\beta)\frac{\partial\hat{f}(\eta;r)}{\partial\eta}\end{array}\right], \tag{4.46}$$

$$\mathcal{N}_\theta\left[\hat{f}(\eta;p),\hat{\theta}(\eta;p),\hat{h}(\eta;p)\right]=\left[\begin{array}{c}\frac{\partial^2\hat{\theta}(\eta;p)}{\partial\eta^2}+\Pr\hat{f}(\eta;p)\frac{\partial\hat{\theta}(\eta;p)}{\partial\eta}\\ -\Pr\frac{\partial\hat{f}(\eta;p)}{\partial\eta}\hat{\theta}(\eta;p)+\Pr N_b\frac{\partial\hat{h}(\eta;p)}{\partial\eta}\frac{\partial\hat{\theta}(\eta;p)}{\partial\eta}\\ +\Pr N_t\left(\frac{\partial\hat{\theta}(\eta;p)}{\partial\eta}\right)^2+Q\frac{\partial\hat{\theta}(\eta;p)}{\partial\eta}\end{array}\right], \tag{4.47}$$

$$\mathcal{N}_h\left[\hat{f}(\eta;p),\hat{\theta}(\eta;p),\hat{h}(\eta;p)\right]=\left[\begin{array}{c}\frac{\partial^2\hat{h}(\eta;p)}{\partial\eta^2}+Le\Pr\hat{f}(\eta;p)\frac{\partial\hat{h}(\eta;p)}{\partial\eta}\\ +\frac{N_t}{N_b}\left(\frac{\partial^2\hat{\theta}(\eta;p)}{\partial\eta^2}\right),\end{array}\right], \tag{4.48}$$

in which, $r\in[0,1]$ is denoted for embedding parameter, $\hbar_f,\hbar_\theta$ and $\hbar_h$ for auxiliary parameters (non-zero) and $\mathcal{N}_f,\mathcal{N}_\theta,$and $\mathcal{N}_h,$ for nonlinear operators.

### 4.3.2 nth-order problem

$$\mathcal{L}_f\left[f_n(\eta)-\chi_n\, f_{n-1}(\eta)\right]=\hbar_f\mathcal{R}_n^f(\eta), \tag{4.49}$$

$$\mathcal{L}_\theta\left[\theta_n(\eta)-\chi_n\,\theta_{n-1}(\eta)\right]=\hbar_\theta\mathcal{R}_n^\theta(\eta), \tag{4.50}$$

$$\mathcal{L}_h\left[h_n(\eta)-\chi_n\, h_{n-1}(\eta)\right]=\hbar_h\mathcal{R}_n^h(\eta), \tag{4.51}$$

$$f_n(0)=f_n'(0)=f_n'(\infty)=0, \tag{4.52}$$

$$\theta_n(0)=\theta_n(\infty)=0, \tag{4.53}$$

$$h_n(0)=h_n(\infty)=0, \tag{4.54}$$

$$\mathcal{R}_n^f(\eta)=f_{n-1}'''(\eta)-\left[\begin{array}{c}\sum_{k=0}^{n-1}\left[2f'_{m-1-k}f'_k+f_{n-1-k}f''_k+\lambda f''_{n-1-k}f'''_k\right]\\ +(-K+M\sin^2\beta)f'_{n-1}\end{array}\right], \tag{4.55}$$

$$\mathbf{R}_n^\theta(\eta)=\theta''_{n-1}(\eta)+\Pr\sum_{k=0}^{n-1}\left[\begin{array}{c}\sum_{k=0}^{n-1}\left(f_{n-1-k}\theta'_k-f'_{n-1-k}\theta_k+N_b\theta'_{n-1-k}h'_k\right.\\ \left.+N_t\theta'_{n-1-k}\theta'_k\right)\end{array}\right]+\Pr Q\theta_{n-1}, \tag{4.56}$$

$$\mathcal{R}_n^h(\eta)=h''_{n-1}(\eta)+\sum_{k=0}^{n-1}[Le\Pr f_{n-1-k}h'_k]+\frac{N_t}{N_b}\theta''_{n-1}], \tag{4.57}$$

$$\chi_n=\begin{cases}0, & n\le 1,\\ 1, & n>1.\end{cases} \tag{4.58}$$

When $r=0$ and $r=1$ then,

$$\widehat{f}(\eta;0)=f_0(\eta),\quad \widehat{f}(\eta;1)=f(\eta), \tag{4.59}$$

$$\widehat{\theta}(\eta;0)=\theta_0(\eta),\quad \widehat{\theta}(\eta;1)=\theta(\eta), \tag{4.60}$$

$$\widehat{h}(\eta;0)=h_0(\eta),\quad \widehat{h}(\eta;1)=h(\eta). \tag{4.61}$$

As $r$ varies from 0 to 1, then $\widehat{f}(\eta;r)$, $\widehat{\theta}(\eta;r)$ and $\widehat{h}(\eta;r)$ change from the initial guesses

$f_0(\eta)$, $\theta_0(\eta)$ and $h_0(\eta)$ to last obtained results $f(\eta), \theta(\eta)$ and $h(\eta)$ respectively. Now expressing through Taylor series, the following expressions are achieved

$$\widehat{f}(\eta;r) = f_0(\eta) + \sum_{n=1}^{\infty} f_n(\eta) r^n, \quad f_n(\eta) = \frac{1}{n!} \frac{\partial^n \widehat{f}(\eta;r)}{\partial r^n}\bigg|_{r=0}, \tag{4.62}$$

$$\widehat{\theta}(\eta;r) = \theta_0(\eta) + \sum_{n=1}^{\infty} \theta_n(\eta) r^n, \quad \theta_n(\eta) = \frac{1}{n!} \frac{\partial^n \widehat{\theta}(\eta;r)}{\partial r^n}\bigg|_{r=0}, \tag{4.63}$$

$$\widehat{h}(\eta;r) = h_0(\eta) + \sum_{n=1}^{\infty} h_n(\eta) r^n, \quad h_n(\eta) = \frac{1}{n!} \frac{\partial^n \widehat{h}(\eta;r)}{\partial r^n}\bigg|_{r=0}. \tag{4.64}$$

Choosing the values of the auxiliary parameters in order to converge the series $(4.62-4.64)$ at $r=1$, we accomplish

$$f(\eta) = f_0(\eta) + \sum_{n=1}^{\infty} f_n(\eta), \tag{4.65}$$

$$\theta(\eta) = \theta_0(\eta) + \sum_{n=1}^{\infty} \theta_n(\eta), \tag{4.66}$$

$$h(\eta) = h_0(\eta) + \sum_{n=1}^{\infty} h_n(\eta). \tag{4.67}$$

The solutions $\left(f_n, \theta_{n,} h_n\right)$ of the respective Eqs. $(4.51-4.53)$ Involving special solutions $(f_n^{\star}, \theta_n^{\star}, h_n^{\star})$ is written down as

$$f_n(\eta) = f_n^{\star}(\eta) + a_1 + a_2 e^{\eta} + a_3 e^{-\eta}, \tag{4.68}$$

$$\theta_n(\eta) = \theta_n^{\star}(\eta) + a_4 e^{\eta} + a_5 e^{-\eta}, \tag{4.69}$$

$$h_n(\eta) = h_n^{\star}(\eta) + a_6 e^{\eta} + a_7 e^{-\eta}, \tag{4.70}$$

It is demonstrated that constants $a_i$ $(i=1-8)$ by means of boundary conditions $(4.52-4.54)$ are given by

$$a_2 = a_4 = a_6 = 0, \quad a_3 = \frac{\partial f_n^{\star}(\eta)}{\partial \eta}\bigg|_{\eta=0} - 1, \quad a_1 = v_w - a_3 - f_n^{\star}(0), \tag{4.71}$$

$$a_5 = 1 - \theta_n^{\star}(0), \ , \ a_7 = 1 - h_n^{*}(0).$$

### 4.3.3 Zeroth order problem (PEHF case)

$$(1-r)\,\mathcal{L}_f\left[\hat{f}(\eta;r)-f_0(\eta)\right]=r\hbar_f\mathcal{N}_f\left[\hat{f}(\eta;r)\right], \tag{4.72}$$

$$(1-r)\,\mathcal{L}_\phi\left[\hat{\phi}(\eta;r)-\phi_0(\eta)\right]=r\hbar_\phi\,\mathcal{N}_\phi\left[\hat{f}(\eta;r),\hat{\phi}(\eta;r),\hat{h}(\eta;r)\right], \tag{4.73}$$

$$(1-r)\,\mathcal{L}_h\left[\hat{h}(\eta;r)-h_0(\eta)\right]=r\hbar_h\,\mathcal{N}_h\left[\hat{f}(\eta;r),\hat{\phi}(\eta;r),\hat{h}(\eta;r)\right], \tag{4.74}$$

$$\hat{f}(0;r)=v_w,\quad \frac{\partial\hat{f}}{\partial\eta}(0;r)=1,\quad \frac{\partial\hat{f}}{\partial\eta}(\infty;r)=0, \tag{4.75}$$

$$\frac{\partial\hat{\phi}}{\partial\eta}(0;r)=-1,\quad \hat{\phi}(\infty;r)=0, \tag{4.76}$$

$$\hat{h}(0;r)=1,\quad \hat{h}(\infty;r)=0, \tag{4.77}$$

$$\mathcal{N}_f\left[\hat{f}(\eta,r)\right]=\left[\begin{array}{c}\frac{\partial^3\hat{f}(\eta;r)}{\partial\eta^3}-2\left(\frac{\partial\hat{f}(\eta;r)}{\partial\eta}\right)^2+\hat{f}(\eta;r)\frac{\partial^2\hat{f}(\eta;r)}{\partial\eta^2}+\lambda\frac{\partial^3\hat{f}(\eta;r)}{\partial\eta^3}\frac{\partial^2\hat{f}(\eta;r)}{\partial\eta^2}\\ -(K+M\sin^2\beta)\frac{\partial\hat{f}(\eta;r)}{\partial\eta}\end{array}\right], \tag{4.78}$$

$$\mathcal{N}_\phi\left[\hat{f}(\eta;r),\hat{\phi}(\eta,r),\hat{h}(\eta;r)\right]=\left[\begin{array}{c}\frac{\partial^2\hat{\phi}(\eta;r)}{\partial\eta^2}+\Pr\hat{f}(\eta;p)\frac{\partial\hat{\phi}(\eta;r)}{\partial\eta}-\Pr\frac{\partial\hat{f}(\eta;r)}{\partial\eta}\hat{\phi}(\eta;r)\\ +\Pr N_b\frac{\partial\hat{h}(\eta;r)}{\partial\eta}\frac{\partial\hat{\phi}(\eta;r)}{\partial\eta}+\Pr N_t\left(\frac{\partial\hat{\phi}(\eta;r)}{\partial\eta}\right)^2\\ +\Pr Q\hat{\phi}(\eta;r)\end{array}\right] \tag{4.79}$$

$$\mathcal{N}_h\left[\hat{f}(\eta;r),\hat{\phi}(\eta,r),\hat{h}(\eta,r)\right]=\frac{\partial^2\hat{h}(\eta;r)}{\partial\eta^2}+Le\Pr\hat{f}(\eta;r)\frac{\partial\hat{h}(\eta;r)}{\partial\eta}+\frac{N_t}{N_b}\frac{\partial^2\hat{\phi}(\eta;r)}{\partial\eta^2}\ , \tag{4.80}$$

where $r\in[0,1]$ is indicated as embedding parameter, $\hbar_f$, $\hbar_\theta$ and $\hbar_h$ as non-zero auxiliary parameters while $\mathcal{N}_f$, $\mathcal{N}_\phi$, and $\mathcal{N}_h$, are represented as nonlinear operators.

### 4.3.4 nth-order Problem

$$\mathcal{L}_f\left[f_n(\eta)-\chi_n\, f_{n-1}(\eta)\right]=\hbar_f\mathcal{R}_n^f(\eta), \tag{4.81}$$

$$\mathcal{L}_\phi\left[\phi_n(\eta)-\chi_n\, \phi_{n-1}(\eta)\right]=\hbar_\phi\mathcal{R}_n^\phi(\eta), \tag{4.82}$$

$$\mathcal{L}_h\left[h_n(\eta)-\chi_n\, h_{n-1}(\eta)\right]=h_h\mathcal{R}_n^h(\eta), \tag{4.83}$$

$$f_n(0)=f_n'(0)=f_n'(\infty)=0, \tag{4.84}$$

$$\phi_n(0)=\phi_n(\infty)=0, \tag{4.85}$$

$$h_n(0)=h_n(\infty)=0, \tag{4.86}$$

$$\mathcal{R}_n^f(\eta)=f_{n-1}'''(\eta)-\left[\begin{array}{c}\sum_{k=0}^{n-1}\left[2[f'_{n-1-k}f'_k]+[f_{n-1-k}f''_k\ ]+\lambda[f''_{n-1-k}f'''_k]\right]\\ +(-K+M\sin^2\beta)f'_{n-1}\end{array}\right], \tag{4.87}$$

$$\mathcal{R}_n^\phi(\eta)=\phi_{n-1}''(\eta)+\Pr\sum_{k=0}^{n-1}\left[\begin{array}{c}\sum_{k=0}^{n-1}f_{n-1-k}\phi'_k-f'_{n-1-k}\phi_k\ +N_b\phi'_{n-1-k}h'_k\\ +N_t\phi'_{n-1-k}\phi'_k\end{array}\right]+\Pr Q\phi_{n-1}, \tag{4.88}$$

$$\mathcal{R}_n^h(\eta)=h_{n-1}''(\eta)+\sum_{k=0}^{n-1}[Le\Pr f_{n-1-k}h'_k]+\frac{N_t}{N_b}\phi''_{n-1}, \tag{4.89}$$

$$\chi_n=\begin{cases}0, & n\le 1\\ 1, & n>1\end{cases}. \tag{4.90}$$

The equations associated with $r=0$ and $r=1$ are

$$\widehat{f}(\eta;0)=f_0(\eta),\quad \widehat{f}(\eta;1)=f(\eta), \tag{4.91}$$

$$\widehat{\phi}(\eta;0)=\phi_0(\eta),\quad \widehat{\phi}(\eta;1)=\phi(\eta), \tag{4.92}$$

$$\widehat{h}(\eta;0)=h_0(\eta),\quad \widehat{h}(\eta;1)=h(\eta). \tag{4.93}$$

As $r$ rises starting from $0$ to $1$, then $\widehat{f}(\eta;r)$, $\widehat{\phi}(\eta;r)$ and $\widehat{h}(\eta;r)$ modify from initial guesses $f_0(\eta)$, $\phi_0(\eta)$ and $h_0(\eta)$ to the ultimate solutions $f(\eta)$, $\phi(\eta)$ and $h(\eta)$ respectively. Now expanding in Taylor series keep in in mind, the parameter $r$ we reach at

$$\widehat{f}(\eta;r) = f_0(\eta) + \sum_{n=1}^{\infty} f_n(\eta) r^n, \quad f_n(\eta) = \frac{1}{n!} \frac{\partial^n \widehat{f}(\eta;r)}{\partial r^n}\bigg|_{r=0}, \tag{4.94}$$

$$\widehat{\phi}(\eta;r) = \phi_0(\eta) + \sum_{n=1}^{\infty} \phi_n(\eta) r^n, \quad \phi_n(\eta) = \frac{1}{n!} \frac{\partial^n \widehat{\phi}(\eta;r)}{\partial r^n}\bigg|_{r=0}, \tag{4.95}$$

$$\widehat{h}(\eta;r) = h_0(\eta) + \sum_{n=1}^{\infty} h_n(\eta) r^n, \quad h_n(\eta) = \frac{1}{n!} \frac{\partial^n \widehat{h}(\eta;r)}{\partial r^n}\bigg|_{r=0}. \tag{4.96}$$

The series $(4.94-4.96)$ converges at $r=1$ for the correct choice of the auxiliary parameters and

$$f(\eta) = f_0(\eta) + \sum_{n=1}^{\infty} f_n(\eta), \tag{4.97}$$

$$\phi(\eta) = \phi_0(\eta) + \sum_{n=1}^{\infty} \phi_n(\eta), \tag{4.98}$$

$$h(\eta) = h_0(\eta) + \sum_{n=1}^{\infty} h_n(\eta), \tag{4.99}$$

The required solutions $\left(f_n, \phi_{n,} h_n\right)$ of the Eqs. $(4.81-4.83)$ is demonstrated as

$$f_n(\eta) = f_n^{\star}(\eta) + a_8 + a_9 e^{\eta} + a_{10} e^{-\eta}, \tag{4.100}$$

$$\phi_n(\eta) = \phi_n^{\star}(\eta) + a_{11} e^{\eta} + a_{12} e^{-\eta}, \tag{4.101}$$

$$h_n(\eta) = h_n^{\star}(\eta) + a_{13} e^{\eta} + a_{14} e^{-\eta}, \tag{4.102}$$

in which the constants $a_i \ (i = 8-14)$ through the boundary conditions $(4.84-4.86)$ are given by

$$b_9 = b_{11} = b_{13} = 0, \quad b_{10} = \frac{\partial f_n^{\star}(\eta)}{\partial \eta}\bigg|_{\eta=0} - 1, \quad b_8 = v_w - b_{10} - f_n^{\star}(0), \tag{4.103}$$

$$b_{12} = 1 + \frac{\partial \phi_n^{\star}(\eta)}{\partial \eta}\bigg|_{\eta=0}, \quad b_{14} = 1 - h_n^{*}(0).$$

## 4.4 Solution Analysis

### 4.4.1 Convergence Discussion

In the methodology, the convergence region is plotted to find solutions of the corresponding momentum, energy and also concentration equations. In addition, befitting values of auxiliary parameters $\hbar$ are obtained by finding convergence region and constructing $\hbar$-curves for the needed solution. These $\hbar$-curves are shown in the Figs. 4.2 & 4.3. The required ranges of the auxiliary parameters $\hbar$ are as follow.

Convergence region for **PEST case**

$$-0.93 \le \hbar_f \le -0.2, \quad -0.98 \le \hbar_\theta \le -0.15, \quad -1 \le \hbar_h \le -0.35. \tag{4.105}$$

Convergence region for **PEHF case**

$$-0.96 \le \hbar_f \le -0.2, \quad -1 \le \hbar_\theta \le -0.2, \quad -1 \le \hbar_h \le -0.15. \tag{4.106}$$

**Table 4.1**. Convergence for the series solutions of different order of approximation when $Q = 1, M = 1,\ K = 1.5,\ \beta = \frac{\pi}{4},\ v_w = 1.5,\ N_b = 1, \Pr = 1.5,\ N_t = 0.2,$ and $\lambda = 0.5$ .

| Order of approximation | $-f''(0)$ | $-\theta'(0)$ PEST case | $-\phi'(0)$ PEHF case | $-h'(0)$ |
|---|---|---|---|---|
| 1 | -1.32083 | -1.20000 | -1.20000 | -0.82500 |
| 5 | -1.55987 | -1.28337 | -1.27525 | -0.41284 |
| 10 | -1.58125 | -1.28926 | -1.27895 | -0.35859 |
| 15 | -1.58286 | -1.28950 | -1.27897 | -0.35577 |
| 20 | -1.58301 | -1.28950 | -1.27897 | -0.35588 |
| 25 | -1.58303 | -1.28950 | -1.27897 | -0.35588 |
| 30 | -1.58303 | -1.28950 | -1.27897 | -0.35588 |

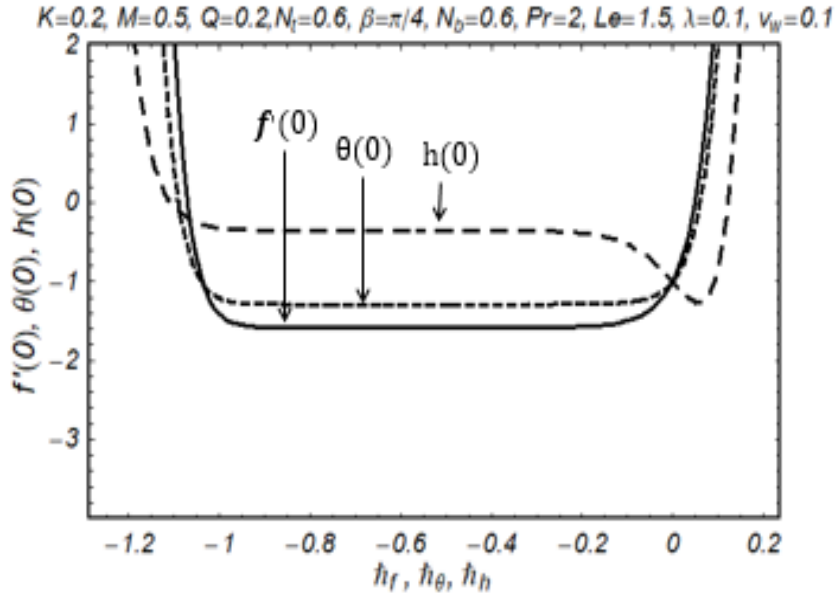


Fig. 4.2. $\hbar$ -curves for PEST case.

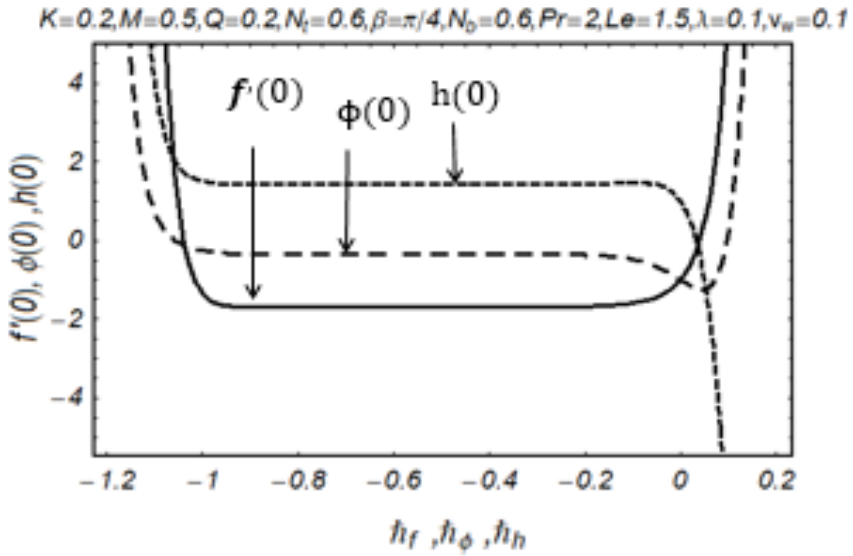


Fig. 4.3. $\hbar$ -curves for PEHF case.

## 4.5 Discussion and Analysis

The purpose of present section is to pursue the ongoing impact of dissimilar parameters corresponding to velocity, temperature and also concentration distributions. Fig. 4.4 is graphed to find how the velocity distribution $f'(\eta)$ changes under the impact of inclined magnetic field angle $\beta$. It is computed that fluid's velocity and the thickness referring to boundary layer lessens down with an intensified $\beta$.The behavior of magnetic parameter represented by $M$ for velocity distribution is examined and displayed in Fig. 4.5. The figure exhibits that velocity profile reduces at larger values of magnetic parameter. Actually, for an amplified magnetic field, a resistive force known to be Lorentz force becomes more active and contributes towards the resistance for the fluid particles, resulting in decrease of the velocity profile. For intensified Prandtl number, temperature profile $\theta(\eta)$ reveals a weaken behavior for both the considered cases of PEST and also PEHF as noticed from Figs. 4.6 & 4.7. It is owing to decrease in thermal diffusivity with enhanced Pr values because Prandtl number and thermal diffusivity have inverse relationship with each other. Impact of heat source $Q$ on temperature profiles are sketched in Figs. 4.8 & 4.9 for the two different cases. It is analyzed that in PEST and also PEHF cases, a better temperature distribution and resultant thermal layer is achieved for boosted heat source $Q$. Influence of dimensionless parameter $N_t$ on temperature profile are displayed in Figs. 4.10 & 4.11. Here temperature profile increases by varying the values of $N_t$ and keeping the rest of the parameters fixed for both the cases. The concentration profile $h(\eta)$ obtained for unalike values of Lewis number $Le$ and in addition, Brownian motion parameter $N_b$ are displayed through the plots. Influence of dimensionless number $Le$ on concentration profiles $h(\eta)$ are presented through Figs. 4.12 & 4.13. In both cases it is apparent that the concentration profile $h(\eta)$ is significantly reduced due to the enhanced values of Lewis number. The concentration distribution and thickness of the boundary layer for distinct value $N_b$ have been observed in Figs. 4.14 & 4.15 and the results show that increasing values of Brownian motion parameter declines the concentration profile $h(\eta)$ for PEHF and PEST cases whereas the effect of $N_b$ for concentration profile in case of PEST is slightly

more prominent as compared to PEHF case. It is to be mentioned that by augmenting $N_b$ the arbitrarily motion of microscopic particles escalates which shortens the mass transfer rate.

The friction drags $C_f$ are determined for the various values of porosity parameter $K$ in accordance with the growing rate of mass suction $v_w$, and this is shown graphically in Fig. 4.16. This image makes it clear that the strength of porosity parameter $K$ greatly influences $C_f$. If $K$ is ignored, then it reaches to its maximum values i.e., a decreasing behavior of skin friction coefficient is observed. In addition to this result, $C_f$ gradually diminishes as the suction parameter gets stronger. According to Fig. 4.17, the heat transfer depicted by Nusselt number $Nu$ is depicted for the various values of $N_b$ with amplified values of suction. It is obvious from the result obtained that though $Nu$ declines with the rise of $N_b$ and it keeps on rising for elevated values of suction. Heat drains due to suction since it results in intensified rate of heat transfer. The conduct of Sherwood number $Sh$ for numerous values of $Le$ are shown with the continuous fluctuation of the suction in Fig. 4.18. This outcome demonstrates that Sherwood number $Sh$ rises when values of $Le$ are elevated. It also shows an interesting behavior as mass suction continues to grow continuously. Table 4.1 show the convergences of series solutions and it exhibits that the solution converges for 30th order of approximation in case of $f''(0)$ for $h'(0)$ at the 25$^{th}$ order of approximation while for $\theta'(0)$ and $\phi'(0)$, at 20th order of approximation, the convergence is achieved. Skin friction coefficient values, in numerical form are also computed and compared with the existing work of Ali *et al.* [33] in Table 4.2. These numerical values of $C_f$ are achieved using the same parametric values of exiting research work, that points to the same situation. Considering this table, we can state that our findings and those of Ali *et al*. [33] are in perfect harmony.

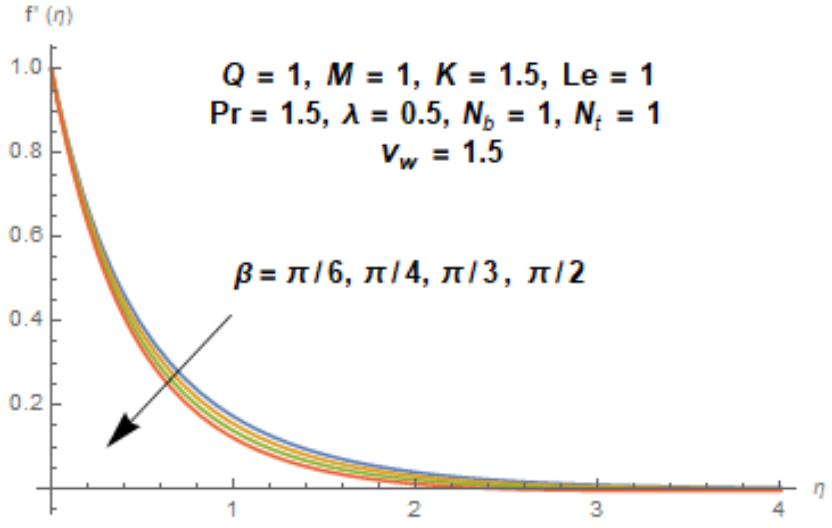


Fig. 4.4. Variation of $f'(\eta)$ for increased $\beta$ values.

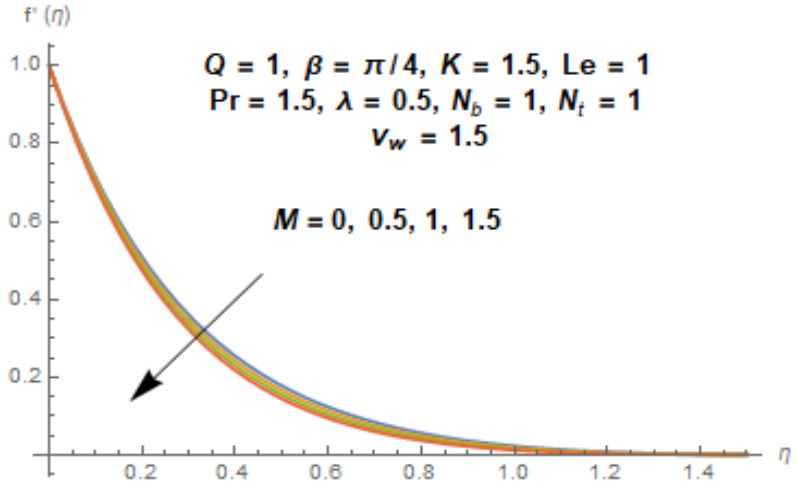


Fig. 4.5. Variation of $f'(\eta)$ for increased $M$ values.

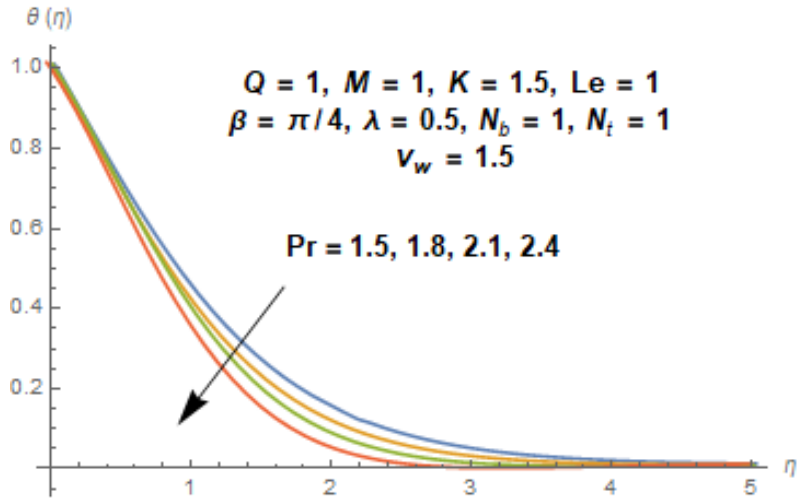


Fig. 4.6. Variation of $\theta(\eta)$ for increased Pr values in case of PEST.

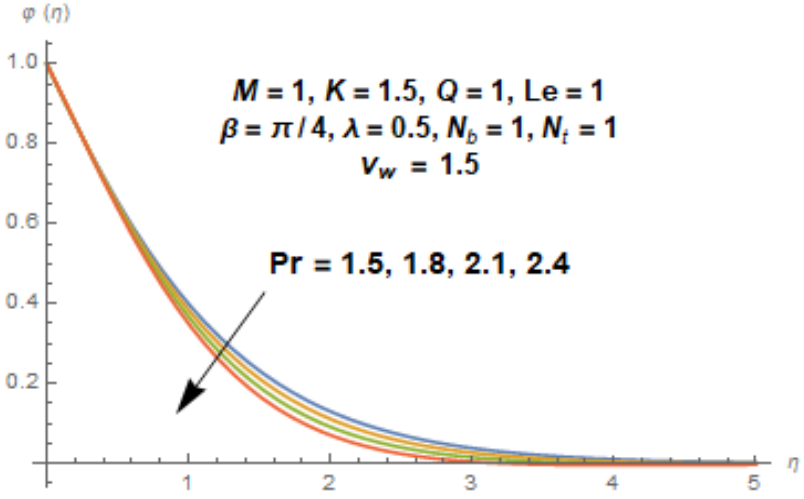


Fig. 4.7. Variation of $\phi(\eta)$ for increased Pr values in case of PEH.

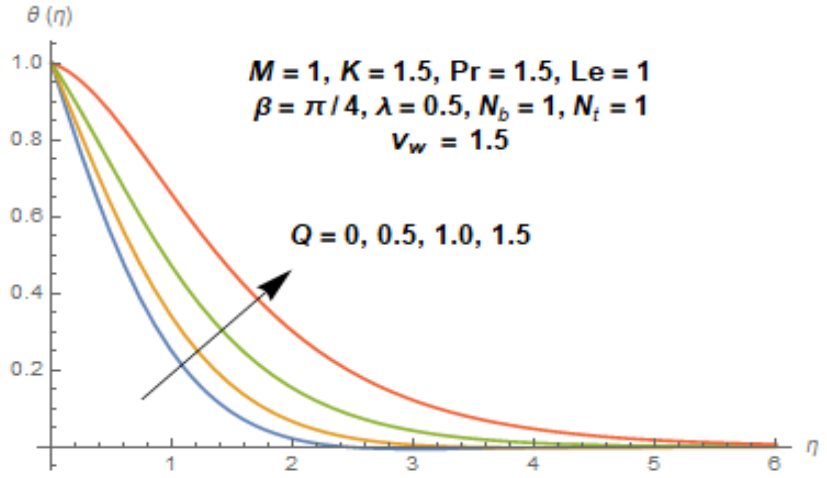


Fig. 4.8. Variation of $\theta(\eta)$ for increased $Q$ values in case of PEST.

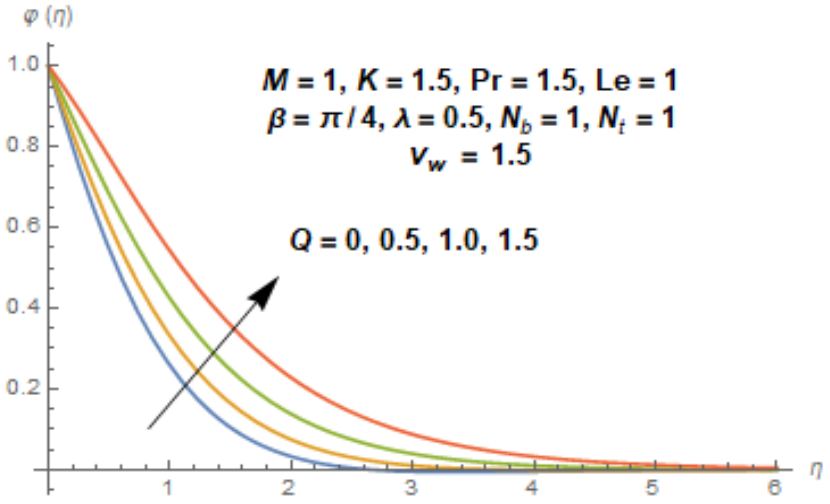


Fig. 4.9. Variation of $\phi(\eta)$ for increased $Q$ values in case of PEHF.

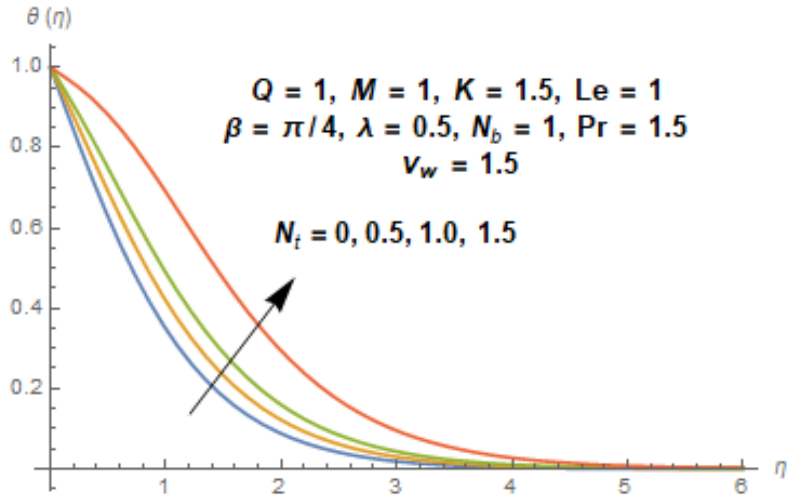


Fig. 4.10. Variation of $\theta(\eta)$ for increased $N_t$ values in case of PEST.

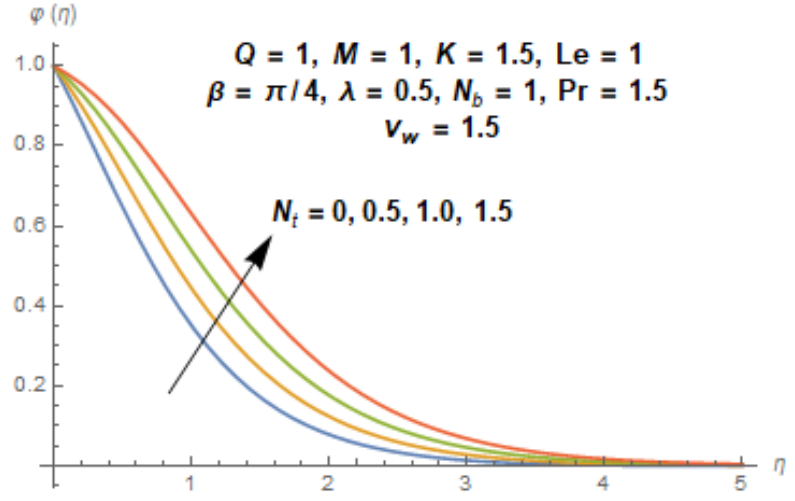


Fig. 4.11. Variation of $\phi(\eta)$ for increased $N_t$ values in case of PEHF.

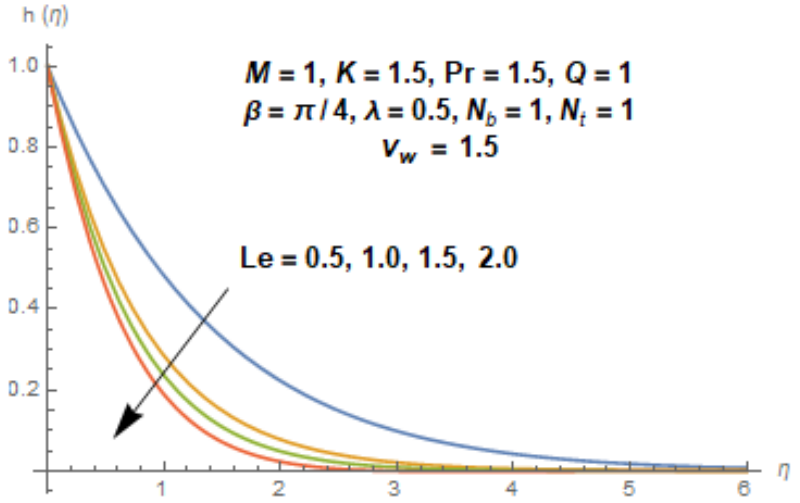


Fig. 4.12. Variation of $h(\eta)$ for increased $Le$ values in case of PEST.

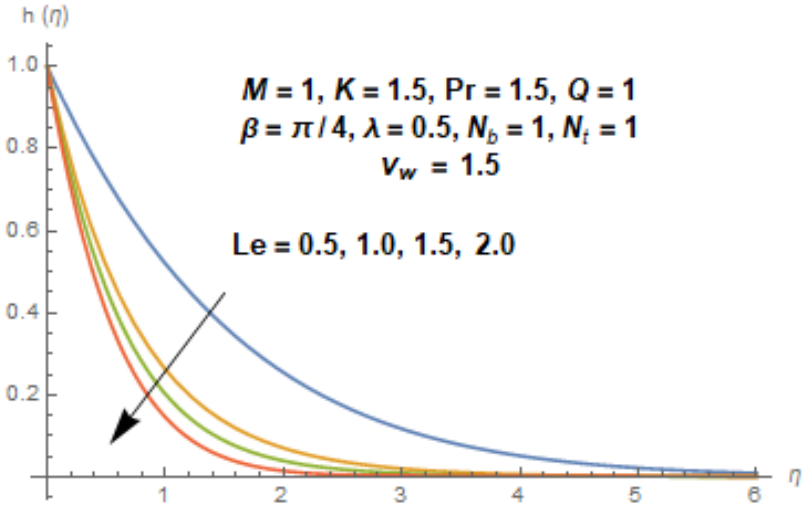


Fig. 4.13. Variation of $h(\eta)$ for increased $Le$ values in case of PEHF.

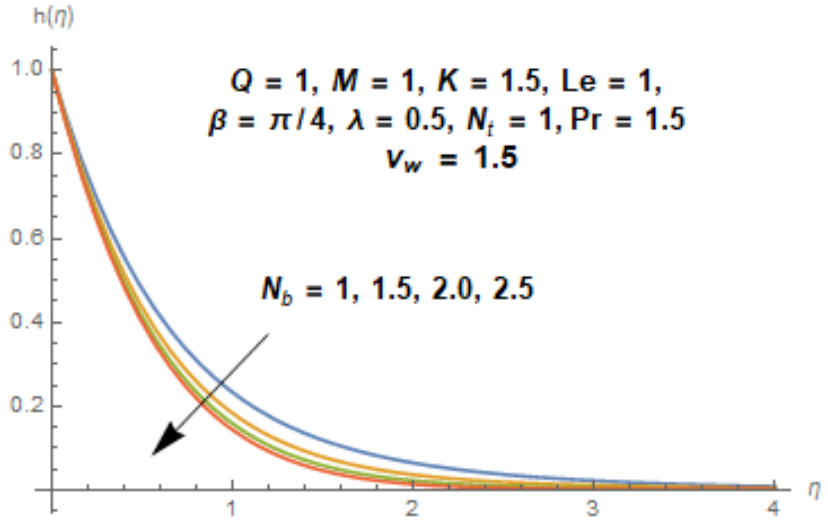


Fig. 4.14. Variation of $h(\eta)$ for increased $N_b$ values in case of PEST.

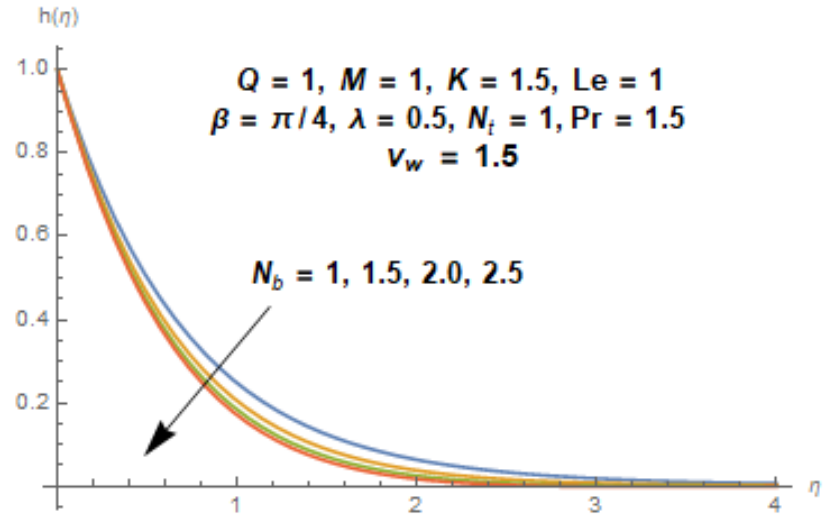


Fig. 4.15. Variation of $h(\eta)$ for increased $N_b$ values in case of PEHF.

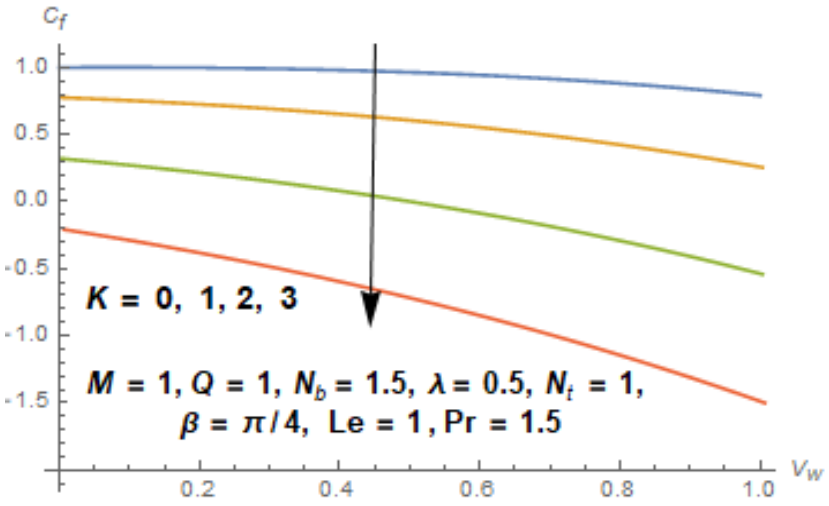


Fig. 4.16. Variation of $C_f$ for increased $K$ values.

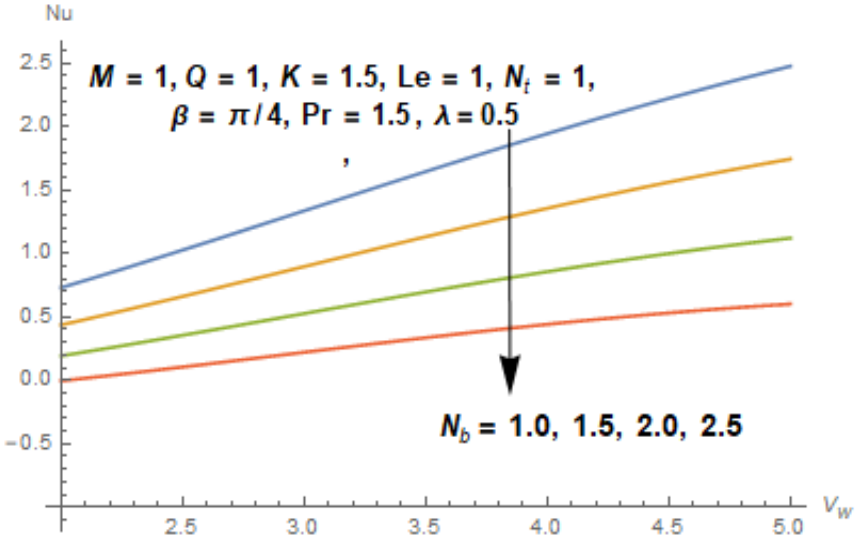


Fig. 4.17. Variation of $Nu$ for increased $N_b$ values.

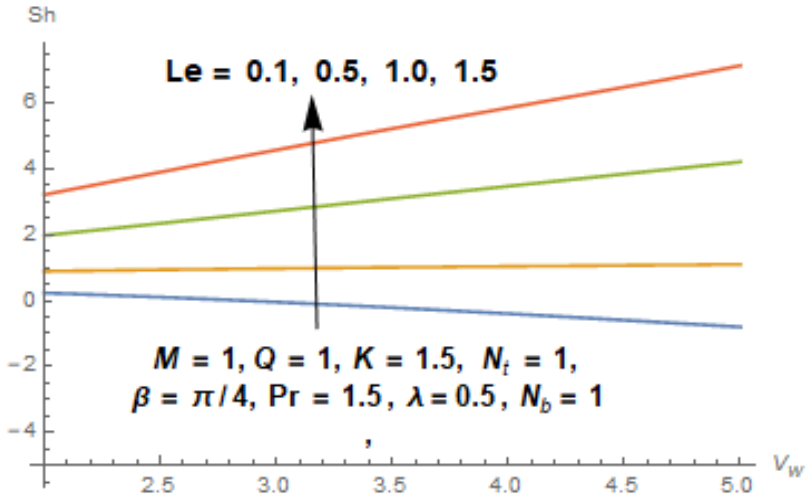


Fig. 4.18. Variation of $Sh$ for increased $Le$ values.

**Table 4.2**. Comparison value of $C_f$ for different values of $\lambda$ and $v_w$ .

| | Ali *et al.* (2021) | | Present results | |
|---|---|---|---|---|
| $\lambda$ | $v_w = 0.10$ | $v_w = 0.20$ | $v_w = 0.10$ | $v_w = 0.20$ |
| 0 | 1.23638 | 1.19298 | 1.23637 | 1.19298 |
| 0.1 | 1.20710 | 1.16468 | 1.20710 | 1.16466 |
| 0.2 | 1.17482 | 1.13365 | 1.17485 | 1.13365 |
| 0.3 | 1.13825 | 1.09881 | 1.13825 | 1.09880 |

# Chapter 5

# Mixed Convection Flow of Williamson Nanofluid over an Exponentially Stretching Surface in the presence of Magnetohydrodynamics

## 5.1 Introduction

In this chapter, the Williamson nanofluid flow over a surface stretching in an exponential form is observed. The heat and also mass transfer examination is performed in the existence of magnetohydrodynamics, chemical reaction, heat generation/absorption and viscous dissipation. The fluid characteristics are also influenced due to the effect of mixed convection. The governing equations are modelled as a system of partial differential equations and are then converted into a system of ordinary differential equations with the aid of similarity transformations. The velocity, temperature and in addition concentration distributions are examined for various important parameters. Furthermore, the graphical influence of different parameters are studied for skin friction, Nusselt number and Sherwood number. The comparative analysis performed in case of obtained results is in accordance with the already existing literature.

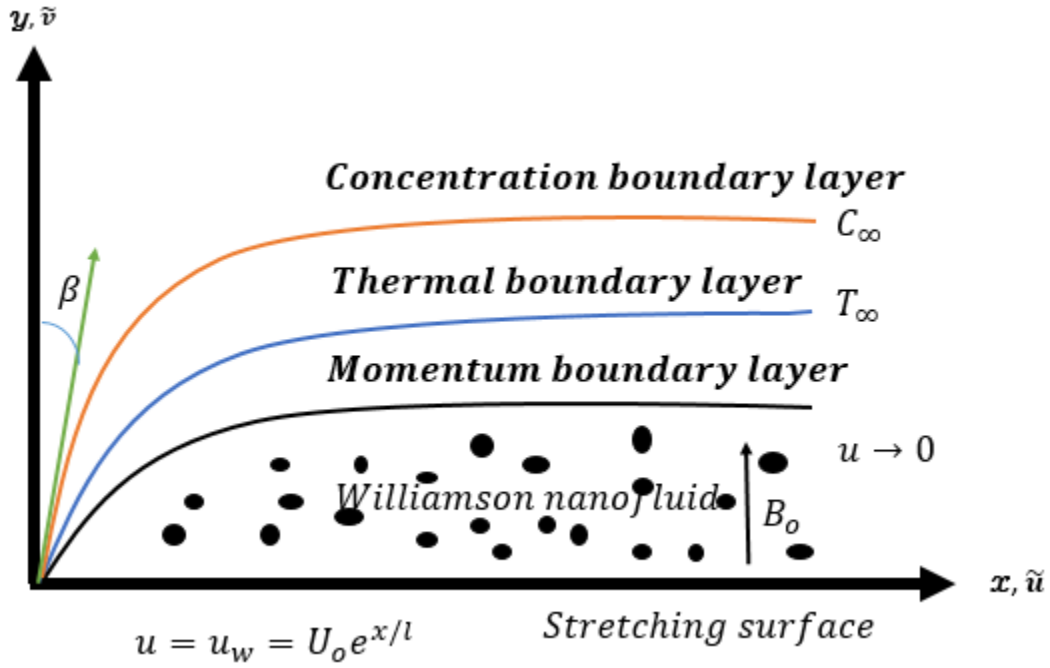


Fig. 5.1. Geometry of the Problem.

## 5.2 Mathematical modelling

This part inspects steady and two-dimensional flow for an incompressible Williamson nanofluid due to the occurrence of mixed convection. The considered flow is instigated by a porous surface stretching exponentially along the *x*-axis and possesses velocity $U_w$. An inclined magnetic field with intensity $B_0$ is applied at an angle $\beta$ to the considered surface. The flow is further influenced by the appearance of heat generation/absorption, chemical reaction and viscous dissipation. The fluid's velocity, its temperature and the relevant nanoparticle concentration close to the surface are assumed in this case to be $U_w$, $T_w$ and $C_w$ respectively. The necessary governing equations for the considered flow model are given as

$$\nabla.\vec{v} = 0, \tag{5.1}$$

$$\rho \frac{d\vec{v}}{dt} = \vec{\nabla}.\vec{S} + \vec{b}\ , \tag{5.2}$$

$$(\rho c_p)_f \frac{dT}{dt} = \nabla.\left(k\ \vec{\nabla}\ T\right) + (\rho c_p)_p \left[ D_B\ \vec{\nabla}\ C.\vec{\nabla}\ T + \frac{D_T}{T_\infty}\left(\vec{\nabla}\ T.\vec{\nabla}\ T\right) + Q_0(T - T_\infty) + \vec{\tau}.\vec{L}\ \right], \tag{5.3}$$

$$\frac{dC}{dt} = \vec{\nabla}.(D_B \vec{\nabla} C + D_T \frac{\vec{\nabla} T}{T_\infty}) - R(C - C_\infty), \tag{5.4}$$

where $\vec{\mathrm{v}} = [\tilde{u}(x,y), \tilde{v}(x,y), 0]$ is noted for velocity, $\vec{S}$ for stress tensor, $\rho$ for nanofluid density, $(\rho c_p)_f$ and $(\rho c_p)_p$ for heat capacities of the fluid and added nanoparticles respectively, $T$ for temperature, $D_B$ for Brownian diffusion coefficient, $Q_\circ$ for heat generation coefficient , $C$ for nanoparticle volumetric fraction, $D_T$ for thermophoretic diffusion coefficient, $C_\infty$ for ambient nanoparticles volume fraction and $T_\infty$ for the ambient fluid temperature.

Williamson fluid holds Cauchy stress tensor $\vec{\mathrm{S}}$ defined to be Nadeem *et al*. [95].

$$\vec{\mathrm{S}} = -p\vec{I} + \vec{\tau}, \tag{5.5}$$

Where

$$\vec{\tau} = \left[ \mu_\infty + \frac{(\mu_0 - \mu_\infty)}{1 - \Gamma\ \dot{\gamma}} \right] A_1, \tag{5.6}$$

where $\tau$ is symbolized for extra stress tensor, $\mu_0$ for limiting viscosity relative to zero shear rate, $\mu_\infty$ for limiting viscosity relative to infinite shear rate and $\Gamma > 0$ for shear stress. It is needed to express $\dot{\gamma}$ as

$$\dot{\gamma} = \sqrt{\frac{1}{2}\pi}, \tag{5.7}$$

$$\pi = trace(A_1^2), \tag{5.8}$$

Taking $\mu_\infty = 0$ and $\Gamma\dot{\gamma} \prec 1$ , we have

$$\vec{\tau} = \mu_0[1 + \Gamma\dot{\gamma}]^{-1} A_1. \tag{5.9}$$

The extra stress tensor in component form are

$$\begin{aligned} \tau_{xx} &= 2\mu_0[1+\Gamma\ \dot{\gamma}]\tfrac{\partial \tilde{u}}{\partial x}, \\ \tau_{xy} &= \tau_{yx} = 2\mu_0[1+\Gamma\ \dot{\gamma}](\tfrac{\partial \tilde{u}}{\partial y}+\tfrac{\partial \tilde{u}}{\partial x}), \\ \tau_{yy} &= 2\mu_0[1+\Gamma\ \dot{\gamma}]\tfrac{\partial \tilde{u}}{\partial y}, \end{aligned} \tag{5.10}$$

and $\tau_{xz}=\tau_{yz}=\tau_{zx}=\tau_{zy}=\tau_{zz}=0.$

The crucial aspects of electromagnetic force is stated to be

$$\vec{\mathrm{J}} \times \vec{\mathrm{B}} = -\sigma B_{\circ}{}^2 sin^2\beta\tilde{u}, \tag{5.11}$$

where $B_0$ is represented for applied magnetic field, $\sigma$ for electrical conductivity and $\vec{E}$ for electric field.

Making use of above Eqs. in $(5.1-5.4)$, we get the following equations under the boundary layer theory

$$\frac{\partial \tilde{u}}{\partial x}+\frac{\partial \tilde{v}}{\partial y}=0, \tag{5.12}$$

$$\begin{aligned} \tilde{u}\frac{\partial \tilde{u}}{\partial x}+\tilde{v}\frac{\partial \tilde{u}}{\partial y} = \nu\frac{\partial^2 \tilde{u}}{\partial y^2}+\sqrt{2}\Gamma\frac{\partial \tilde{u}}{\partial y}\frac{\partial^2 \tilde{u}}{\partial y^2}-\nu\frac{\tilde{u}}{k_1}-\frac{\sigma B^2}{\rho}sin^2\beta\tilde{u} \\ +g\beta_T(T-T_\infty)+g\beta_c(C-C_\infty), \end{aligned} \tag{5.13}$$

$$\tilde{u}\frac{\partial T}{\partial x}+\tilde{v}\frac{\partial T}{\partial y}=\alpha\frac{\partial^2 T}{\partial y^2}+\frac{Q_0}{(\rho c_p)_f}(T-T_\infty)+\frac{(\rho c_p)_p}{(\rho c_p)_f}\left[D_{\boldsymbol{B}}\frac{\partial T}{\partial y}\frac{\partial C}{\partial y}+\frac{D_T}{T_\infty}\left(\frac{\partial T}{\partial y}\right)^2+\frac{\mu}{(\rho C_p)_f}(\frac{\partial \tilde{u}}{\partial y})^2\right], \tag{5.14}$$

$$\tilde{u}\ \frac{\partial C}{\partial x}+\tilde{v}\ \frac{\partial C}{\partial y}=D_B\left(\frac{\partial^2 C}{\partial y^2}\right)+\frac{D_T}{T_\infty}\left(\frac{\partial^2 T}{\partial y^2}\right)-R(C-C_\infty). \tag{5.15}$$

The necessary conditions for above equations can be stated as Li *et al*. [96].

$$\tilde{u}=U_w=U_0e^{\frac{x}{l}},\ v_w=-\delta(x). \tag{5.16}$$

For **PEST** case:

$$T = T_w = T_\infty + (T_w - T_\infty)e^{\frac{x}{2l}},\ C = C_w \text{ at } y = 0, \tag{5.17}$$

For **PEHF** case.

$$-k\left(\frac{\partial T}{\partial y}\right)_w = (T_w - T_\infty)e^{\frac{x}{l}},\ C = C_w \text{ at } y = 0, \tag{5.18}$$

and the conditions when $y \to \infty$ are

$$\tilde{u} = u_e \to 0,\ T \to T_\infty, C \to C_\infty. \tag{5.19}$$

In above stated expressions $u_1$ and $v_1$ are characterized for velocity components in orthogonal directions, $U_0$ for reference velocity, $\rho$ for fluid's density, $\sigma$ for electrical conductivity, $\alpha$ for thermal diffusivity, $k_1$ for permeability of the porous medium, $\nu$ for kinematic viscosity, $\beta_T$ for temperature expansion coefficient and $\beta_c$ for concentration expansion coefficient.

Exercising the succeeding transformations Lie *et al*. [96].

$$\begin{aligned} \tilde{u} &= U_0 e^{\frac{x}{l}} f'(\eta), \\ v_w &= -\sqrt{\frac{\nu U_\circ}{2l}} e^{\frac{x}{2l}} [(f(\eta) + \eta f'(\eta)], \\ \eta &= \sqrt{\frac{U_\circ}{2\nu l}} y e^{\frac{x}{2l}}. \end{aligned} \tag{5.20}$$

**Case for PEST:**

$$\begin{aligned} T &= T_\infty + (T_w - T_\infty)e^{\frac{x}{2l}}\theta(\eta), \\ h &= \frac{C - C_\infty}{C_w - C_\infty}. \end{aligned} \tag{5.21}$$

**Case for PEHF:**

$$\begin{aligned} T &= T_\infty + \frac{T_w - T_\infty}{k} e^{\frac{x}{2l}} \sqrt{\frac{2\nu l}{U_\circ}}\,\phi(\eta), \\ h &= \frac{C - C_\infty}{C_w - C_\infty}. \end{aligned} \tag{5.22}$$

Applying similarity transformations $(5.9 - 5.13)$ in equations $(5.3 - 5.5)$ we get

(5.23)

$$f''' - 2(f')^2 + ff'' + \lambda f'''f'' - (K + M\sin^2\beta)f' + Gr_t\theta + Gr_c h = 0.$$

**PEST case**

$$\theta'' + \Pr\left(f\theta' - f'\theta + N_b h'\theta' + N_t\theta'^2 + Q\theta + Ecf''^2\right) = 0, \tag{5.24}$$

$$h'' + Le\Pr(fh' - \gamma h) + \frac{N_t}{N_b}\theta'' = .0 \tag{5.25}$$

**PEHF case**

$$\phi'' + \Pr\left(f\phi' - f'\phi + N_b h'\phi' + N_t\phi'^2 + Q\phi + Ecf''^2\right) = 0, \tag{5.26}$$

$$h'' + Le\Pr(fh' - \gamma h) + \frac{N_t}{N_b}\phi'' = 0. \tag{5.27}$$

and the boundary conditions become,

$$f(0) = v_w, \quad f'(0) = 1, \quad f'(\infty) = 0. \tag{5.28}$$

The requisite conditions for **PEST** are

$$\theta(0) = 1, \ \theta(\infty) = 0, \quad h(0) = 1, \quad h(\infty) = 0, \tag{5.29}$$

and for **PEHF** are

$$\phi'(0) = -1, \quad \phi(\infty) = 0, \quad h(0) = 1, \ h(\infty) = 0 \ , \tag{5.30}$$

where $\lambda$ is indicated for Williamson parameter, $K$ for porosity parameter, $\Pr$ for Prandtl number, $Ec$ for Eckert number, $Gr_t$ for temperature Grashof number, $Gr_c$ for concentration Grashof number, $M$ for Hartmann number, $N_t$ and $N_b$ for Brownian and thermophoresis motion parameter, $Q$ for heat source parameter, $Le$ for Lewis number and $\gamma$ for chemical reaction parameter. These parameters are demonstrated as follows:

$$\lambda = \frac{\Gamma}{\sqrt{\nu l}} U_{\circ}^{3/2} e^{\frac{3x}{2l}}, \quad M = \frac{2\sigma B_{\circ}^2 l}{\rho U_0} e^{-\frac{x}{l}}, \quad K = \frac{2\nu l}{k_1 U_{\circ}} e^{-\frac{x}{l}},$$
$$\gamma = \frac{2Rl}{U_{\circ}} e^{-\frac{x}{l}}, \quad Ec = \frac{U_0^2}{(C_p)_f (T_w - T_{\infty})} e^{\frac{3x}{2l}}, \quad \Pr = \frac{\nu}{\alpha},$$
$$Gr_c = \frac{2\beta_c g l \nu^2}{U_{\circ} \nu^2} (C_w - C_{\infty}) e^{\frac{2x}{l}}, \quad N_t, = \frac{D_T}{T_{\infty}} \frac{(\rho C_p)_p}{(\rho C_p)_f} \frac{(T_w - T_{\infty})}{\nu} e^{\frac{x}{l}},$$
$$N_b = \frac{D_B}{\nu} \frac{(\rho C_p)_p}{(\rho C_p)_f} (C_w - C_{\infty}), \quad Q = \frac{Q_{\circ}}{(\rho C_p)_f} \frac{2l}{U_{\circ}} e^{-\frac{x}{l}},$$
$$Le = \frac{\alpha}{D_B}, \quad Gr_t = \frac{2\beta_T g l \nu^2}{U_0^2 \nu^2} (T_w - T_{\infty}) e^{-\frac{x}{l}}. \tag{5.31}$$

The skin friction coefficient, the Sherwood number $(Sh)$ and 1ocal Nusselt number ( $Nu_x$) are defined as

$$C_f = \frac{\tau_w}{\rho U_w^2}, \quad Nu_x = \frac{x \tilde{q}_w}{k(T_w - T_{\infty})}, \quad Sh = \frac{x \tilde{q}_m}{D_B (T_w - T_{\infty})}, \tag{5.32}$$

$$\tau_w = \mu \left[ \frac{\partial u_1}{\partial y} + \frac{\Gamma}{\sqrt{2}} \left( \frac{\partial u_1}{\partial y} \right)^2 \right]_{y=0}, \quad \tilde{q}_w = -k \left[ \frac{\partial T}{\partial y} \right]_{y=0}, \quad \tilde{q}_n = -D_B \left[ \frac{\partial C}{\partial y} \right]_{y=0}, \tag{5.33}$$

$$(2\,\mathrm{Re}_x)^{1/2} C_f = (f'' + \frac{\lambda}{2} f'^2)_{\eta=0}, \quad e^{-\frac{x}{2l}} (2\,\mathrm{Re}_x)^{-1/2} Nu = -\theta'(0),$$
$$e^{-\frac{x}{2l}} (2\,\mathrm{Re}_x)^{-1/2} Sh = -h'(0), \tag{5.34}$$

where $\mathrm{Re} = \frac{U_{\circ} x^2 e^{\frac{x}{l}}}{2\nu l}$ .

## 5.3 Homotopic solution

The requisite initial guesses $(f_0, \theta_0, h_0)$ and associated linear operators $(\mathcal{L}_f, \mathcal{L}_\theta, \mathcal{L}_h)$ for the momentum, energy and also concentration equations can be adopted in the following way:

$$f_0(\eta) = 1 + v_w - \exp(-\eta), \quad \theta_0(\eta) = \exp(-\eta), \quad h_0(\eta) = \exp(-\eta), \tag{5.35}$$

$$\mathcal{L}_f(f) = \frac{d^3 f}{d\eta^3} - \frac{df}{d\eta}, \quad \mathcal{L}_\theta(\theta) = \frac{d^2\theta}{d\eta^2} - \theta, \quad \mathcal{L}_h(h) = \frac{d^2 h}{d\eta^2} - h, \tag{5.36}$$

and

$$\mathcal{L}_f[b_1 + b_2 \exp(\eta) + b_3 \exp(-\eta)] = 0, \tag{5.37}$$

$$\mathcal{L}_\theta[b_4 \exp(\eta) + b_5 \exp(-\eta)] = 0, \tag{5.38}$$

$$\mathcal{L}_h[b_6 \exp(\eta) + b_7 \exp(-\eta)] = 0, \tag{5.39}$$

where $b_i$ $(i = 1-7)$ give arbitrary constants.

The problems relative to zeroth and nth orders are stated as:

### 5.3.1 Zeroth-order problem (PEST case)

$$(1-r)\,\mathcal{L}_f\left[\hat{f}(\eta;r) - f_0(\eta)\right] = r\hbar_f \mathcal{N}_f\left[\hat{f}(\eta;r)\right], \tag{5.40}$$

$$(1-r)\,\mathcal{L}_\theta\left[\hat{\theta}(\eta;r) - \theta_0(\eta)\right] = r\hbar_\theta \mathcal{N}_\theta\left[\hat{f}(\eta;r), \hat{\theta}(\eta;r), \hat{h}(\eta;r)\right], \tag{5.41}$$

$$(1-r)\,\mathcal{L}_h\left[\hat{h}(\eta;r) - h_0(\eta)\right] = r\hbar_h \mathcal{N}_h\left[\hat{f}(\eta;r), \hat{\theta}(\eta;p), \hat{h}(\eta;r)\right], \tag{5.42}$$

$$\hat{f}(0;r) = v_w, \quad \frac{\partial \hat{f}}{\partial \eta}(0;r) = 1, \quad \frac{\partial \hat{f}}{\partial \eta}(\infty;r) = 0, \tag{5.43}$$

$$\hat{\theta}(0;r) = 1, \quad \hat{\theta}(\infty;r) = 0, \tag{5.44}$$

$$\hat{h}(0;r) = 1, \quad \hat{h}(\infty;r) = 0, \tag{5.45}$$

$$\mathcal{N}_f\left[\,\widehat{f}(\eta;r),\widehat{\theta}(\eta;r),\widehat{h}(\eta;r)\,\right]=\left[\begin{array}{c}\frac{\partial^3\widehat{f}(\eta;r)}{\partial\eta^3}-2\left(\frac{\partial\widehat{f}(\eta;r)}{\partial\eta}\right)^2+\widehat{f}(\eta;r)\frac{\partial^2\widehat{f}(\eta;r)}{\partial\eta^2}+\\ +\lambda\frac{\partial^3\widehat{f}(\eta;r)}{\partial\eta^3}\frac{\partial^2\widehat{f}(\eta;r)}{\partial\eta^2}-(K+M\sin^2\beta)\frac{\partial\widehat{f}(\eta;r)}{\partial\eta}\\ +Gr_t\widehat{\theta}(\eta;r)+Gr_c\widehat{h}(\eta;r)\end{array}\right], \tag{5.46}$$

$$\mathcal{N}_\theta\left[\,\widehat{f}(\eta;r),\widehat{\theta}(\eta;r),\widehat{h}(\eta;r)\,\right]=\left[\begin{array}{c}\frac{\partial^2\widehat{\theta}(\eta;r)}{\partial\eta^2}+\Pr\widehat{f}(\eta;r)\frac{\partial\widehat{\theta}(\eta;r)}{\partial\eta}-\Pr\frac{\partial\widehat{f}(\eta;r)}{\partial\eta}\widehat{\theta}(\eta;r)\\ +\Pr N_b\frac{\partial\widehat{h}(\eta;r)}{\partial\eta}\frac{\partial\widehat{\theta}(\eta;r)}{\partial\eta}+\Pr N_t\left(\frac{\partial\widehat{\theta}(\eta;r)}{\partial\eta}\right)^2\\ +\Pr Q\widehat{\theta}(\eta;r)+\Pr Ec\left(\frac{\partial^2\widehat{f}(\eta;r)}{\partial\eta^2}\right)^2\end{array}\right], \tag{5.47}$$

$$\mathcal{N}_h\left[\,\widehat{f}(\eta;r),\widehat{\theta}(\eta;r),\widehat{h}(\eta;r)\,\right]=\left[\begin{array}{c}=\frac{\partial^2\widehat{h}(\eta;r)}{\partial\eta^2}+Le\Pr\widehat{f}(\eta;r)\frac{\partial\widehat{h}(\eta;r)}{\partial\eta}\\ -\Pr Le\gamma\widehat{h}(\eta;r)+\frac{N_t}{N_b}\frac{\partial^2\widehat{\theta}(\eta;r)}{\partial\eta^2}\end{array}\right], \tag{5.48}$$

For the above equations $\hbar_f,\hbar_\theta$ , $\hbar_h$ are the auxiliary parameters and $r\in[0,1]$.

### 5.3.2 nth-order problem

$$\mathcal{L}_f\left[\,f_n(\eta)-\chi_n f_{n-1}(\eta)\,\right]=\hbar_f\mathcal{R}_n^f(\eta), \tag{5.49}$$

$$\mathcal{L}_\theta\left[\,\theta_n(\eta)-\chi_n\theta_{n-1}(\eta)\,\right]=\hbar_\theta\mathcal{R}_n^\theta(\eta), \tag{5.50}$$

$$\mathcal{L}_h\left[\,h_n(\eta)-\chi_n h_{n-1}(\eta)\,\right]=\hbar_h\mathcal{R}_n^h(\eta), \tag{5.51}$$

$$f_n(0)=f_n'(0)=f_n'(\infty)=0, \tag{5.52}$$

$$\theta_n(0)=\theta_n(\infty)=0, \tag{5.53}$$

$$h_n(0)=h_n(\infty)=0, \tag{5.54}$$

$$\mathcal{R}_n^f(\eta) = f'''_{n-1}(\eta) - \left[ \begin{array}{c} \sum_{k=0}^{n-1}\left[ 2f'_{n-1-k}f'_k + f_{n-1-k}f''_k + \lambda f'''_{n-1-k}f''_k \right] \\ -(K + M\sin^2\beta)f'_{n-1}, + Gr_t\ \theta_{n-1} + Gr_c h_{n-1}, \end{array} \right], \tag{5.55}$$

$$\mathcal{R}_n^\theta(\eta) = \theta''_{n-1}(\eta) + \Pr \sum_{k=0}^{n-1} \left[ \begin{array}{c} f_{n-1-k}\theta'_k - f_{n-1-k}\theta'_k + N_b\theta'_{n-1-k}h'_k \\ +N_t\theta'_{n-1-k}\theta'_k + Ecf''_{n-1-k}f''_k \end{array} \right] + \Pr Q\theta_{n-1}, \tag{5.56}$$

$$\mathcal{R}_n^h(\eta) = h''_{n-1}(\eta) + \sum_{k=0}^{m-1}[Le\Pr f_{n-1-k}h'_k] - Le\Pr\gamma h_{n-1} + \frac{N_t}{N_b}\theta''_{n-1}], \tag{5.57}$$

$$\chi_n = \begin{cases} 0, & n \le 1, \\ 1, & n > 1. \end{cases} \tag{5.58}$$

$r = 0$ and $r = 1$ correspond to

$$\widehat{f}(\eta;0) = f_0(\eta), \quad \widehat{f}(\eta;1) = f(\eta), \tag{5.59}$$

$$\widehat{\theta}(\eta;0) = \theta_0(\eta), \quad \widehat{\theta}(\eta;1) = \theta(\eta), \tag{5.60}$$

$$\widehat{h}(\eta;0) = h_0(\eta), \quad \widehat{h}(\eta;1) = h(\eta). \tag{5.61}$$

As $r$ changes increases from $0$ to $1$, then $\widehat{f}(\eta;r)$, $\widehat{\theta}(\eta;r)$ and $\widehat{h}(\eta;r)$ modifies from $f_0(\eta)$, $\theta_0(\eta)$ and $h_0(\eta)$ to $f(\eta)$, $\theta(\eta)$ and $h(\eta)$ respectively. Taylor series expression with regard to the parameter $r$ results in the following forms.

$$\widehat{f}(\eta;p) = f_0(\eta) + \sum_{n=1}^{\infty} f_n(\eta)r^n, \quad f_n(\eta) = \frac{1}{n!}\frac{\partial^n \widehat{f}(\eta;r)}{\partial r^n}\bigg|_{r=0}, \tag{5.62}$$

$$\widehat{\theta}(\eta;r) = \theta_0(\eta) + \sum_{n=1}^{\infty} \theta_n(\eta)r^n. \quad \theta_n(\eta) = \frac{1}{n!}\frac{\partial^n \widehat{\theta}(\eta;r)}{\partial r^n}\bigg|_{r=0}, \tag{5.63}$$

$$\widehat{h}(\eta;r) = h_0(\eta) + \sum_{n=1}^{\infty} h_n(\eta)r^n, \qquad h_n(\eta) = \frac{1}{n!}\frac{\partial^n \widehat{h}(\eta;r)}{\partial r^n}\bigg|_{r=0}. \tag{5.64}$$

Choosing the values of the auxiliary parameters to obtain the convergence at $r=1$ results in

$$f(\eta) = f_0(\eta) + \sum_{n=1}^{\infty} f_n(\eta), \tag{5.65}$$

$$\theta(\eta) = \theta_0(\eta) + \sum_{n=1}^{\infty} \theta_n(\eta), \tag{5.66}$$

$$h(\eta) = h_0(\eta) + \sum_{n=1}^{\infty} h_n(\eta). \tag{5.67}$$

The obtained solutions $\left(f_n, \theta_{n,}, h_n\right)$ of the Eqs. $(5.48-5.50)$ are illustrated as

$$f_n(\eta) = f_n^{\star}(\eta) + b_1 + b_2 e^{\eta} + b_3 e^{-\eta}, \tag{5.68}$$

$$\theta_n(\eta) = \theta_n^{\star}(\eta) + b_4 e^{\eta} + b_5 e^{-\eta}, \tag{5.69}$$

$$h_n(\eta) = h_n^{\star}(\eta) + b_6 e^{\eta} + b_7 e^{-\eta}, \tag{5.70}$$

which express the constants $b_i$ $(i=1-8)$ utilizing boundary conditions $(5.51-5.3)$ are given by

$$b_2 = b_4 = b_6 = 0, \quad b_3 = \left.\frac{\partial f_n^{\star}(\eta)}{\partial \eta}\right|_{\eta=0} - 1, \quad b_1 = v_w - f_n^{\star}(0), \tag{5.71}$$
$$b_5 = 1 - \theta_n^{\star}(0), \quad b_7 = -h_n^{*}(0).$$

### 5.3.3 Zeroth-order problem (PEHF case)

$$(1-r)\mathcal{L}_f\left[\widehat{f}(\eta;r) - f_0(\eta)\right] = r\hbar_f \mathcal{N}_f\left[\widehat{f}(\eta;r), \widehat{\theta}(\eta;r), \widehat{h}(\eta;r)\right], \tag{5.72}$$

$$(1-r)\mathcal{L}_\phi\left[\widehat{\phi}(\eta;r) - \phi_0(\eta)\right] = r\hbar_\phi \mathcal{N}_\phi\left[\widehat{f}(\eta;r), \widehat{\phi}(\eta;r), \widehat{h}(\eta;r)\right], \tag{5.73}$$

$$(1-r)\mathcal{L}_h\left[\widehat{h}(\eta;r) - h_0(\eta)\right] = r\hbar_h \mathcal{N}_h\left[\widehat{f}(\eta;r), \widehat{\phi}(\eta;r), \widehat{h}(\eta;r)\right], \tag{5.74}$$

$$\widehat{f}(0;r) = v_w, \quad \frac{\partial \widehat{f}}{\partial \eta}(0;r) = 1, \quad \frac{\partial \widehat{f}}{\partial \eta}(\infty;r) = 0, \tag{5.75}$$

$$\frac{\partial \widehat{\phi}}{\partial \eta}(0;r) = -1, \quad \widehat{\phi}(\infty;r) = 0, \tag{5.76}$$

$$\widehat{h}(0;r) = 1, \quad \widehat{h}(\infty;r) = 0, \tag{5.77}$$

$$\mathcal{N}_f\left[\widehat{f}(\eta;r), \widehat{\theta}(\eta;r), \widehat{h}(\eta;r)\right] = \begin{bmatrix} \frac{\partial^3 \widehat{f}(\eta;r)}{\partial \eta^3} - 2\left(\frac{\partial \widehat{f}(\eta;r)}{\partial \eta}\right)^2 + \widehat{f}(\eta;r)\frac{\partial^2 \widehat{f}(\eta;r)}{\partial \eta^2} + \\ +\lambda \frac{\partial^3 \widehat{f}(\eta;r)}{\partial \eta^3}\frac{\partial^2 \widehat{f}(\eta;r)}{\partial \eta^2} - (K + M\sin^2\beta)\frac{\partial \widehat{f}(\eta;r)}{\partial \eta} \\ +Gr_t\widehat{\theta}(\eta;r) + Gr_c\widehat{h}(\eta;r) \end{bmatrix}, \tag{5.78}$$

$$\mathcal{N}_\phi\left[\widehat{f}(\eta,r), \widehat{\phi}(\eta,r), \widehat{h}(\eta,r)\right] = \begin{bmatrix} \frac{\partial^2 \widehat{\phi}(\eta;r)}{\partial \eta^2} + \Pr \widehat{f}(\eta;r)\frac{\partial \widehat{\phi}(\eta;r)}{\partial \eta} - \Pr \frac{\partial \widehat{f}(\eta;r)}{\partial \eta}\widehat{\phi}(\eta;r) \\ +\Pr N_b \frac{\partial \widehat{h}(\eta;r)}{\partial \eta}\frac{\partial \widehat{\phi}(\eta;r)}{\partial \eta} + \Pr N_t\left(\frac{\partial \widehat{\phi}(\eta;r)}{\partial \eta}\right)^2 \\ +\Pr Q\widehat{\phi}(\eta;r) + \Pr Ec\left(\frac{\partial^2 \widehat{f}(\eta;r)}{\partial \eta^2}\right)^2 \end{bmatrix}, \tag{5.79}$$

$$\mathcal{N}_h\left[\widehat{f}(\eta;r), \widehat{\theta}(\eta;r), \widehat{h}(\eta;r)\right] = \begin{bmatrix} = \frac{\partial^2 \widehat{h}(\eta;r)}{\partial \eta^2} + Le\,[\Pr \widehat{f}(\eta;r)\frac{\partial \widehat{h}(\eta;r)}{\partial \eta} \\ -\Pr \gamma \widehat{h}(\eta;r)] + \frac{N_t}{N_b}\frac{\partial^2 \widehat{\theta}(\eta;r)}{\partial \eta^2} \end{bmatrix}, \tag{5.80}$$

Stating that $r \in [0,1]$ represents embedding parameter.

### 5.3.4 nth-order problem

$$\mathcal{L}_f[f_n(\eta) - \chi_n f_{n-1}(\eta)] = \hbar_f \mathcal{R}_n^f(\eta), \tag{5.81}$$

$$\mathcal{L}_\phi[\phi_n(\eta) - \chi_n \phi_{n-1}(\eta)] = \hbar_\phi \mathcal{R}_n^\phi(\eta), \tag{5.82}$$

$$\mathcal{L}_h[h(\eta) - \chi_n h_{n-1}(\eta)] = \hbar_h \mathcal{R}_n^h(\eta), \tag{5.83}$$

$$f_n(0) = f_n'(0) = f_n'(\infty) = 0, \tag{5.84}$$

$$\phi_n(0) = \phi_n(\infty) = 0, \tag{5.85}$$

$$h_n(0) = h_n(\infty) = 0, \tag{5.86}$$

$$\overset{f}{}_n(\eta) = f_{n-1}'''(\eta) - \left[ \begin{array}{c} \sum_{k=0}^{n-1}\left[ 2f_{n-1-k}'f_k' + f_{n-1-k}f_k'' + \lambda f'''_{n-1-k}f_k'' \right] \\ -(K + M\sin^2\beta)f_{n-1}', + Gr_t\ \phi_{n-1} + Gr_c h_{n-1}, \end{array} \right], \tag{5.87}$$

$$\mathcal{R}_n^{\phi}(\eta) = \phi_{n-1}''(\eta) + \Pr \sum_{k=0}^{n-1} \left[ \begin{array}{c} f_{n-1-k}\phi_k' - f_{n-1-k}\phi_k' + N_b\phi'_{n-1-k}h_k' \\ +N_t\phi'_{n-1-k}\phi_k' + Ecf''_{n-1-k}f_k'' \end{array} \right] + \Pr Q\phi_{n-1}, \tag{5.88}$$

$$\mathcal{R}_n^h(\eta) = h_{n-1}''(\eta) + \sum_{k=0}^{n-1}[Le\Pr f_{n-1-k}h_k'] + \frac{N_t}{N_b}\phi''_{n-1}, \tag{5.89}$$

$$\chi_n = \begin{cases} 0, & n \le 1, \\ 1, & n > 1. \end{cases} \tag{5.90}$$

At $r = 0$ and $r = 1$,

$$\widehat{f}(\eta;0) = f_0(\eta), \quad \widehat{f}(\eta;1) = f(\eta), \tag{5.91}$$

$$\widehat{\phi}(\eta;0) = \phi_0(\eta), \quad \widehat{\phi}(\eta;1) = \phi(\eta), \tag{5.92}$$

$$\widehat{h}(\eta;0) = h_0(\eta), \quad \widehat{h}(\eta;1) = h(\eta). \tag{5.93}$$

As $r$ varies from 0 to 1, then $\widehat{f}(\eta;r)$, $\widehat{\phi}(\eta;r)$ and $\widehat{h}(\eta;r)$ change from guesses $f_0(\eta)$, $\phi_0(\eta)$ and $h_0(\eta)$ to the $f(\eta)$, $\phi(\eta)$ and $h(\eta)$ respectively. Using Taylor series expansion,

$$\widehat{f}(\eta;r) = f_0(\eta) + \sum_{n=1}^{\infty} f_n(\eta)r^n, \quad f_n(\eta) = \frac{1}{n!}\frac{\partial^n \widehat{f}(\eta;r)}{\partial r^n}\bigg|_{r=0}, \tag{5.94}$$

$$\widehat{\phi}(\eta;r) = \phi_0(\eta) + \sum_{n=1}^{\infty} \phi_n(\eta) r^n, \quad \phi_n(\eta) = \frac{1}{n!} \frac{\partial^n \widehat{\phi}(\eta;r)}{\partial r^n} \bigg|_{r=0}, \tag{5.95}$$

$$\widehat{h}(\eta;r) = h_0(\eta) + \sum_{n=1}^{\infty} h_n(\eta) r^r, \qquad h_n(\eta) = \frac{1}{n!} \frac{\partial^n \widehat{h}(\eta;r)}{\partial r^n} \bigg|_{r=0}. \tag{5.96}$$

Choice of the auxiliary parameters leads to the convergence of $(5.94-5.96)$ at $r=1$ and

$$f(\eta) = f_0(\eta) + \sum_{n=1}^{\infty} f_n(\eta), \tag{5.97}$$

$$\phi(\eta) = \phi_0(\eta) + \sum_{n=1}^{\infty} \phi_n(\eta), \tag{5.98}$$

$$h(\eta) =_0 (\eta) + \sum_{n=1}^{\infty} h_n(\eta). \tag{5.99}$$

The general solutions of the Eqs. $(5.80-5.82)$ is expressed as

$$f_n(\eta) = f_n^{\star}(\eta) + b_8 + b_9 e^{\eta} + b_{10} e^{-\eta}, \tag{5.100}$$

$$\phi_n(\eta) = \phi_n^{\star}(\eta) + b_{11} e^{\eta} + b_{12} e^{-\eta}, \tag{5.101}$$

$$h_n(\eta) = h_n^{\star}(\eta) + b_{13} e^{\eta} + b_{14} e^{-\eta}, \tag{5.102}$$

in which the constants $b_i$ $(i=8-11)$ through the boundary conditions $(5.83-5.85)$ are given by

$$b_9 = b_{11} = b_{13} = 0, \quad b_{10} = \frac{\partial f_n^{\star}(\eta)}{\partial \eta} \bigg|_{\eta=0} - 1, \quad b_8 = v_w - b_{10} - f_n^{\star}(0), \tag{5.103}$$

$$b_{12} = 1 + \frac{\partial \phi_n^{\star}(\eta)}{\partial \eta} \bigg|_{\eta=0}, \quad b_{14} = 1 - h_n^{*}(0).$$

## 5.4 Analysis

### 5.4.1 Convergence of solution

The methodology greatly rely on the correct choice of the auxiliary parameter which can be achieved. For this, convergence region is obtained by plotting three $\hbar$ -curves for the equations displayed in Figs. 5.2 & 5.3. The permissible ranges of the auxiliary parameters $\hbar_f$, $\hbar_\theta$, $\hbar_\phi$, and $\hbar_h$ can be clearly seen through these $\hbar$-curves. These plots guarantee the convergence of the series solution. The following ranges of auxiliary parameters are gained.

**PEST case**:

$$-0.97 \le \hbar_f \le -0.3, \quad -0.98 \le \hbar_\theta \le -0.18, \quad -1 \le \hbar_h \le -0.3. \tag{5.104}$$

**PEHF case**:

$$-0.9 \le \hbar_f \le -0.3, \quad -1 \le \hbar_\phi \le -0.3, \quad -0.97 \le \hbar_h \le -0.25. \tag{5.105}$$

**Table 5.1**. Convergence for the solution when

$Q = 1,\ M = 1,\ \gamma = 0.1,\ K = 1.5,\ Gr_t = 1, Gr_c = 1,\ \beta = \frac{\pi}{4},\ v_w = 1.5,\ Ec = 0.1,$

$N_b = 1,\ \Pr = 1.5,\ N_t = 0.2$ and $\lambda = 0.5$ .

| Order of approximation | $-f''(0)$ | $-\theta'(0)$ PEST case | $-\phi'(0)$ PEHF case | $-h'(0)$ |
|---|---|---|---|---|
| 1 | -1,28750 | -1.16667 | -1.28750 | -0.52417 |
| 5 | -1.50637 | -1.28571 | -1.30102 | -0.27391 |
| 10 | -1.54249 | -1.35012 | -1.35012 | -0.71751 |
| 15 | -1.58246 | -1.35013 | -1.37012 | -0.71862 |
| 20 | -1.58247 | -1.35013 | -1.37112 | -0.82463 |
| 25 | -1.58249 | -1.35013 | -1.37112 | -0.82463 |
| 30 | -1.58249 | -1.35013 | -1.37112 | -0.82463 |

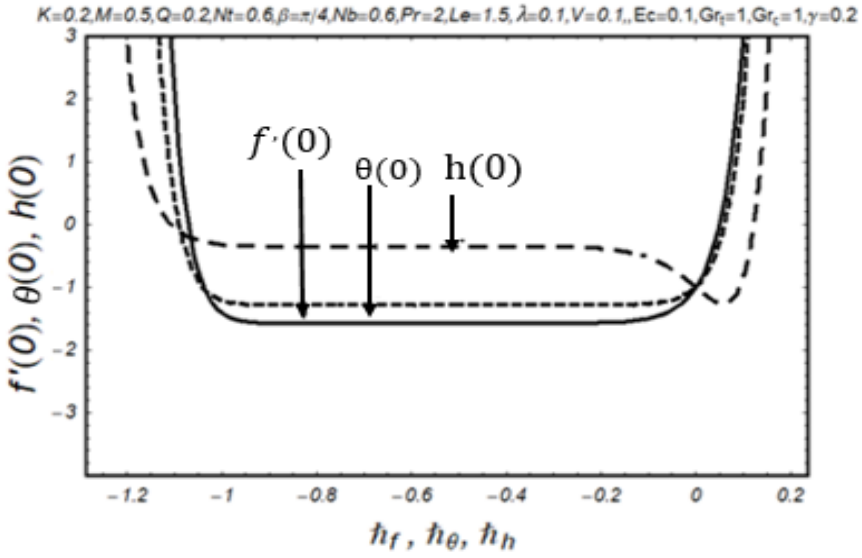


Fig. 5.2. $\hbar$-curves for PEST case.

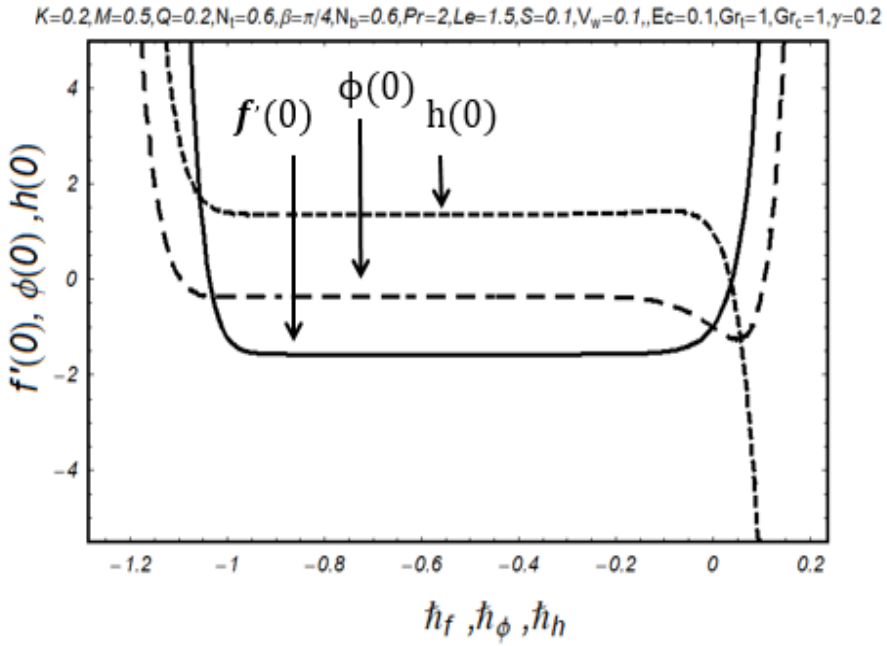


Fig. 5.3. $\hbar$-curves for PEHF case.

## 5.5 Graphical Results and Discussion

The response of velocity, temperature and concentration distributions in terms of various dimensionless quantities for steady, Williamson nanofluid flow is analyzed when the surface over which the fluid is flowing is stretching exponentially and different considered factors control the flow. The outcomes are derived in the form of graphical illustration for the dimensionless parameters. Fig. 5.4. depicts the velocity distribution $f'(\eta)$ and thickness of the boundary layer for increased values of inclined magnetic field angle $\beta$. It is evident from the figure that velocity profile decreases when increased values of $\beta$ are incorporated. The conduct of magnetic parameter given by $M$ on velocity distribution is apparent in Fig. 5.5. Through which a decreasing velocity profile is noticeable for larger magnetic parameter's values. This is in line with the fact that raised magnetic parameter brings resistance to the fluid motion due to Lorentz force, thus decreasing the profile. Figs. 5.6 and 5.7 elucidate the outcome of varying thermal Grashof number on the velocity $f'(\eta)$. A rise in value of Grashof number $Gr_t$ and $Gr_c$ amplifies the velocity profile. Figs. 5.8 to 5.11 indicate the variation of Grashof number $Gr_t$ and $Gr_c$ on temperature profile $\theta(\eta)$. Increasing values of $Gr_t$ and $Gr_c$ reduce temperature distribution $\theta(\eta)$.The impact of $Gr_c$ instigate a similar pattern to that of $Gr_t$ on all profiles and for geometries. The change in Prandtl number $\mathrm{Pr}$ and its result for temperature distribution is seen in Figs. 5.12 and 5.13. For higher Prandtl number's values, the temperature appear to lessen down for both PEST and PEHF case. The reason behind this lies in the decrease of thermal diffusivity since Prandtl number and thermal diffusivity are related inversely with each other. When compared the results for PEST case and PEHF case, the later experiences somewhat more influence of Prandtl number for the same values. The temperature distribution $\theta(\eta)$ for elevated heat source values $Q$ is sketched in Figs. 5.14 & 5.15 for the considered cases. It is analyzed that in PEST and even in PEHF case, the profile elevated with the rising values of heat source $Q$. The variation in thermophoresis motion parameter $N_t$

relative to temperature profile $\theta(\eta)$ is presented through Figs. 5.16 & 5.17. Here the temperature profile $\theta(\eta)$ enhances for $N_t$ for the dual cases. The changing Eckert number $Ec$ for temperature is seen through Figs. 5.18 & 5.19. These figures indicate that when $Ec$ increases, temperature and related thickness of boundary layer rise for both cases. From figure, it is clear that heat is generated within the fluid as value of Eckert number enhances. The frictional heating is the main cause of this phenomenon, so the fluid temperature increases with higher Eckert number. In general, Eckert number is demonstrated as the percentage of kinetic energy with specific enthalpy difference calculated between the wall and fluid. Thus, the work that is done as the Eckert number increases raises the liquid's temperature by transforming the kinetic energy to internal energy. The thermal energy is saved within the fluid as the Eckert number rises as a result of frictional or drag forces, increasing the temperature profile. The concentration profile $h(\eta)$ for Brownian motion parameter $N_b$ values have been acquired through the Figs. 5.20 & 5.21. It is noticed that intensifying the values of $N_b$ brings down the mass transfer rate, since through enhancement of $N_b$, the haphazard movement of tiny particles amplifies, thus reducing mass transfer rate. The concentration profile $h(\eta)$ for increasing Lewis number $Le$ is displayed in Figs. 5.22 & 5.23. In both cases, it can be perceived that concentration $h(\eta)$ is remarkably reduced by increasing Lewis number. Figs. 5.24 & 5.25 are plotted for the chemical reaction parameter $\gamma$ versus concentration profile $h(\eta)$. In both PEST and PEHF case, a declined concentration profile is noticeable from the figures. Growing values of $\gamma$ cause mass concentration to decline. The reason is that, the number of molecules experiencing chemical reaction lead to decrease in fluid concentration. From the figures, it can be observed that PEST case shows more prominent results than PEHF case.

The skin friction coefficient, being an important parameter is investigated through different findings. It is plotted for different values of porosity parameter $K$ with increasing mass suction and the outcomes are shown graphically in Fig. 5.26 which shows the reduced drag for intensified porosity parameter $K$ and the same is observed for the case of suction. Fig. 5.27. Show the behavior of local Nusselt number on Eckert number $Ec$. With increasing values of Eckert number reduce the local Nusselt number. The impact of $Sh$ number for different values of chemical reaction parameter is displayed in Fig. 5.28. Table 5.1 manifests the convergences of series solutions. The convergent solution for $f''(0)$ is obtained at the 30$^{th}$ order of approximation, for

$\theta'(0)$ it can be seen of the 20$^{th}$ order of approximation, for $\phi'(0)$ at 15$^{th}$ order of approximation and for $h'(0)$ at the 25$^{th}$ order of approximation. The numerically calculated values of the skin friction coefficient are also calculated and compared with the existing work done by Ali *et al*. [33] in Table 5.2. These numerical values of $C_f$ are obtained using the same parametric values of exiting research work. Considering this table, we can state that our findings and those of Ali *et al.* [33] are in perfect harmony.

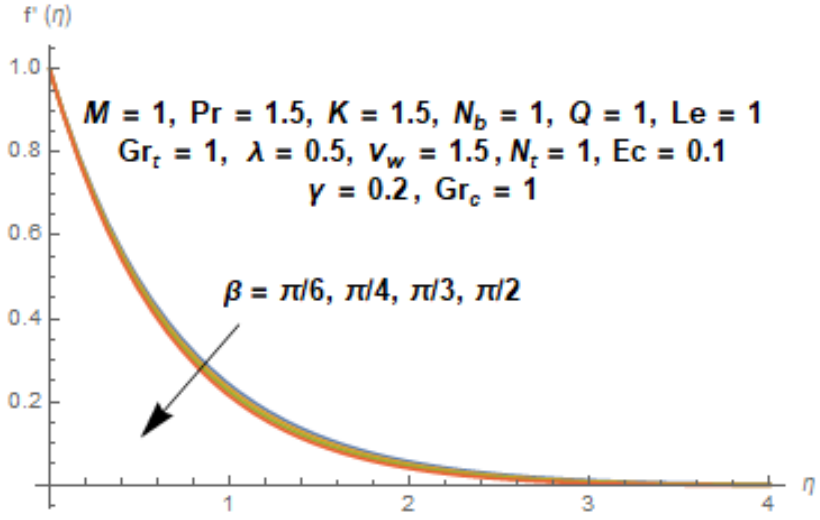


Fig. 5.4. Variation of profile $f'(\eta)$ for increased $\beta$ values.

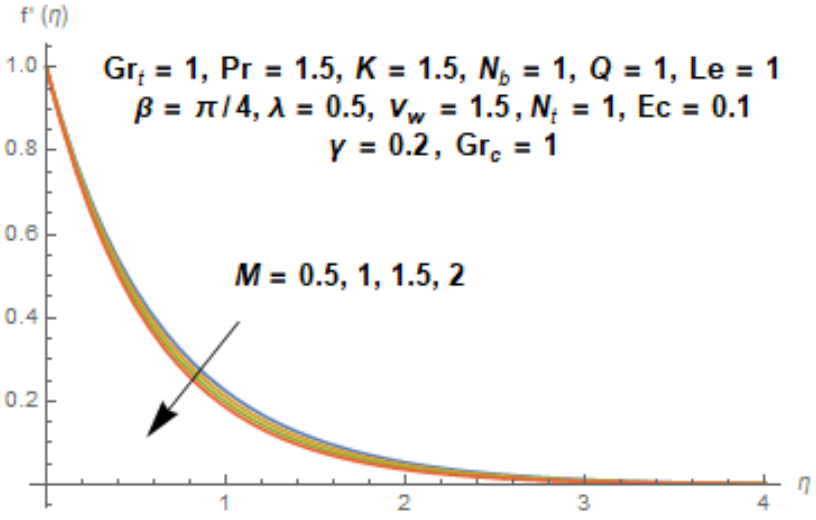


Fig. 5.5. Variation of profile $f'(\eta)$ for increased $M$ values.

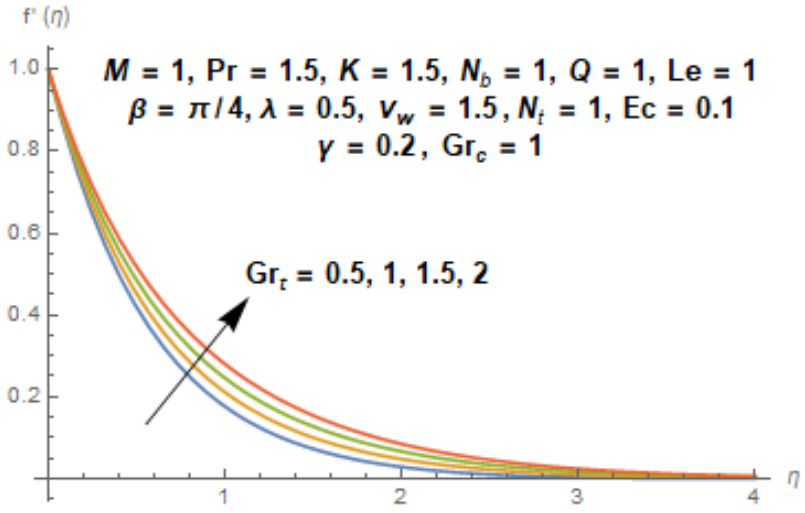


Fig. 5.6. Variation of profile $f'(\eta)$ for increased $Gr_t$ values.

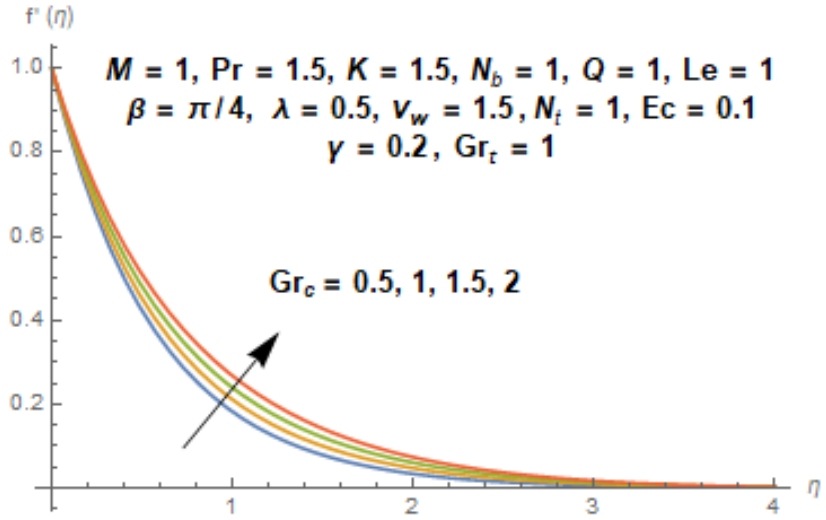


Fig. 5.7. Variation of profile $f'(\eta)$ for increased $Gr_c$ values.

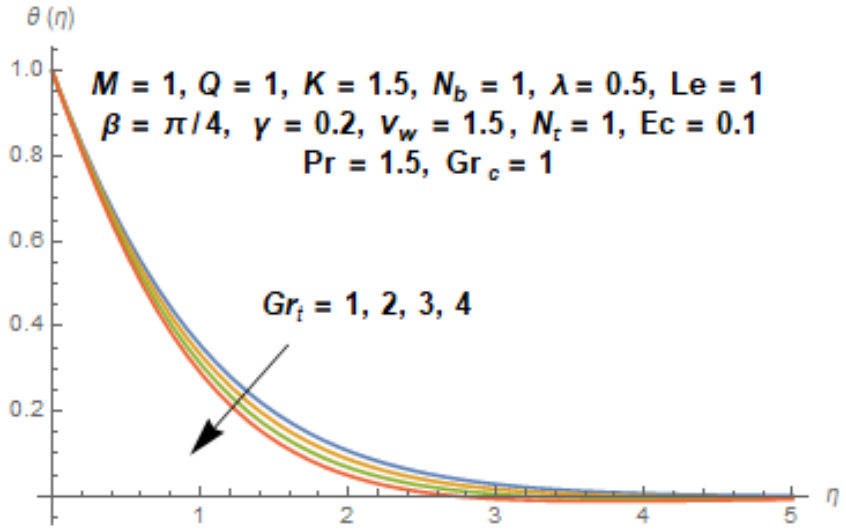


Fig. 5.8. Variation of profile $\theta(\eta)$ for increased $Gr_t$ values in case of PEST.

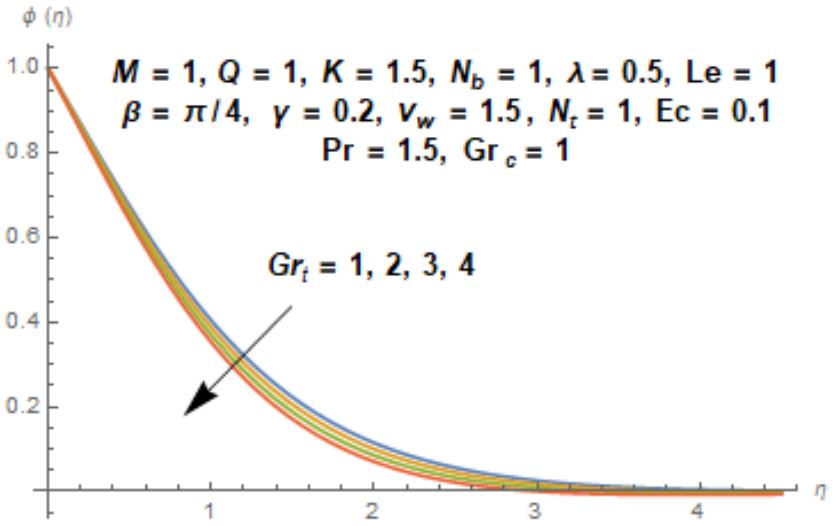


Fig. 5.9. Variation of profile $\phi(\eta)$ for increased $Gr_t$ values in case of PEHF.

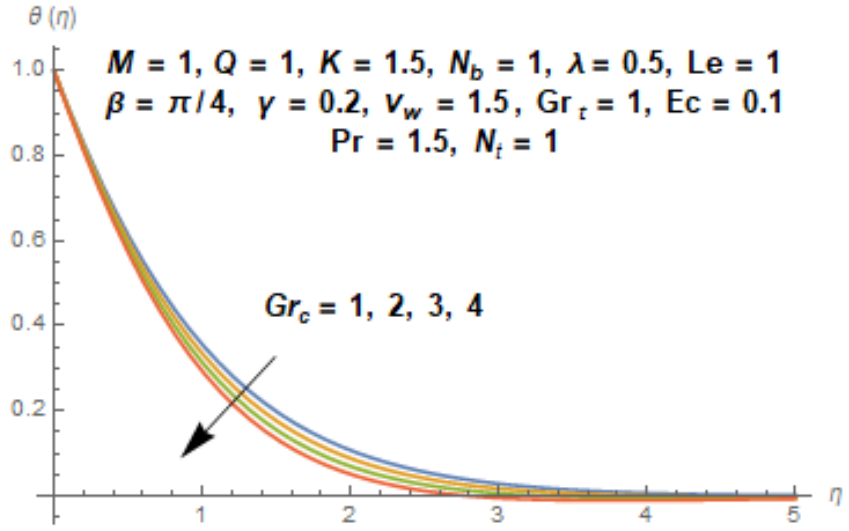


Fig. 5.10. Variation of profile $\theta(\eta)$ for increased $Gr_c$ values in case of PEST.

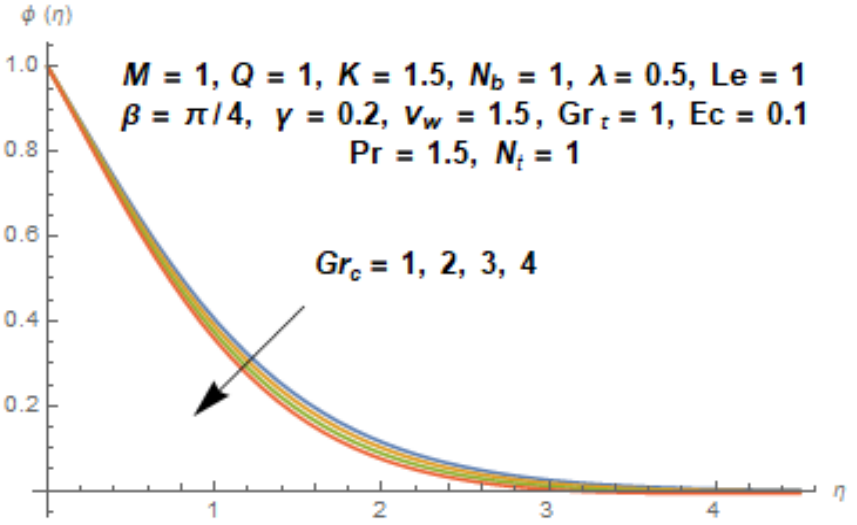


Fig. 5.11. Variation of profile $\phi(\eta)$ for increased $Gr_c$ values in case of PEHF.

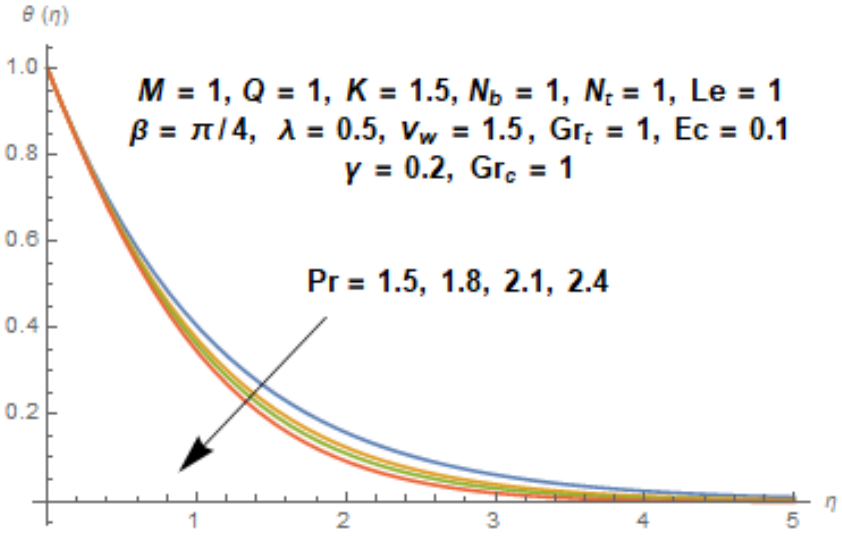


Fig. 5.12. Variation of profile $\theta(\eta)$ for increased Pr values in case of PEST.

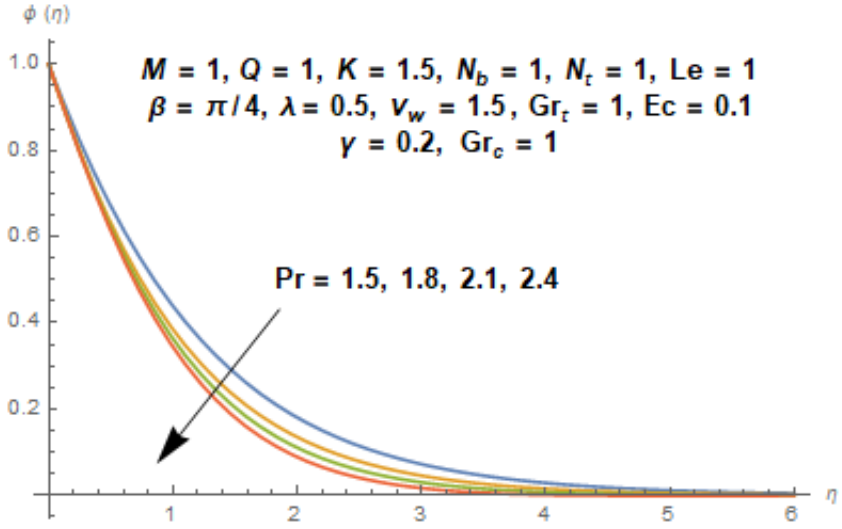


Fig. 5.13. Variation of profile $\phi(\eta)$ for increased Pr values in case of PEHF.

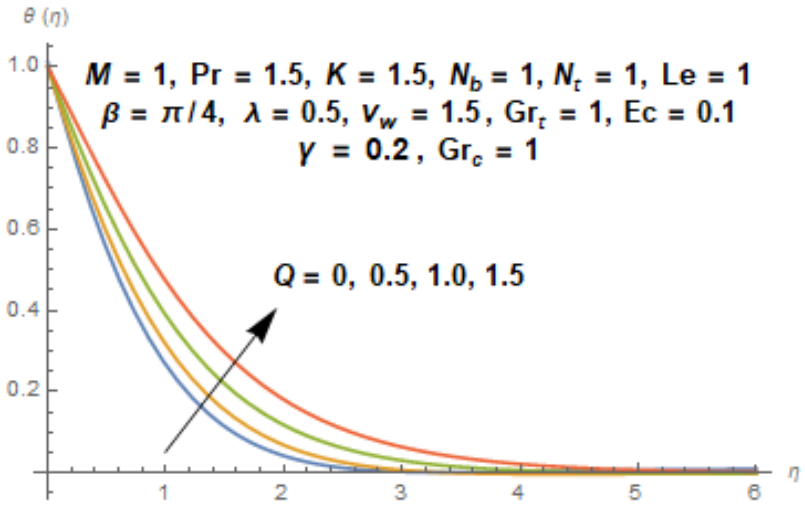


Fig. 5.14. Variation of profile $\theta(\eta)$ for increased $Q$ values in case of PEST.

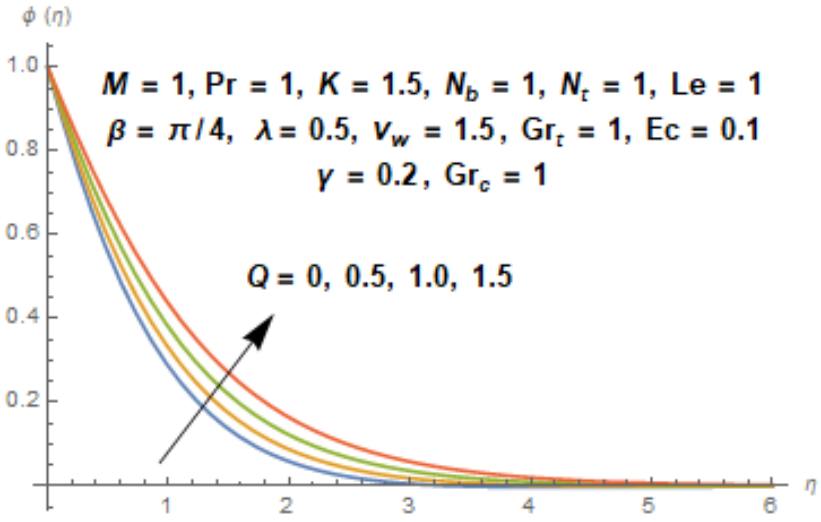


Fig. 5.15. Variation of profile $\phi(\eta)$ for increased $Q$ values in case of PEHF.

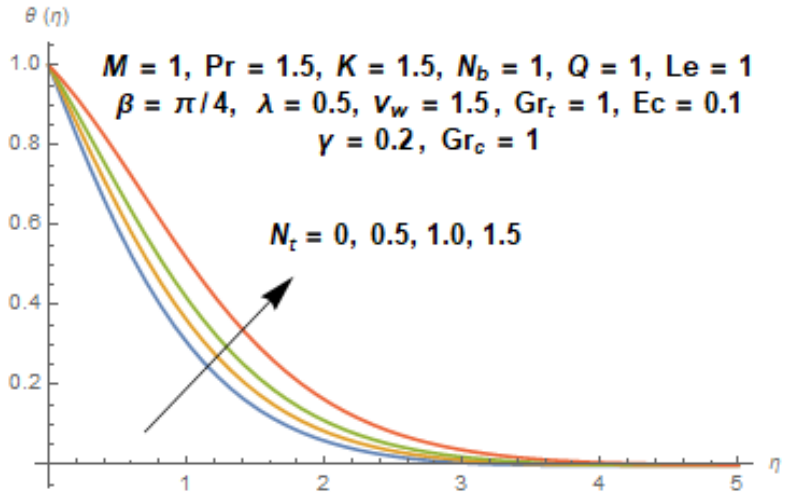


Fig. 5.16. Variation of profile $\theta(\eta)$ for increased $N_t$ values in case of PEST.

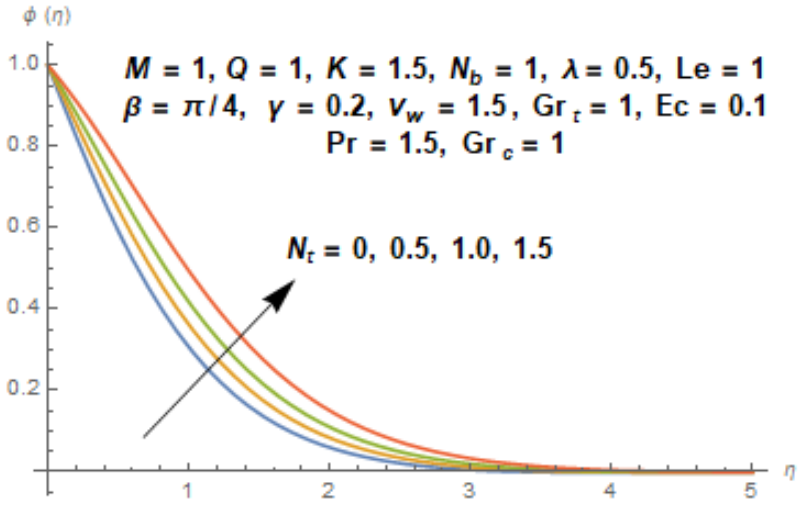


Fig. 5.17. Variation of profile $\phi(\eta)$ for increased $N_t$ values in case of PEHF.

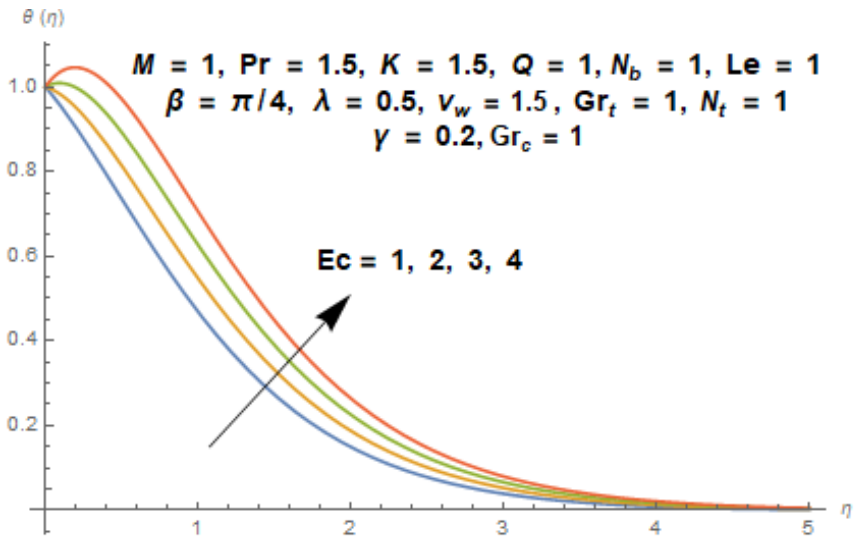


Fig. 5.18. Variation of profile $\theta(\eta)$ for increased $Ec$ values in case of PEST.

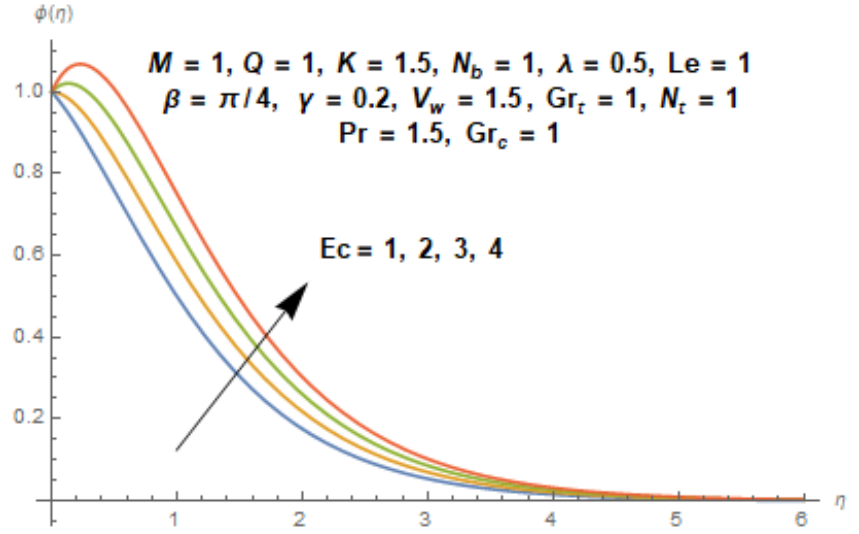


Fig. 5.19. Variation of profile $\phi(\eta)$ for increased $Ec$ values in case of PEHF.

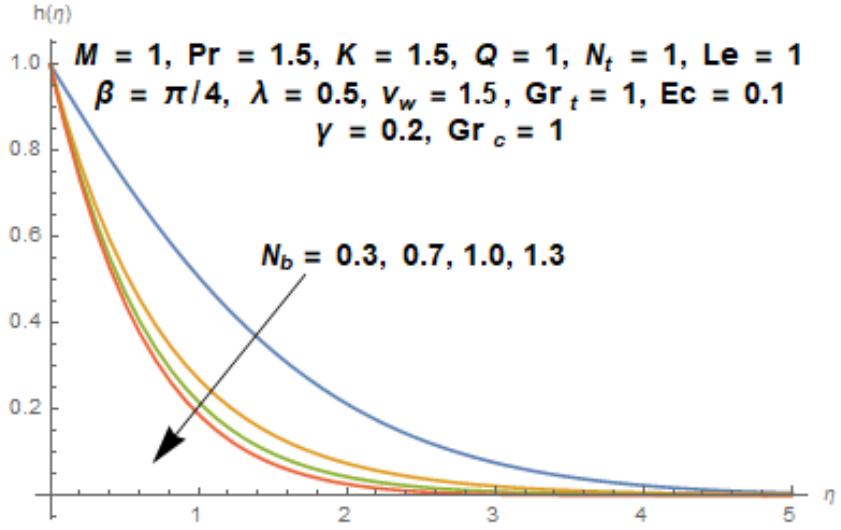


Fig. 5.20. Variation of profile $h(\eta)$ for increased $N_b$ values in case of PEST.

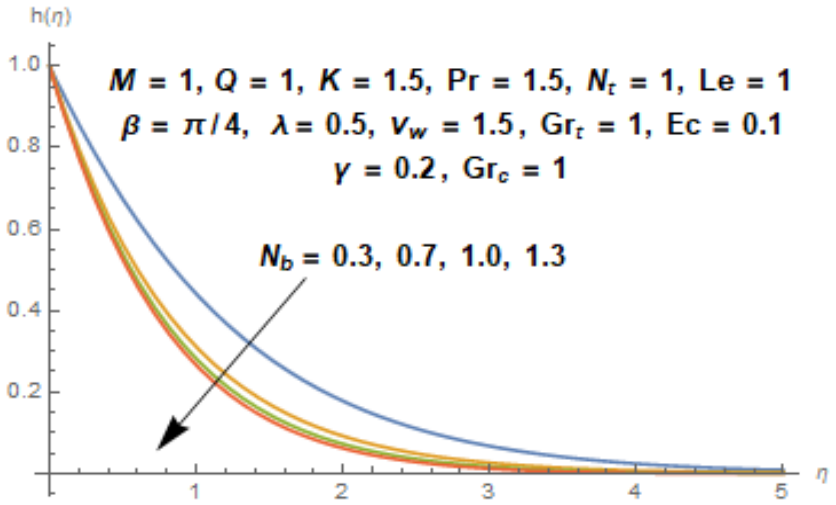


Fig. 5.21. Variation of profile $h(\eta)$ for increased $N_b$ values in case of PEHF.

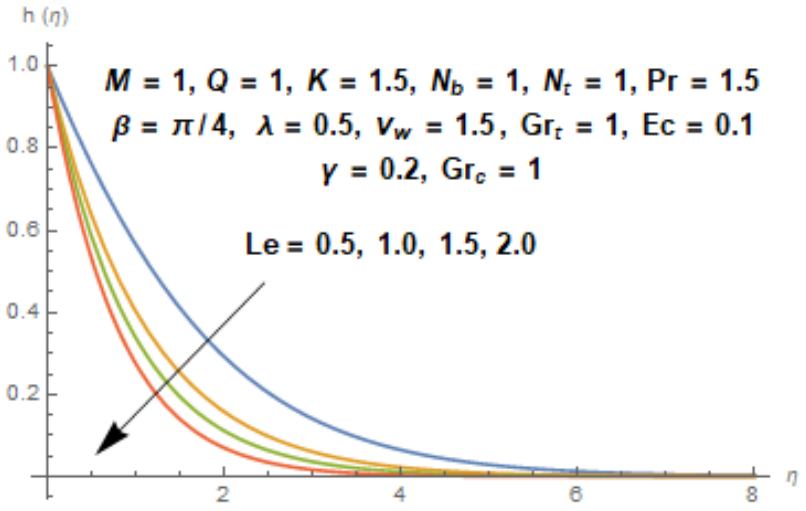


Fig. 5.22. Variation of profile $h(\eta)$ for increased $Le$ values in case of PEST.

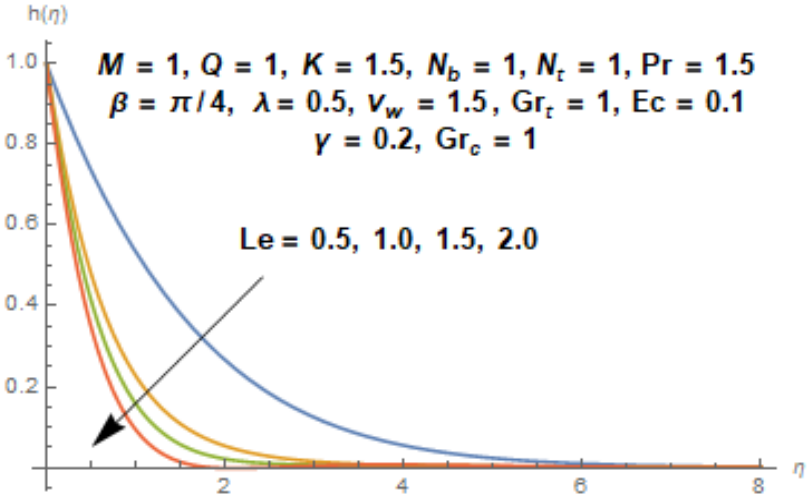


Fig. 5.23. Variation of profile $h(\eta)$ for increased $Le$ values in case of PEHF.

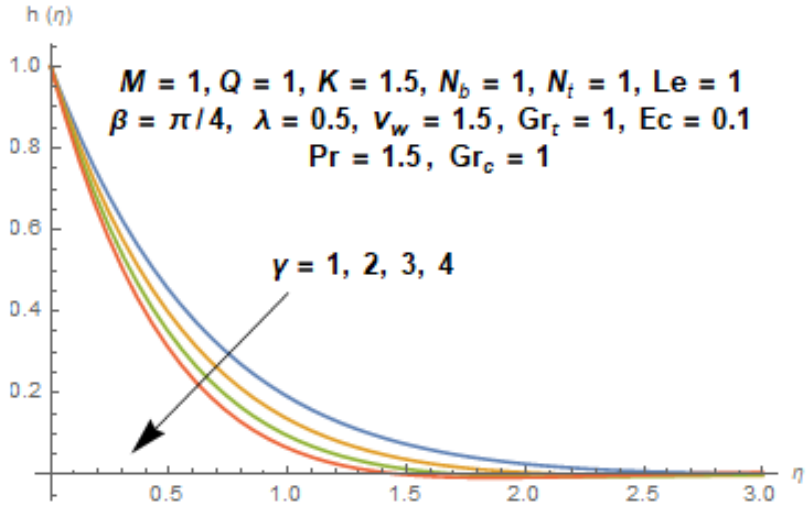


Fig. 5.24. Variation of profile $h(\eta)$ for increased $\gamma$ values in case of PEST.

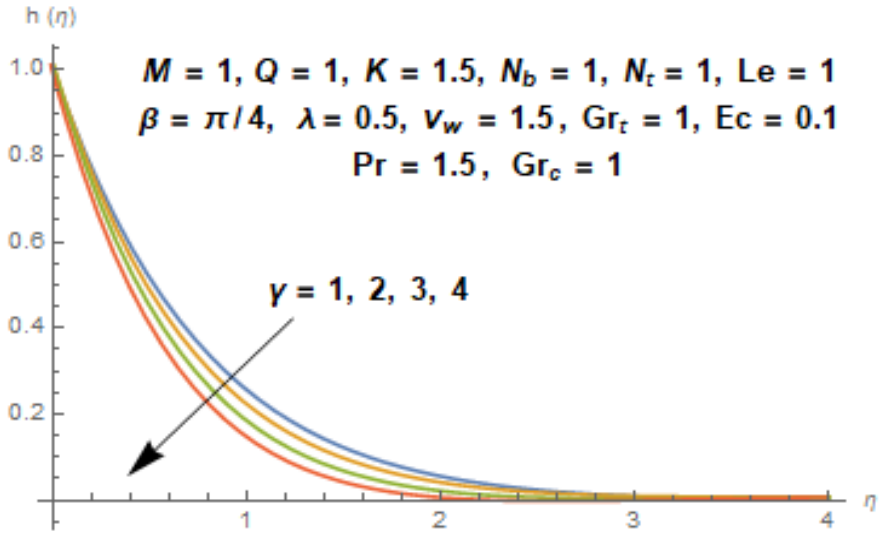


Fig. 5.25. Variation of profile $h(\eta)$ for increased $\gamma$ values in case of PEHF.

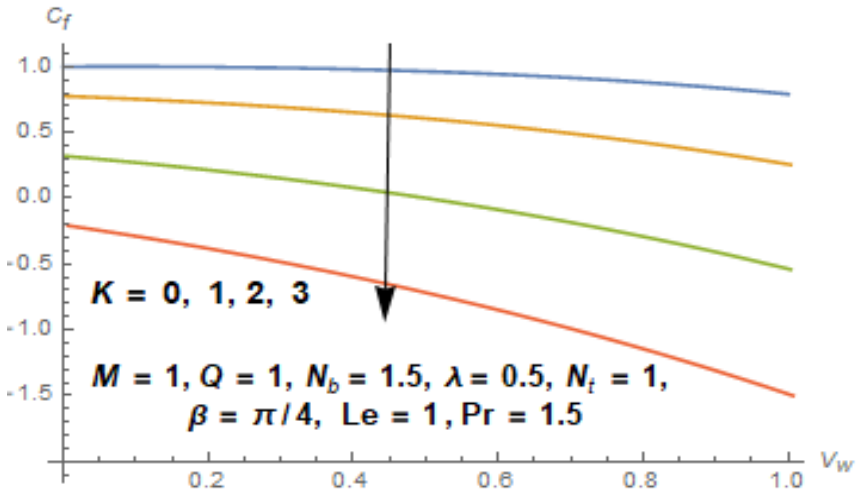


Fig. 5.26. Variation of $C_f$ for increased $K$ values.

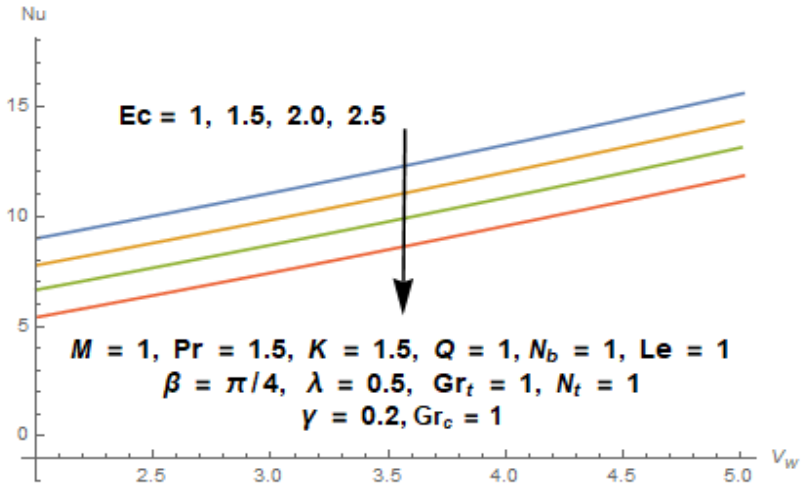


Fig. 5.27. Variation of $Nu$ for increased $Ec$ values

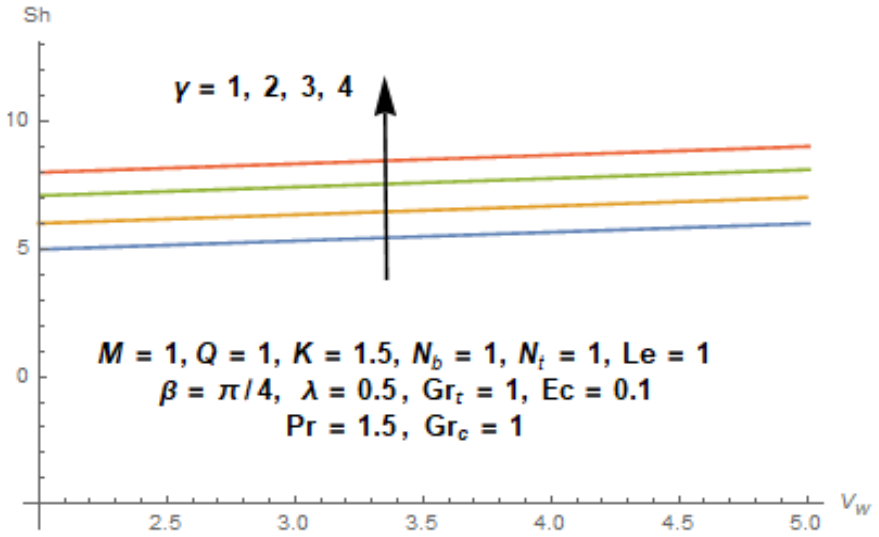


Fig. 5.28. Variation of $Sh$ for increased $\gamma$ values.

**Table 5.2**. Comparison results of $C_f$ for different values of $\lambda$ and $v_w$ .

| | Xia *et al.* (2021) | | Present results | |
|---|---|---|---|---|
| $\lambda$ | $v_w = 0.10$ | $v_w = 0.20$ | $v_w = 0.10$ | $v_w = 0.20$ |
| 0 | 1.23638 | 1.19298 | 1.23637 | 1.19298 |
| 0.1 | 1.20710 | 1.16468 | 1.20710 | 1.16466 |
| 0.2 | 1.17482 | 1.13365 | 1.17485 | 1.13365 |
| 0.3 | 1.13825 | 1.09881 | 1.13825 | 1.09880 |

# Chapter 6

# Conclusion

## 6.1 Conclusions

The ongoing study is executed to examine the heat and also mass transfer phenomenon in Williamson nanofluid flow instigated due to a porous surface stretching with velocity in exponential form. Two different cases of heat and mass transfer i.e., PEST and PEHF have been explored. The fluid model is influenced due to inclined magnetic field and heat generation/absorption. Further, the mixed convection flow is investigated for a Williamson nanofluid with the existence of an inclined MHD, chemical reaction and heat generation/absorption. The flow is investigated through homotopy analysis method (HAM) is used to secure the key findings mentioned as follows.

The velocity lessens down when values of $\beta$ and $M$ jump up. The velocity distribution increases with increasing values of $Gr_t$ and $Gr_c$. For consideration of PEST and PEHF, the temperature distribution strengthens by raising the values of $Ec$, $N_t$ and $Q$. Temperature distribution diminishes for the enhanced values of $\Pr$ , $Gr_t$ and $Gr_c$ for PEST and PEHF considered cases. The increasing values of $Le$, $N_b$ and $\gamma$ leads to reduce concentration distributions. Huge values of $K$ and $v_w$ result in less friction drag . $Nu$ lowers down with the improved values of $N_b$ and the opposite is seen for $v_w$ .The increasing values of $Le$ is associated with higher Sherwood number $Sh$ .

## 6.2 Future work

Within this work, the effects of mixed convection for Williamson nanofluid flowing by an exponentially stretching surface with the existence of magnetohydrodynamics have been analyzed with few considered assumptions. However, this carried out research provides a pathway towards more interesting works. The following are a few intriguing potential works that might be fascinating in the future.

The research can be extended for any other non-Newtonian fluid with suitable boundary conditions. The rotating Williamson nanofluid flow over a Riga surface with activation energy can be looked into. Bio-convection effects on three dimensional Williamson nanofluid flow between circular plates can also be explored.

# References


1. Choi. U.S. (1995) Enhancing Thermal Conductivity of Fluids with Nanoparticles, Developments and Application of Non-Newtonian Flows. *ASME Journal of Heat Transfer*. 66, 99-105.
2. Williamson. R. Vo. (1996). The flow of pseudoplastic materials. *Industrial and Engineering Chemistry* .21(11), 1108-1111.
3. Khan. N. A., Khan. S. and Riaz. F. (2014). Boundary layer flow of Williamson fluid with chemically reactive species using scaling transformation and homotopy analysis method. *Mathematical Sciences Letters*. 3(3), 199.
4. Pal. D. and Mandal. G. (2015). Hydromagnetic convective--radiative boundary layer flow of nanofluids induced by a non-linear vertical stretching/shrinking sheet with viscous Ohmic dissipation. *Powder Technology*. 279, 61-74.
5. Krishnamurthy. M. R., Prasannakumara. B. C., Gireesha. B. J. and Gorla. R. S. R. (2016). Effect of chemical reaction on MHD boundary layer flow and melting heat transfer of Williamson nanofluid in porous medium. *Engineering Science and Technology an International Journal*. 19(1), 53-61.
6. Khan. M., Malik. M. Y., Salahuddin. T., Rehman. K. U. and Naseer. M. (2017). MHD flow of Williamson nanofluid over a cone and plate with chemically reactive species. *Journal of Molecular Liquids*. 231, 580-588.
7. Hamid. A. and Khan. M. (2018). Unsteady mixed convective flow of Williamson nanofluid with heat transfer in the presence of variable thermal conductivity and magnetic field. *Journal of Molecular Liquids*. 260, 436-446 2558-2570.
8. Ali. H., and Nandy. S. K. (2023). Scrutinization of Unsteady Magnetohydrodynamics Williamson Nanofluid Flow and Heat Transfer past a Permeable Sheet. *Journal of Nanofluids*. 12(4), 1095-1106.
9. Nadra. K. L., (2016). Micropolar nanofluid flow with MHD and mixed convection flow effects towards a stretching sheet with multimedia feature. *International Journal of Heat and Mass Transfer*. 112, 983-990.
10. Rashidi. M. M., Nasiri. M., Khezerloo. M. and Laraqi. N. (2017). Numerical investigation

of magnetic field effect on mixed convection heat transfer of nanofluid in a channel with sinusoidal walls. *Journal of Magnetism and Magnetic Materials*. 401, 159-168.

11. Selimefendigil. F. and Öztop. H. F. (2018). Mixed convection of nanofluids in a three dimensional cavity with two adiabatic inner rotating cylinders. *International Journal of Heat and Mass Transfer*. 117, 331-343.
12. Aly. A. M., and Raizah. Z. A. S. (2019). Mixed convection in an inclined nanofluid filled-cavity saturated with a partially layered porous medium. *Journal of Thermal Science and Engineering Application*. 11(4).
13. Pal. D. and Mandal. G. (2015). Hydromagnetic convective--radiative boundary layer flow of nanofluids induced by a non-linear vertical stretching/shrinking sheet with viscous Ohmic dissipation. *Powder Technology*. 279, 61-74.
14. Hayat. T., Muhammad. T., Shehzad. S. A. and Alsaedi. A. (2017). An analytical solution for magnetohydrodynamic Oldroyd-B nanofluid flow induced by a stretching sheet with heat generation/absorption. *International Journal of Thermal Sciences*. 111, 274-288.
15. Prasad. P. D., Kumar. R. K. and Varma. S. V. K. (2018). Heat and mass transfer analysis for the MHD flow of nanofluid with radiation absorption. *Ain Shams Engineering Journal*. 9(4), 801-813.
16. Mohyud-Din. S. T., Khan. U., Ahmed. N. and Rashidi. M. M. (2018). A study of heat and mass transfer on magnetohydrodynamic (MHD) flow of nanoparticles. *Propulsion and Power Research*. 7(1), 72-77.
17. Umavathi. J. C., Sheremet. M. A. and Mohiuddin. S. (2016). Combined effect of variable viscosity and thermal conductivity on mixed convection flow of a viscous fluid in a vertical channel in the presence of first order chemical reaction. *European Journal of Mechanics-B/Fluids*. 58, 98-108.
18. Badruddin. I. A. and Quadir. G. A. (2016, June). Radiation and viscous dissipation effect on square porous annulus. In AIP Conference Proceedings (Vol. 1738, No. 1, p. 480127).
19. Hsiao. K. L. (2017). Micropolar nanofluid flow with MHD and viscous dissipation effects towards a stretching sheet with multimedia feature. *International Journal of Heat and Mass Transfer*. 112, 983-990.
20. Hayat. T., Khan. M. I., Alsaedi. A. and Khan. M. I. (2017). Joule heating and viscous dissipation in flow of nanomaterial by a rotating disk. *International Communications in*

*Heat and Mass Transfer*. 89, 190-197.

21. Saleem. S., Nadeem. S., Rashidi. M. M. and Raju. C. S. K. (2019). An optimal analysis of radiated nanomaterial flow with viscous dissipation and heat source. *Microsystem Technologies*. 25(2), 683-689.
22. Abbas. Z., Naveed, M. and Sajid. M. (2016). Hydromagnetic slip flow of nanofluid over a curved stretching surface with heat generation and thermal radiation. *Journal of Molecular Liquids*. 215, 756-762.
23. Bilal. S., Malik. M. Y., Hussain. A. and Khan. M. (2017). Effects of temperature dependent conductivity and absorptive/generative heat transfer on MHD three dimensional flow of Williamson fluid due to bidirectional non-linear stretching surface. *Results in Physics*. 7, 204-212.
24. Upreti. H., Pandey. A. K. and Kumar. M. (2018). MHD flow of Ag-water nanofluid over a flat porous plate with viscous-Ohmic dissipation, suction/injection and heat generation/ absorption. *Alexandria engineering journal*. 57(3), 1839-1847.
25. Saba. F., Ahmed. N., Hussain. S., Khan. U., Mohyud-Din. S. T. and Darus. M. (2018). Thermal analysis of nanofluid flow over a curved stretching surface suspended by carbon nanotubes with internal heat generation. *Applied Sciences*. 8(3), 395.
26. Eid. M. R. and Mahny. K. L. (2018). Flow and heat transfer in a porous medium saturated with a Sisko nanofluid over a nonlinearly stretching sheet with heat generation/absorption. *Heat Transfer Asian Research*. 47(1), 54-71.
27. Hayat. T., Qayyum. S., Shehzad, S. A. and Alsaedi, A. (2016). Simultaneous effects of heat generation/absorption and thermal radiation in magnetohydrodynamics (MHD) flow of Maxwell nanofluid towards a stretched surface. *Results in physics*. 7, 562-573.
28. Nayak. M. K., Dash. G. C. and Singh. L. P. (2017). Heat and mass transfer effects on MHD viscoelastic fluid over a stretching sheet through porous medium in presence of chemical reaction. *Propulsion and Power Research*. 5(1), 70-80.
29. Saqib. M., Ali. F., Khan. I. and Sheikh. N. A. (2018). Heat and mass transfer phenomena in the flow of Casson fluid over an infinite oscillating plate in the presence of first-order chemical reaction and slip effect. *Neural Computing and Applications*. 30(7), 2159-2172.
30. Mjankwi. M. A., Masanja. V. G., Mureithi. E. W. and James. M. N. O. (2019). Unsteady MHD flow of nanofluid with variable properties over a stretching sheet in the presence of

thermal radiation and chemical reaction. *International Journal of Mathematics and Mathematical Sciences*. 21(3), 12-18.

31. Sabir. Z., Akhtar. R., Zhiyu. Z., Umar. M., Imran. A., Wahab. H. A. and Raja. M. A. Z. (2019). A computational analysis of two-phase casson nanofluid passing a stretching sheet using chemical reactions and gyrotactic microorganisms. *Mathematical Problems in Engineering*. 9(1), 99-129.
32. Waqas. M., Khan. M. I., Asghar. Z., Kadry. S., Chu. Y. M. and Khan. W. A. (2020). Interaction of heat generation in nonlinear mixed/forced convective flow of Williamson fluid flow subject to generalized Fourier's and Fick's concept. *Journal of Materials Research and Technology*. 9(5), 11080-11086.
33. Ali. R., Khan. M. R., Abidi. A., Rasheed. S. and Galal. A. M. (2021). Application of PEST and PEHF in magneto-Williamson nanofluid depending on the suction/injection. *Case Studies in Thermal Engineering*. 27, 101329.
34. Yusuf. T. A., Mabood, F., Prasannakumara, B. C. and Sarris. I. E. (2021). Magneto-bioconvection flow of Williamson nanofluid over an inclined plate with gyrotactic microorganisms and entropy generation. *Fluids*. 6(3), 109.
35. Nazir. U., Sadiq. M. A. and Nawaz. M. (2021). Non-Fourier thermal and mass transport in hybridnano-Williamson fluid under chemical reaction in Forchheimer porous medium. *International Communications in Heat and Mass Transfer*. 127, 105536.
36. Srinivasulu. T. and Goud. B. S. (2021). Effect of inclined magnetic field on flow, heat and mass transfer of Williamson nanofluid over a stretching sheet. *Case Studies in Thermal Engineering*. 23, 100819.
37. Dawa. A., Shah. Z. and Islam. S. (2021). Mathematical modeling and study of MHD flow of Williamson nanofluid over a nonlinear stretching plate with activation energy. *Heat Transfer*. 50(3), 2558-2570.
38. Habib. U., Abdal. S., Siddique. I. and Ali, R. (2021). A comparative study on micropolar, Williamson, Maxwell nanofluids flow due to a stretching surface in the presence of bioconvection, double diffusion and activation energy. *International Communications in Heat and Mass Transfer*. 127, 105551.
39. Loganathan, P. and Sangeetha, S. (2022). Effect of Williamson parameter on Cu-water Williamson nanofluid over a vertical plate. *International Communications in Heat and*

*Mass Transfer*. 137, 106273.

40. Patil. P. M., Benawadi. S. and Muttannavar. V. T. (2022). Mixed Bioconvective Flow of Williamson Nanofluid Over a Rough Vertical Cone. *Arabian Journal for Science and Engineering*. 1-12.
41. Sharma. R. P., Mishra. S. R., Tinker. S. and Kulshrestha. B. K. (2022). Effect of Non-linear Thermal Radiation and Binary Chemical Reaction on the Williamson Nanofluid Flow past a Linearly Stretching Sheet. *International Journal of Applied and Computational Mathematics.* 8(4), 1-13.
42. Reddy. M. G., Krishnamurth. M. R., Praveena. M. M., Naik. L. S., Prakasha. D. G. and Ganesh. K. K. (2022). Unsteady absorption flow and dissipation heat transfer over a non-Newtonian fluid. *Waves in Random and Complex Media*. 1-15.
43. Reddy. M. V. and Lakshminarayana. P. (2022). MHD radiative flow of Williamson nanofluid with Cattaneo-Christov model over a stretching sheet through a porous medium in the presence of chemical reaction and suction/injection. *Journal of Porous Media*. 25.
44. Sulochana. C. and Mahalaxmi. B. (2022). Thermophoresis and Brownian motion effects on Williamson nanofluid flow past a stretching surface with thermal radiation and chemical reaction. *Heat Transfer*. 51(3), 2761-2779.
45. Son. Y. Q., Hamid. A., Sun. T. C., Khan. M. I., Qayyum. S., Kumar. R. N. and Chinram. R. (2022). Unsteady mixed convection flow of magneto-Williamson nanofluid due to stretched cylinder with significant non-uniform heat source/sink features. *Alexandria Engineering Journal*. 61(1), 195-206.
46. Hussain. A. and Malik. M. Y. (2021). MHD nanofluid flow over stretching cylinder with convective boundary conditions and Nield conditions in the presence of gyrotactic swimming microorganism: A biomathematical model. *International Communications in Heat and Mass Transfer*. 126, 105425.
47. Zhang. X. H., Abidi. A., Ahmed. A. E., S., Khan. M. R., El-Shorbagy. M., A. Shutaywi. M. and Galal, A. M. (2021). MHD stagnation point flow of nanofluid over a curved stretching/shrinking surface subject to the influence of Joule heating and convective condition. *Case Studies in Thermal Engineering*. 26, 101184.
48. Ali. B., Shafiq. A., Manan. A., Wakif. A. and Hussain. S. (2022). Bioconvection: Significance of mixed convection and mhd on dynamics of Casson nanofluid in the

stagnation point of rotating sphere via finite element simulation. *Mathematics and Computers in Simulation*. 194, 254-268.

49. Arafa. A. A., Sameh. E. A. and Allan. M. M. (2022). Peristaltic flow of non-homogeneous nanofluids through variable porosity and heat generating porous media with viscous dissipation: Entropy analyses. *Case Studies in Thermal Engineering*. 32, 101882.
50. Sharada. K. (2022): Heat and mass transfer effects on MHD mixed convection flow of viscoelastic fluid with constant viscosity and thermal conductivity. *Heat Transfer*. 51.1, 1213-1236.
51. Arshad. M., Hussain. A., Hassan. A., Shah. S. A. G. A., Elkotb. M. A., Gouadria. S.and Galal. A. M. (2022). Heat and mass transfer analysis above an unsteady infinite porous surface with chemical reaction. *Case Studies in Thermal Engineering*. 36, 102140.
52. Haq. I., Bilal. M., Ahammad. N. A., Ghoneim. M. E., Ali. A. and Weera. W. (2022). Mixed convection nanofluid flow with heat source and chemical reaction over an inclined irregular surface. *ACS omega*. 7(34), 30477-30485.
53. Hamzah. H. K., Ali, F. H. and Hatami, M. (2022). MHD mixed convection and entropy generation of CNT-water nanofluid in a wavy lid-driven porous enclosure at different boundary conditions. *Scientific Reports*. 12(1), 1-27.
54. Safadr. J., Mahabaleshwar. U. S. and Bognár. G. (2022).Maxwell nanofluid flow under mass transpiration in nonlinear MHD flow due to porous stretching sheet. *Scientific reports*. 9(1), 1-15.
55. Sudarsana. R. P. and Sreedevi. P. (2022). Impact of chemical reaction and double stratification on heat and mass transfer characteristics of nanofluid flow over porous stretching sheet with thermal radiation. *International Journal of Ambient Energy*. 43(1), 1626-1636.
56. Almaneea. A., (2022). Numerical study on heat and mass transport enhancement in MHD Williamson fluid via hybrid nanoparticles. *Alexandria Engineering Journal*. 61(10), 8343-8354.
57. Salawu. S. O., Fatunmbi. E. O. and Okoya. S. S. (2021). MHD heat and mass transport of Maxwell Arrhenius kinetic nanofluid flow over stretching surface with nonlinear variable properties. *Results in Chemistry*. 3, 100125.
58. Zhou. J. C., Abidi. A., Shi. Q. H., Khan. M. R., Rehman. A., Issakhov. A. and Galal. A.

M. (2021). Unsteady radiative slip flow of MHD Casson fluid over a permeable stretched surface subject to a non-uniform heat source. *Case Studies in Thermal Engineering*. 26, 101141.

59. Adigun. J. A., Adeniyan. A. and Abiala. I. O. (2021). Stagnation point MHD slip-flow of viscoelastic nanomaterial over a stretched inclined cylindrical surface in a porous medium with dual stratification. *International Communications in Heat and Mass Transfer*. 126, 105479.
60. Warke. A. S., Ramesh. K., Oudina. F. M., Abidi. A. (2021). Numerical investigation of the stagnation point flow of radiative magnetomicropolar liquid past a heated porous stretching sheet, *Journal of Thermal Analysis and Calorimetry*. (doi.org/10.1007/s10973-021-10976-z).
61. Yahya. A. U., Salamat. N., Huang. W. H., Siddique. I., Abdal. S. and Hussain. S. (2021). Thermal charactristics for the flow of Williamson hybrid nanofluid (MoS2+ ZnO) based with engine oil over a streched sheet. *Case Studies in Thermal Engineering*. 26, 101196.
62. Gopal. D., Saleem. S., Jagadha. S., Ahmad. F., Almatroud. A. O. and Kishan. N. (2021). Numerical analysis of higher order chemical reaction on electrically MHD nanofluid under influence of viscous dissipation. *Alexandria Engineering Journal*. 60(1). 1861-1871.
63. Hayat. T., Khan. M. I., Alsaedi. A., and Khan. M. I. (2021). Joule heating and viscous dissipation in flow of nanomaterial by a rotating disk. International Communications in *Heat and Mass Transfer*. 89, 190-197.
64. Megahed. A. M., Reddy. M. G. and Abbas. W. (2021). Modeling of MHD fluid flow over an unsteady stretching sheet with thermal radiation, variable fluid properties and heat flux. *Mathematics and Computers in Simulation*. 185, 583-593.
65. Vinodkumar. R. M. and Lakshminarayana. P. (2022). Higher Order Chemical Reaction and Radiation Effects on Magnetohydrodynamic Flow of a Maxwell Nanofluid With Cattaneo--Christov Heat Flux Model Over a Stretching Sheet in a Porous Medium. *Journal of Fluids Engineering*. 144(4), 041204.
66. Abdelmalek. Z., Hussain. A., Bilal. S., Sherif. E. S. M. and Thounthong. P., (2022). Brownian motion and thermophoretic diffusion influence on thermophysical aspects of

electrically conducting viscoinelastic nanofluid flow over a stretched surface. *Journal of Materials Research and Technolog*. 9(5), 11948-11957.

67. Biswas. R., Hossain. M. S., Islam. R., Ahmmed. S. F., Mishra. S. R. and Afikuzzaman. M. (2022). Computational treatment of MHD Maxwell nanofluid flow across a stretching sheet considering higher-order chemical reaction and thermal radiation. *Journal of Computational Mathematics and Data Science*. 4, 100048.
68. Bejawada and S. Goud, et al. (2022). Radiation effect on MHD Casson fluid flow over an inclined non-linear surface with chemical reaction in a Forchheimer porous medium. *Alexandria Engineering Journal* 61(10) 8207-8220.
69. Hamid. A. (2020). Terrific effects of Ohmic-viscous dissipation on Casson nanofluid flow over a vertical thin needle: buoyancy assisting & opposing flow. *Journal of Materials Research and Technology*. 9(5), 11220-11230.
70. Lund. L. A., Omar. Z., Khan. I., Seikh. A. H., Sherif. E. S. M. and Nisar. K. S. (2020). Stability analysis and multiple solution of Cu--Al2O3/H2O nanofluid contains hybrid nanomaterials over a shrinking surface in the presence of viscous dissipation. *Journal of Materials Research and Technology*. 9(1), 421-432.
71. Chu. Y. M., Khan. U., Zaib. A., Shah. S. H. A. M. and Marin. M. (2020). Numerical and computer simulations of cross-flow in the streamwise direction through a moving surface comprising the significant impacts of viscous dissipation and magnetic fields: stability analysis and dual solutions. *Mathematical Problems in Engineerin*g. 2020, 1-11.
72. Aziz. A., Jamshed. W., Aziz. T., Bahaidarah. H. and Ur Rehman. K. (2021). Entropy analysis of Powell--Eyring hybrid nanofluid including effect of linear thermal radiation and viscous dissipation. *Journal of Thermal Analysis and Calorimetric*. 143(2), 1331-1343.
73. Abbas. M. A., Ahmed. B., Chen. L., Rehman. S. U., Saleem. M. and Khudair. W. S., (2022). Analysis of Entropy Generation on Magnetohydrodynamic Flow with Mixed Convection through Porous Media. *Energies*. 15(3), 1206.
74. Rikitu. B. H., Makinde. O. D., and Enyadene. L. G. (2022). Unsteady mixed convection of a radiating and reacting nanofluid with variable properties in a porous medium microchannel. *Archive of Applied Mechanics*. 92(1), 99-119.
75. Saeed. A., Algehyne. E. A., Aldhabani. M. S., Dawar. A., Kumam. P., and Kumam.

W., (2022). Mixed convective flow of a magnetohydrodynamic Casson fluid through a permeable stretching sheet with first-order chemical reaction. *Plos one*. 17(4), e0265238.

76. Nandi. S. and Kumbhakar. B. (2022). Viscous Dissipation and Chemical Reaction Effects on Tangent Hyperbolic Nanofluid Flow Past a Stretching Wedge with Convective Heating and Navier's Slip Conditions. *Iranian Journal of Science and Technology, Transactions of Mechanical Engineering*. 46(2), 379-397.
77. Nalivela. N. R., Vempati. S. R., Ravindra R. B. and Dharmendar. R. Y. (2022). Viscous dissipation and thermal radiation impact on MHD mass transfer natural convective flow over a stretching sheet. *Proceedings of the Institution of Mechanical Engineers, Part E*: *Journal of Process Mechanical Engineering*. 09544089221081339.
78. Hussian. M. and Prakash. J. (2022). Effects of thermal radiation parameter and magnetic field on the peristaltic motion of nanofluids in a tapered asymmetric channel. International *Journal of Heat and Mass Transfer*. 81, 234-245.
79. Khan. M. R., Mao. S., Deebani. W. and Elsiddieg. A. M. (2022). Numerical analysis of heat transfer and friction drag relating to the effect of Joule heating, viscous dissipation and heat generation/absorption in aligned MHD slip flow of a nanofluid. *International Communications in Heat and Mass Transfer*. 131, 105843.
80. Chen. C. H., (2009). Magneto-hydrodynamic mixed convection of a power-law fluid past a stretching surface in the presence of thermal radiation and internal heat generation/absorption. *International Journal of Non-Linear Mechanics*. 44(6), 596-603.
81. Ahmed. N., Mohyud-Din. S. T. and Hassan. S. M. (2016). Flow and heat transfer of nanofluid in an asymmetric channel with expanding and contracting walls suspended by carbon nanotubes: a numerical investigation. *Aerospace Science and Technology*. 48, 53-60.
82. Nuwaira. M., Hafeez. A., Khalid. A. and Aldhafeeri. A. (2022). Multiple solutions of melting heat transfer of MHD hybrid based nanofluid flow influenced by heat generation/absorption. *Case Studies in Thermal Engineering*. 35, 101988.
83. Johnson. B. A. and I. O. (2022). Impact of radiation and heat generation/absorption in a Walters' B fluid through a porous medium with thermal and thermo diffusion in the presence of chemical reaction. *International Journal of Modelling and Simulation*.1-14.
84. Yaseen. M., Rawat. S. K., Shafiq. A., Kumar. M. and Nonlaopon. K. (2022). Analysis of

heat transfer of mono and hybrid nanofluid flow between two parallel plates in a Darcy porous medium with thermal radiation and heat generation/absorption. *Symmetry*. 14(9), 1943.

85. Eid. M. R. and Nafe. M. A. (2022). Thermal conductivity variation and heat generation effects on magneto-hybrid nanofluid flow in a porous medium with slip condition. *Waves in Random and Complex Media.* 32(3), 1103-1127.
86. Yesodha. P., Bhuvaneswari. M., Sivasankaran. S. and Saravanan. K. (2022). Nanofluid flow with activation energy and heat generation under slip boundary condition with convective heat and mass transfer. *Materials Today: Proceedings*. 59, 959-967.
87. Shah. S. S., Haq. R., McCash. L. B., Bahaidarah. H. M. and Aziz. T. (2022). Numerical simulation of lid driven flow in a curved corrugated porous cavity filled with CuO-water in the presence of heat generation/absorption. *Alexandria Engineering Journal*. 61(4), 2749-2767.
88. Gajbhiye. S., Warke. A. and Ramesh. K. (2022). Analysis of energy and momentum transport for Casson nanofluid in a microchannel with radiation and chemical reaction effects. *Waves in Random and Complex Media*. 1-29.
89. Khan. N. S., Kumam. P. and Thounthong. P. (2020). Second law analysis with effects of Arrhenius activation energy and binary chemical reaction on nanofluid flow. *Scientific reports*. 10(1), 1-16.
90. Khan. M. and Alzahrani. F. (2020). Activation energy and binary chemical reaction effect in nonlinear thermal radiative stagnation point flow of Walter-B nanofluid: Numerical computations. *International Journal of Modern Physics B*. 34(13), 2050132.
91. Uddin. I., Ullah. I., Ali. R., Khan. I. and Nisar. K. S. (2021). Numerical analysis of nonlinear mixed convective MHD chemically reacting flow of Prandtl--Eyring nanofluids in the presence of activation energy and Joule heating. *Journal of Thermal Analysis and Calorimetry*. 145(2), 495-505.
92. Punith. G. R. J., Naveen K. R., Jyothi. A. M., Prasannakumara. B. C. and Nisar. K. S. (2021). KKL correlation for simulation of nanofluid flow over a stretching sheet considering magnetic dipole and chemical reaction. *ZAMM-Journal of Applied Mathematics and Mechanics/Zeitschrift für Angewandte Mathematik und Mechanik*. 101(11). e202000372.

93. Raja. M. A. Z., Tabassum. R., El-Zahar. E. R., Shoaib. M., Khan. M. I., Malik. M. Y. and Qayyum. S. (2022). Intelligent computing through neural networks for entropy generation in MHD third-grade nanofluid under chemical reaction and viscous dissipation. *Waves in Random and Complex Media*. 1-25.
94. Varun. K. R. S., Gunderi. D. P., Naveen. K. R. P., Gowda. R. J. and Prasannakumara. B. C. (2022). Modeling and theoretical investigation on Casson nanofluid flow over a curved stretching surface with the influence of magnetic field and chemical reaction. *International Journal for Computational Methods in Engineering Science and Mechanics.* 23(1), 12-19.
95. Nadeem, S., S. T. Hussain, and Changhoon Lee. Flow of a Williamson fluid over a stretching sheet. *Brazilian journal of chemical engineering.* 30 (2013), 619-625.
96. Li. Y. X., Alshbool. M. H., Lv. Y. P., Khan. I., Khan. M. R. and Issakhov. A. (2021). Heat and mass transfer in MHD Williamson nanofluid flow over an exponentially porous stretching surface. *Case Studies in Thermal Engineering*. 26, 100975.
97. Dowling. D. R., Kundu. P. K., and Cohen, I. M. (2012). *Fluid Mechanics*. (6th ed.) Germany: Elsevier Science.
98. McDonald, A. T., Fox, R. W., and Pritchard, P. J. (2009). *Introduction to fluid mechanics*. (8th ed.) India.: Wiley.
99. Whitaker, S. (1977). *Fundamental Principles of Heat Transfer*. (1st ed.) United Kingdom.: Elsevier Science and Technology Books.
100. Durst, F. (2008). *Fluid Mechanics*: *An Introduction to the Theory of Fluid Flows*. Germany.: Springer Berlin Heidelberg.
101. Musharafa (2021). *Lie group study of some non-newtanion fluid flow with heat transfer anaylsis*. MS Thesis pages 30-34, University of engineering and technology, Lahore.
102. Liao, S. (2012). *Homotopy Analysis Method in Nonlinear Differential Equations*. Germany.: Higher Education Press.